



UNIVERSIDADE ESTADUAL DE CAMPINAS

INSTITUTO DE GEOCIÊNCIAS

Pós-Graduação em Geociências - Área de Metalogênese

**AUTOR:** Renato Dantas Neder

**ORIENTADOR:** Prof. Dr. Bernardino Ribeiro de Figueiredo

Aprovada em: 24/05/02

**PRESIDENTE:** Prof. Dr. Prof. Dr. Bernardino Ribeiro de Figueiredo

**EXAMINADORES:**

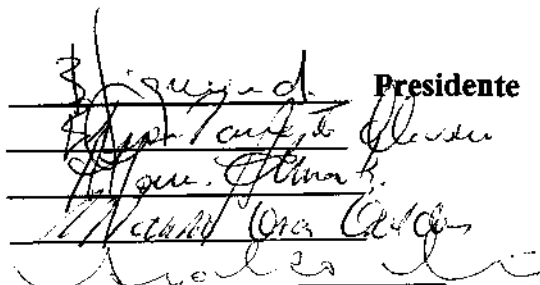
Prof. Dr. Bernardino Ribeiro de Figueiredo

Prof. Dr. Elson Paiva de Oliveira

Prof. Dr. Alfonso Schrank

Prof. Dr. MauroCesar Geraldes

Prof. Dr. Aroldo Misi

  
Presidente

Campinas, 24 de maio de 2002



**UNICAMP**

**UNIVERSIDADE ESTADUAL DE CAMPINAS**

**INSTITUTO DE GEOCIÊNCIAS**

**Pós-Graduação em Geociências**

**Área de Metalogênese**

**RENATO DANTAS NEDER**

Depósitos de sulfeto maciço associados à rochas vulcânicas: O caso do depósito Zn-Pb do Expedito,  
Ariuanã, MT, Brasil.

Tese apresentada ao Instituto de Geociências como parte dos  
requisitos para obtenção do título de Doutor em Ciências.

ntador: Prof. Dr. Bernardino Ribeiro de Figueiredo

Este exemplar corresponde à  
redação final da tese defendida  
por Renato Dantas Neder  
e aprovada pela Comissão Julgadora  
em 24/10/2002

B. Figueiredo  
\_\_\_\_\_  
ORIENTADOR

**CAMPINAS - SÃO PAULO**

Maio - 2002

**UNICAMP**  
**BIBLIOTECA**

**UNICAMP**  
**BIBLIOTECA CENTRAL**  
**SEÇÃO CIRCULANTE**

UNIDADE Be  
Nº CHAMADA T/UNICAMP  
N 284d  
V EX  
TOMBO BC/ 49903  
PROC 16-837102  
C DX  
PREÇO R\$11,00  
DATA \_\_\_\_\_  
Nº CPD \_\_\_\_\_

CM00170299-6

BIB ID 249926

FICHA CATALOGRÁFICA ELABORADA PELA  
BIBLIOTECA DO IG - UNICAMP

Neder, Renato Dantas

N284d      Depósitos de sulfeto maciço associados a rochas vulcânicas: o caso do depósito Zn-Pb do Expedito, Aripuanã, MT, Brasil / Renato Dantas Neder.- Campinas,SP.: [s.n.], 2002.

Orientador: Bernardino Ribeiro de Figueiredo  
Tese (doutorado) Universidade Estadual de Campinas, Instituto de Geociências.

1. Geologia Econômica – Aripuanã, MT. 2. Jazidas – Aripuanã, MT. 3. Zinco. 4. Chumbo. 5. Minas e Mineração. I. Figueiredo, Bernardino Ribeiro de. II. Universidade Estadual de Campinas, Instituto de Geociências III. Título.

À minha querida esposa Maria Lucia e a meus filhos Renato e Luciana.

## **AGRADECIMENTOS**

Em primeiro lugar agradeço a Bernardino Ribeiro de Figueiredo pela orientação incentivo e amizade e aos professores Jayme Alfredo Dexheymer Leite, Colombo Celso Gaeta Tassinari, Asit Chouduri, Jacinta Enzweiler, Roberto Xavier e aos funcionários Dalton Silva e Maria Aparecida Vendemiatto que colaboraram diretamente com este trabalho.

Agradecimentos são devidos ao Instituto de Geociências da Universidade de Campinas pelo curso, pela utilização dos laboratórios e ao CNPq pela concessão da bolsa de doutorado bem como ao Centro de Pesquisas Geocronológicas do IG-USP que me franqueou a preparação das amostras isotópicas e realizou as análises, e à Universidade Federal de Mato Grosso pelo afastamento concedido.

Um agradecimento especial é dado ao Dr. Willian Randall Van Schmus pela extrema boa vontade na correção, críticas, discussões e sugestões que enriqueceram em muito um dos trabalhos que fazem parte desta tese, o que foi feito mesmo sem me conhecer pessoalmente.

Agradeço também aos colegas da UFMT, Márcia Aparecida S. B. Pinho e Francisco Egídio C. Pinho pelas discussões e sugestões ao trabalho.

Agradeço a Jayme Alfredo Dexheymer Leite e Neal J. McNaughton pelas análises Shrimp.

Especiais agradecimentos são dados à Noranda Exploração Mineral Ltda. pelo apoio nos trabalhos de campo.

Agradeço também aos colegas Heitor Neves Maia, Carlos Humberto Calle Tapias, Fernando Buco Tallarico e Hector Barrueto pela amizade e apoio durante os períodos em que estive em Campinas.

## SUMÁRIO

<b>1. INTRODUÇÃO .</b>	<b>1</b>
1-1 . Considerações Preliminares	1
1-2 . Histórico da Descoberta	2
1-3 . Depósitos Vulcanogênicos de Sulfetos Maciços .	10
1-4. Objetivos	13
1-5. Metodologia	14
1-5-1. Mapeamento	14
1-5-2. Análise de Testemunhos de Sondagem	15
1-5-3. Análises Isotópicas .	15
1-5-4. Análises Químicas	16
1-5-5. Conteúdo da Tese .	17
<b>2. THE EXPEDITO MASSIVE SULFIDE DEPOSIT, MATO GROSSO .</b>	<b>18</b>
2-1.Introduction	18
2-2.Local geology	19
2-3.The Valley Deposit	22
2-4.Discussion	26
Acknowledgements	27
References	28
<b>3. 1.76 GA VOLCANO-PLUTONISM IN THE SOUTHWESTERN AMAZONIAN CRATON, ARIPUANÃ-MT, BRASIL: TECTONO-STRATIGRAPHIC IMPLICATIONS FROM SHRIMP U-PB ZIRCON DATA AND ROCK GEOCHEMISTRY</b>	<b>29</b>
3-1. Introduction	30
3-2. Regional geology	30
3-3. Characterization of the volcanic-plutonic association of Aripuanã	32
3-4. Major and Trace Element Chemistry	34
3-5. U-Pb methodology	38
3-6. Geochronology results	39
3-6-1. Sample 01 - Massaranduba dacites	39

3-6-2. Sample 02 - Paraibão granite	42
3-7. Discussion	44
3-8. Tectonic Model	45
3-9. Conclusions	48
Acknowledgements	48
References	49
<b>4. MINERALOGY, ISOTOPIC DATA AND MINERALIZATION STYLES OF THE VOLCANIC - HOSTED MASSIVE SULFIDE ZN - PB EXPEDITO DEPOSIT IN ARIPUANÃ, MATO GROSSO-BRAZIL</b>	<b>52</b>
4-1. Introduction	53
4-2. Background	54
4-3. Regional geology	55
4-4. Geology of the Ore Deposit	56
4-5. Materials and Analytical Techniques	59
4-6. Results	60
Petrologic Studies	60
4-7. Mineral Chemistry	63
4-7-1. Geothermometric and geobarometric estimations	63
4-7-2. Chlorite Geothermometry	64
4-7-3 Arsenopyrite Geothermometry	64
4-7-4. Sphalerite Geobarometry	67
4-8. Isotopic studies	69
4-8-1. Strontium Isotopes	69
4-8-2. Lead Isotopes	71
4-9. Discussion and Conclusions	75
References	77
<b>5. CONSIDERAÇÕES FINAIS</b>	<b>79</b>
5-1. Conclusões	79
5-1-1. Estratigrafia	79

5-1-2. Ambiente Tectônico	80
5-1-3.. Mineralização	81
5-1-4. Alteração Hidrotermal	82
5-1-5. Gênese e Classificação	83
5-2. Critérios Prospectivos	85
5-3. Recomendações	86
Bibliografia	87
 ANEXOS	 90

## **LISTA DE FIGURAS**

### **1. INTRODUÇÃO**

Figura 1	Mapa Logístico e de Localização.	3
Figura 2	Esboço geológico regional.	4
Figura 3	Em primeiro plano, trabalhos de rebaixamento executados pelos garimpeiros até 1992. Em segundo plano, no vale, o aluvião lavrado margeado pelo Gossan Hill.	6
Figura 4	Trincheira de acesso à Cava do Expedito vista no último plano .	7
Figura 5	Vista geral do Gossan Hill. No primeiro plano a drenagem(Grota do Maranhão), mineralizada em ouro a partir da represa, à esquerda .	8
Figura 6	Vista a partir do vale dos trabalhos de rebaixamento executados pelos garimpeiros.	8

### **2. THE EXPEDITO MASSIVE SULFIDE DEPOSIT, MATO GROSSO**

Figura 1	Location map and regional geology of the Aripuanã Region.	19
Figura 2	Simplified Geology of the Area of the Expedito Deposit ( modified from Collins et al. 1998).	21
Figura 3	Winchester and Floyd 1977, discriminant plots for representative volcanic rocks of the Expedito District.	22
Figura 4	Magmatic affinity of volcanic rocks: (A) AFM diagram for basalts and (B) Total Alkali X SiO <sub>2</sub> diagram of basalts and felsic rocks (Fields according Irvine and Baragar 1971).	24
Figura 5	Sketch of relationship of mineralization and alteration zone	25
Figura 6	Pb isotopic reservoir growth curves of the plumbotectonic model (Zartman and Doe 1981) (Version II), applied to the Expedito sulfide deposits.	26

**3. 1.76 GA VOLCANO-PLUTONISM IN THE SOUTH-WESTERN AMAZONIAN CRATON, ARIPUANÁ-MT, BRASIL: TECTONO-STRATIGRAPHIC IMPLICATIONS FROM SHRIMP U-PB ZIRCON DATA AND ROCK GEOCHEMISTRY**

- Figura 1 Simplified geology of the Aripuanã District. The locations of the samples dated in this paper are also shown. 30
- Figura 2 Bivariate plots for acid (squares) and basic (circles) rocks of the Aripuanã District (Table 1). a) Total alkalis (Irvine & Baragar, 1971) and FeOt / MgO versus SiO<sub>2</sub> (Miyashiro, 1974); b) AFM (Irvine & Baragar, 1971) and c) Modified Winchester & Floyd (1977) petrographic discriminant diagram. 34
- Figura 3 Discriminant diagrams for the acidic rocks of the Aripuanã District: a)K<sub>2</sub>O vs. silica diagram showing the subdivisions of Le Maitre et al., (1989) b)Ratios between molar values diagram of Maniar & Piccoli (1989). 35
- Figura 4 Tectonic setting discriminant diagrams for acidic rocks of the Aripuanã District. Boundaries are from: a) Maniar & Piccoli (1989); b) Pearce (1984). 36
- Figura 5 Tectonic setting discriminant diagrams for the basalts of the Aripuanã district. Boundaries are from Pearce and Cann (1973). 36
- Figura 6 Back-scattered electrons image of zircons of the Massaranduba Dacite with spots marked by white circles. (See text for explanation).; - (A)- Euhedral short prismatic crystal showing faint euhedral zoning; (B)- Zircon displaying a similar habit with well defined euhedral zoning and overgrowth by magmatic crystallization; (C ) - Zircons with overgrowth features; (D)- Crystal showing corrosion features in borders and embayments. 39
- Figura 7 U-Pb concordia diagram of the Massaranduba dacite zircons. 40

Figura 8	Back scattered electrons image of zircons of the Paraibão Granite (A) Euhedral short prismatic crystal showing faint euhedral zoning; and (B) Crystal showing sector zoning and corrosion features in borders and embayments.	43
Figura 9	U-Pb concordia diagram of zircons of the Paraibão Granite.	44
Figura 10	Series of block diagrams showing the sequence of tectonic episodes in the Aripuanã Region. (1) Initial configuration. (2). Mantle underplating of mafic magma and upwelling of hot asthenosphere. (3) Extensive plutonism and volcanism with predominance of massive acid flows. (4) Caldera subsidence originating a large basin-shaped volcanic depression. (5) Caldera initially filling with huge amounts of pyroclastic, followed by chemical sedimentation and by detritic material in the vanishing stages of the volcanism. (6) Rifting stage and block faulting by crustal extension in response to dextral transtension. (7) Isostatic adjustments.	47

**4. MINERALOGY, ISOTOPIC DATA AND MINERALIZATION STYLES OF THE VOLCANIC - HOSTED MASSIVE SULFIDE ZN - PB EXPEDITO DEPOSIT IN ARIPUANÃ, MATO GROSSO-BRAZIL**

Figura 1	Geologic map of the Aripuanã Area showing the location of the metallogenic district (rectangle) and of the investigated deposit.	54
Figura 2	Geologic map of the Serra do Expedito area after Collins and Monteiro (1998).	57
Figura 3	Vertical cross-section showing the relationship between mineralization and hydrothermal alteration zones. For localization see Geologic map (Fig. 2).	58
Figure 4	Fig 4. Microphotographs of representatives examples of ores. A. Sphalerite in massive sulfide ore with inclusions of galena and very fine chalcopyrite disseminated and euhedral pyrite. B.	61

Galena intruding cavities in sphalerite groundmass. C. Pyrrhotite substituting sphalerite. D. Sphalerite and calchopyrite filling fractures in pyritic ore. D.Euhedral and anhedral pyrites with sphalerite and galena displaying characteristic pits. E. Magnetite replacing sphalerite. F. Fractured arsenopyrite injected by arsenopyrite in pyrrhotite sphalerite groundmass. G.Fractured arsenopyrite with inclusion of sphalerite in chloritic groundmass. I..Aggregates of acicular actinolite in chloritic groundmass. J. Crustiform vein with quartz, calcite and sphalerite in tuff.

Figura 5	Fig. 5. Plots of the Expedito deposit chlorite compositions in the cationic diagram of Hey, (1964)	67
Figura 6	As content (%) in arsenopyrite from the Expedito Deposit. Temperatures after Sundblad et al. (1984)	67
Figura 7	Fig. 7- FeS content (Mole%) in sphalerite from the Expedito Deposit. Pressures after Shimizu & Shimazaki, 1981.	69
Figura 8	$^{87}\text{Sr}/^{86}\text{Sr}$ intermediate composition of calcites in relation to disseminated sulfides and one sphalerite lixiviate. One isochron referring to an event of 1,1 Ga in age is shown.	71
Figura 9	Fig. 9. Galena and K-feldspar lead isotopic data with reference to the average crustal growth curve of Stacey and Kramers (1975)	73
Figura 10	Fig. 10. Galena lead isotopic data with reference to the reservoir growth curves of Zartman and Doe (1981).	75

## **LISTA DE TABELAS**

### **1. INTRODUÇÃO**

Tabela 1	Relação de amostras e metodologias isotópicas utilizadas.	16
----------	---	----

### **2. THE EXPEDITO MASSIVE SULFIDE DEPOSIT, MATO GROSSO**

Tabela 1	Average chemical composition of least altered rocks. (n) = number of samples.	20
----------	---	----

Tabela 2	Correlation matrix of ore samples (288 Samples).	23
----------	--	----

Tabela 3	Isotopic composition of galena crystals.	24
----------	--	----

### **3. 1.76 GA VOLCANO-PLUTONISM IN THE SOUTH-WESTERN AMAZONIAN CRATON, ARIPUANÃ-MT, BRASIL: TECTONO-STRATIGRAPHIC IMPLICATIONS FROM SHRIMP U-PB ZIRCON DATA AND ROCK GEOCHEMISTRY**

Tabela 1	Representative Analyses of Plutonic and Volcanic Rocks from the Aripuanã District.	37
----------	--	----

Tabela 2	Shrimp data of Sample 1 zircons - Massaranduba Dacite	39
----------	---	----

Tabela 3	SHRIMP data of the zircons of the Sample 2 _ Paraibão Granite	42
----------	---	----

### **4. MINERALOGY, ISOTOPIC DATA AND MINERALIZATION STYLES OF THE VOLCANIC - HOSTED MASSIVE SULFIDE ZN - PB EXPEDITO DEPOSIT IN ARIPUANÃ, MATO GROSSO-BRAZIL**

Tabela I	Chemical composition of chlorite (n=25) from hydrothermal alteration zone in the Valley Deposit chlorites.	65
----------	--	----

Tabela II	Electron microprobe results of calcic amphiboles of the Valley Deposit.	66
-----------	---	----

Tabela III	Compilation of electron microprobe results of 26 analyses of arsenopyrite of the Valley Deposit.	66
------------	--	----

Tabela IV	Compilation of electron microprobe results from sphalerites of the Valley Deposit (n=36). Pressures in Kb were calculated using the equation $P = 42.30 - 32.10 \times \log M_{FeS}$ (Shimizu & Shimazaki, 1981).	69
Tabela V	Rb and Sr isotopic data of sulfides and carbonate minerals.	72
Tabela VI	Pb-Pb isotopic data of galenas, K-feldspar and Paraibão granite.	74



UNIVERSIDADE ESTADUAL DE CAMPINAS/  
INSTITUTO DE GEOCIÊNCIAS/DEPTO DE  
METALOGÊNESE E GEOQUÍMICA

Pós-Graduação em Geociências - Área de Metalogênese

**UNICAMP**

**Depósitos de sulfeto maciço associados a rochas vulcânicas:  
O caso do depósito Zn-Pb do Expedito, Aripuanã, MT, Brasil.**

**RESUMO**

**TESE DE DOUTORADO**

**Renato Dantas Neder**

Os depósitos de sulfeto maciço de filiação vulcânica constituem importantes fontes de chumbo, zinco, cobre e metais preciosos em vários países do mundo. Este estudo é uma contribuição para um melhor entendimento da origem dos depósitos de sulfeto maciço a Zn-Pb da Serra do Expedito, município de Aripuanã, Mato Grosso, Brasil. Esses depósitos localizam-se na porção SW do Cráton Amazônico e são associados às rochas vulcânicas e plutônicas felsicas, de idade Paleoproterozóica, relacionadas ao Magmatismo Teles Pires. Os trabalhos compreenderam mapeamento geológico, descrição de testemunhos de sondagens, estudos litogegeoquímicos e geocronológicos, análises petrográficas e de microssonda eletrônica de minerais de minério, encaixantes e zonas de alteração hidrotermal, bem como, aplicações de geoquímica isotópica de Sr e Pb no estudo da gênese do depósito do Expedito. Os estudos litogegeoquímicos indicaram o enquadramento das rochas ácidas no tipo A, origem anorogênica ou pós-orogênica, possivelmente resultante de ativação mantélica durante um evento extensional de grande duração, em ambiente ensílico. Foram obtidas idades Shrimp U-Pb em zircões de  $1762 \pm 6$  Ma para as rochas extrusivas e de  $1755 \pm 5$  Ma para as rochas plutônicas. As rochas vulcânicas encaixantes do depósito incluem tufo de cristal e lapilli que são interpretados como registros distais subaquáticos de um centro vulcânico de localização desconhecida. Evidências de campo sugerem que os corpos de minério conformam um cinturão mineralizado ao longo de um sistema de falhas que canalizaram os fluidos hidrotermais e a deposição dos sulfetos. Esses corpos apresentam uma paragênese metálica constituída de pirita, pirrotita, esfalerita, galena, calcopirita e arsenopirita subordinada. Por outro lado, apresentam uma alteração hidrotermal atípica com abundante clorita localmente associada a actinolita e magnetita. Estudos de química mineral indicaram um evento principal de formação do depósito no intervalo 300-350°C em condições de pressões parciais de O<sub>2</sub> e S<sub>2</sub> elevadas. Porções do minério foram submetidas a aquecimento e interação de fluido que deram origem à formação da assembléia de alteração cálcio-silicática e magnetita. Foram obtidas idades modelo de chumbo em galena em torno de 1.75 Ga que indicam contemporaneidade entre o evento vulcânico-plutônico e a deposição do sulfeto maciço. A ocorrência de um episódio pós-mineralização a 1.1 Ga foi demonstrado pela composição isotópica de chumbo de K-feldspato e uma isócrona Rb-Sr em lixiados de esfalerita. As composições isotópicas de estrôncio de carbonato são claramente indicativas de sua origem hidrotermal e confirmam, em combinação com as elevadas razões isotópicas de chumbo em galena, a origem dos fluidos hidrotermais em reservatórios da Crosta Superior. Esses dados em conjunto conduzem à conclusão de que a deposição das rochas encaixantes ocorreu em ambiente sub-aquático e o depósito de sulfeto maciço se formou em níveis crustais epizonais, ao longo de zonas de falhas sin-vulcânicas que funcionaram como canais para os fluidos mineralizantes de origem plutônica e supra-crustal. Esses processos são coerentes com o enquadramento do depósito do Expedito no modelo VHMS – *Volcanic Hosted Massive Sulfide*.



**UNICAMP**

**UNIVERSIDADE ESTADUAL DE CAMPINAS/  
INSTITUTO DE GEOCIÊNCIAS/DEPTO DE  
METALOGÊNESE E GEOQUÍMICA**

**Pós-Graduação em Geociências - Área de Metalogênese**

**Volcanic-associated massive sulfide deposits: a case study on the  
Expedito Zn-Pb deposit, Aripuanã, State of Mato Grosso, Brazil.**

**ABSTRACT**

**Ph.D. Thesis**

**Renato Dantas Neder**

Volcanic-associated massive sulfide deposits represent important sources of lead, zinc, copper and precious metals worldwide. The present study is a contribution to a better understanding of the origin of the Zn-Pb sulfide deposits of the Serra do Expedito, State of Mato Grosso, Brazil. These deposits are located in the SW portion of the Amazonian Craton, associated with Paleoproterozoic felsic volcanic and plutonic rocks, correlated to Magmatismo Teles Pires. Studies undertaken included geological mapping, drill-core examination, lithogeochemical and geochronological studies, petrographic and electron-microprobe analyses of minerals in the ore, wall-rocks and hydrothermal alteration zones, as well as applications of Sr and Pb isotope geochemistry to ore-deposit modeling. Geochemical data place the acid rocks in A-type, indicating an anorogenic or post-orogenic origin, possibly due to mantle activation during a long lasting extensional event, in an ensialic environment. SHRIMP U-Pb zircon ages at  $1762 \pm 6$  Ma and  $1755 \pm 5$  Ma were obtained for volcanic and plutonic rocks, respectively. The predominant volcanic host rocks include crystal and lapilli tuffs that are interpreted as a sub-aqueous record of a distal volcanic center of unknown localization. Field evidence suggests that the orebodies form one single belt, representing the actual trace of a system of synvolcanic fault that channeled the hydrothermal fluids and sulfide deposition. The orebodies present normal sulfide mineralogy for volcanogenic deposits with pyrite, pyrrhotite, sphalerite, galena, chalcopyrite and with locally accessory arsenopyrite. On the other hand, the alteration is atypical since it presents chloritic zones locally associated with actinolite and magnetite. Mineral chemical studies indicate that the main mineralization event occurred in the interval 300-350°C at elevated O<sub>2</sub> e S<sub>2</sub> partial pressures whereas some portions of ore bodies underwent heating and fluid interaction that yielded the calc-silicate and magnetite assemblage overprint. A Pb-Pb model age in galena was obtained at 1.75 Ga which indicates that the deposit was formed during the last stages of a magmatic-tectonic-hydrothermal event that occurred in the interval 1,76-1,75 Ga. The lead isotopic data for K-feldspar and a Rb-Sr isochron for sphalerite leachates indicate a later post-depositional event at 1,1 Ga. The Sr-isotope compositions of carbonate are clearly suggestive of its hydrothermal origin and, in conjunction with elevated lead-isotope ratios in galena, point to hydrothermal sources located in the Upper Crust. These results lead to consider a sub-aqueous deposition of wall-rocks, sulfide deposition in epizonal crustal levels, along synvolcanic fault zones that channeled mineralizing fluids of plutonic and supracrustal origin. These processes are consistent with the VHMS – Volcanic Hosted Massive Sulfide model presently attributed to the Expedito Zn-Pb deposit.

## CAPÍTULO 1 - INTRODUÇÃO

### 1-1. CONSIDERAÇÕES PRELIMINARES

A descoberta em 1996 do depósito de sulfeto maciço de Pb-Zn da Serra do Expedito, onde antes havia operado o garimpo de ouro de Aripuanã (NW do Mato Grosso), representou um acontecimento muito importante para o futuro da exploração mineral e pesquisas metalogenéticas de uma extensa região da Amazônia onde afloram as vulcânicas félscicas do Grupo Uatumã.

A presente tese reúne, de forma inédita, os resultados obtidos nos primeiros estudos das mineralizações metálicas da Serra do Expedito, em particular, do maior corpo de minério até o momento descoberto, o depósito Valley.

A área estudada, incluindo a Serra do Expedito, situa-se no município de Aripuanã na região noroeste do Estado de Mato Grosso, a aproximadamente 700 km em linha reta de Cuiabá. O acesso se faz por rodovia pavimentada a partir de Cuiabá até Campo Novo do Parecis passando por Tangará da Serra, num percurso de 300 Km. A partir daí até Aripuanã, o percurso é realizado por estradas não pavimentadas em uma extensão de 700 Km, passando pelas cidades de Juína, Castanheira e Juruena, perfazendo um total de 1000 Km (Figura 1). De Aripuanã, o acesso à Serra do Expedito é feito por estradas vicinais num percurso de 20 Km.

A cidade de Aripuanã é sede de um município com aproximadamente 18.000 habitantes, cuja área é de 8.000 Km<sup>2</sup>, com aproximadamente 1/3 dessa área ocupada por reservas indígenas, constituindo pólo de uma região que engloba todo o limite noroeste do povoamento do Estado de Mato Grosso, não tendo nenhum acesso rodoviário aos estados vizinhos de Rondônia e Amazonas.

Até meados da década de 70, as únicas atividades econômicas existentes em toda a região eram as extrativistas de borracha e castanha do Pará, sendo os produtos escoados para Manaus, por via fluvial pelos rios Aripuanã, Roosevelt e Amazonas. No final dessa década, trabalhos de colonização em toda a Amazônia, fomentados pelo regime militar vigente, promoveram de forma indireta a incorporação econômica da região ao estado de Mato Grosso. A partir daí, a região teve grande desenvolvimento em função de intensa

atividade extrativista madeireira, que persistiu até o final da década passada. O esgotamento das reservas madeireiras, cujo ‘front’ extrativo está atualmente no Estado do Amazonas, 200 Km a norte da cidade de Aripuanã, aliado ao isolamento rodoviário, fez com que a economia da região ficasse bastante prejudicada.

O conhecimento geológico disponível está baseado nos resultados obtidos pelo Projeto RADAMBRASIL (Silva et al., 1980), compreendendo mapeamento geológico regional na escala 1:1.000.000 (Figura 2), baseado na interpretação de imagens de radar de visada lateral e em dados geocronológicos Rb/Sr e K/Ar. Trabalhos posteriores tiveram um foco notadamente geocronológico e compilações dos dados disponíveis são apresentadas por Tassinari (1996), Tassinari & Macambira (1999) e Tassinari et al. (2000).

Os depósitos estão localizados na porção SW do Craton Amazônico na região limítrofe entre as Províncias Geocronológicas Rio Negro-Juruena e Ventuari Tapajós (Tassinari et al., 1996). Outras compartimentações utilizadas na região incluem estas mineralizações no denominado Bloco Juruena (Costa e Hasui, 1997) ou, no mais recentemente proposto, Cinturão Juruena-Rondônia (Santos et al., 2000).

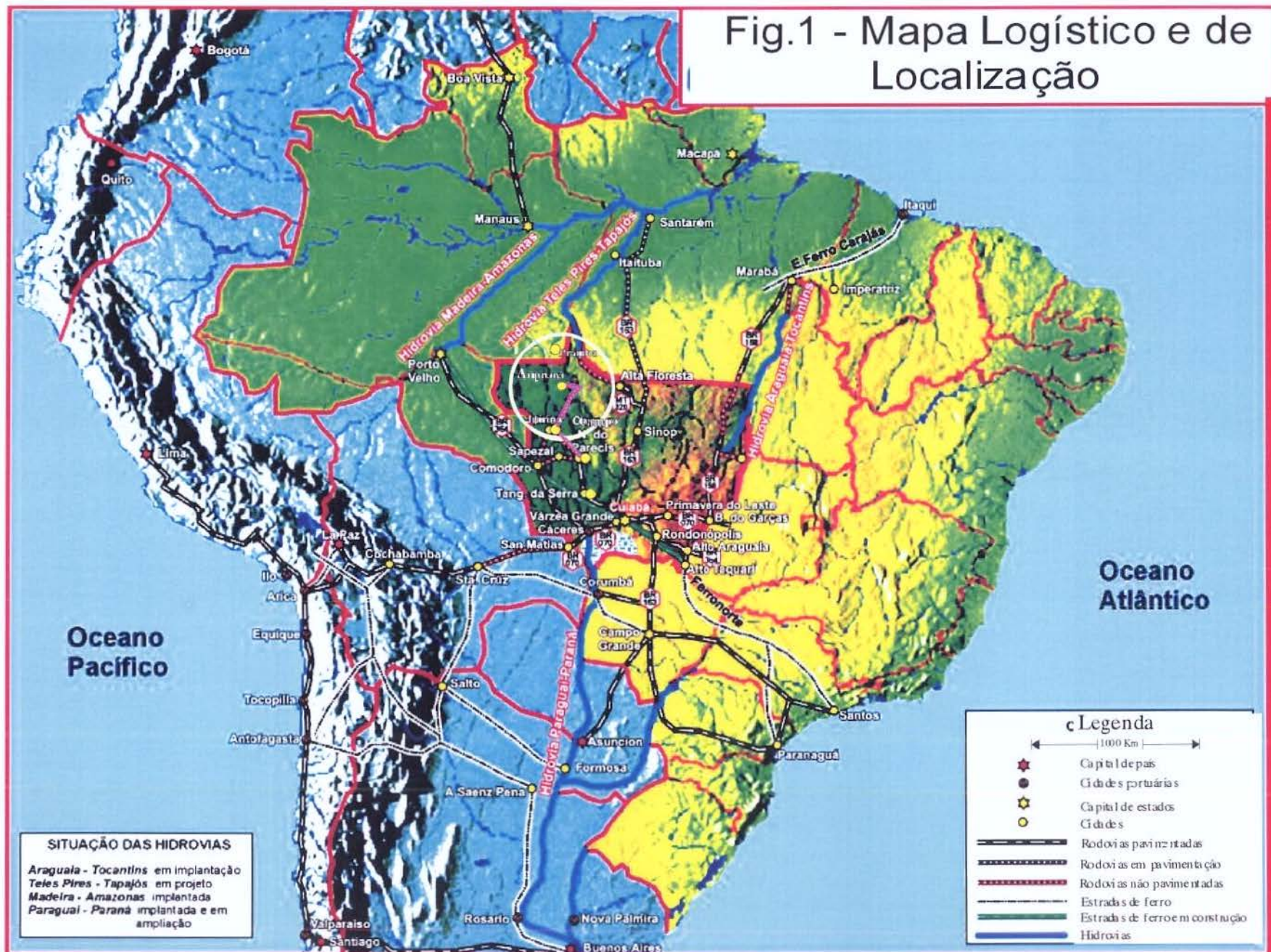
Os trabalhos geológicos, a partir da descoberta dos depósitos da Serra do Expedito em 1996, propiciaram investimentos da ordem de US\$ 15.000.000,00 pelas empresas de mineração envolvidas (Noranda, Anglo American e Ambrex). Embora a maior parte destes recursos tenha sido dirigida ao pagamento de serviços especializados de empresas estrangeiras e de outras regiões do país, a geração de empregos em nível de pessoal sem especialização tem sido uma importante fonte de recursos para a região.

A importância econômica do ambiente geológico foi salientada, portanto, na última década, depois da descoberta dos depósitos de sulfetos maciços e disseminados, que definiu um importante distrito metalogenético com características únicas em todo o Craton Amazônico.

## **1-2 . HISTÓRICO DA DESCOBERTA**

A descoberta de ouro no município de Aripuanã se deu no final dos anos 70, quando toda a região Amazônica brasileira foi alvo de intensa atividade garimpeira, como reflexo dos altos preços alcançados pelo metal, decorrentes das instabilidades econômicas em nível mundial.

Fig.1 - Mapa Logístico e de Localização



Uma drenagem secundária, denominada Grotão do Maranhão, se constituiu na mais importante zona de concentração aluvionar de ouro encontrada na região de Aripuanã e para ela afluiu significativa parcela da população garimpeira de outras regiões, particularmente da região de Peixoto de Azevedo-MT. Dessa atividade, resultou a extração de, aproximadamente, 5 toneladas de ouro, com o emprego de mão de obra de cinco mil garimpeiros.

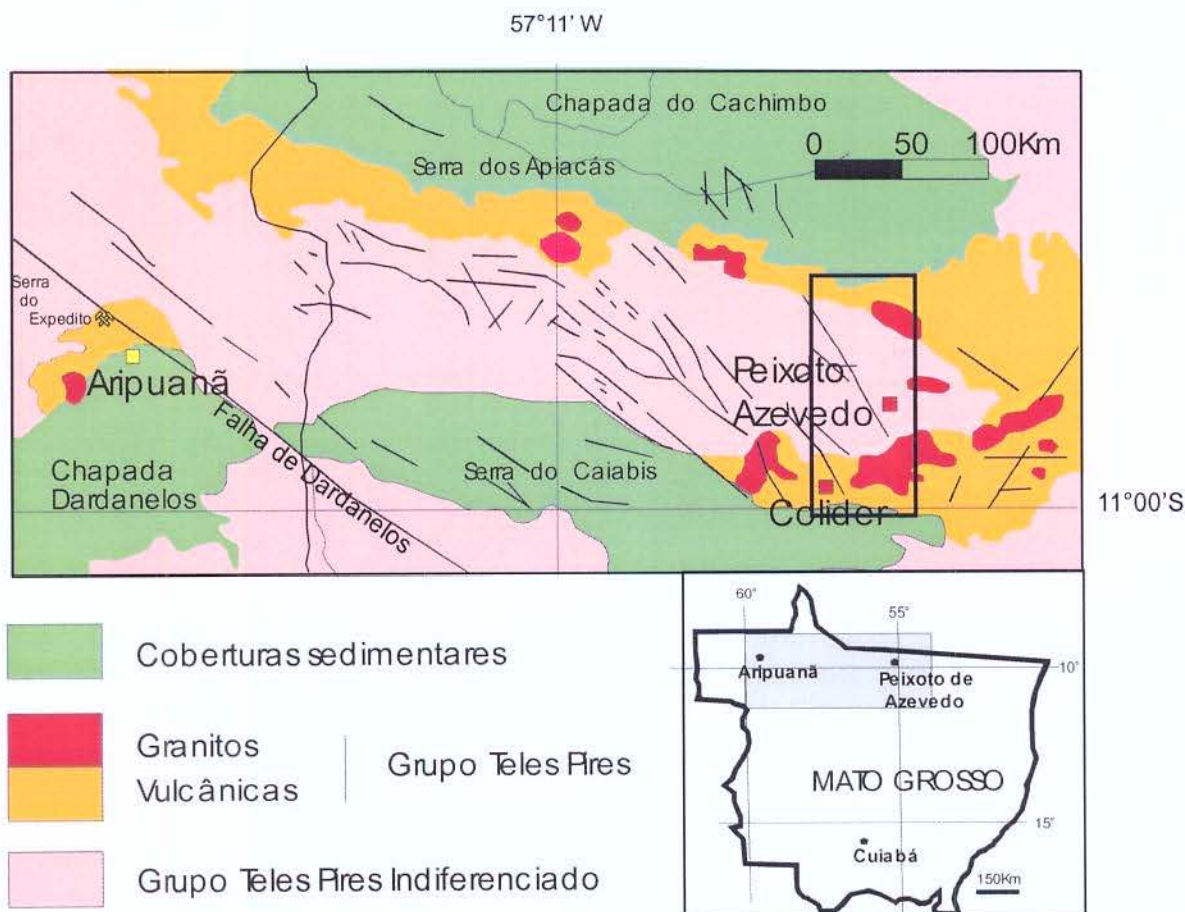


Figura 2. Esboço geológico regional.

A descoberta da fonte primária do ouro por um grupo de garimpeiros, liderados por Expedito José Rodrigues, nas encostas que margeiam o aluvião na Serra do Expedito, se deu em decorrência do esgotamento das reservas aluvionares. Tratava-se, esta descoberta, que foi denominada Buraco do Expedito, de uma zona hidrotermalizada à clorita e biotita

enriquecida em ouro, com teores de até 80 ppm, onde era comum a ocorrência de ouro visível.

O desenvolvimento da lavra da mineralização aurífera foi realizado com dificuldade pelos garimpeiros, dado que, além de não possuírem prática em trabalhos subterrâneos de desmonte com a utilização de explosivos, os serviços eram prejudicados pelas precárias condições de acesso e pela localização em escarpa íngreme. Além disto, a recuperação do ouro por processos rudimentares era dificultada pela granulometria muito fina, pelas associações paragenéticas do ouro com sulfetos e pelo alto teor de Cu e Ag na liga aurífera que se apresentava, depois de refinada, com uma cor esverdeada peculiar. Esta dificuldade foi contornada pelo tratamento do rejeito, em diversas repassagens pelo processo, com intervalos de meses, período em que provavelmente a oxidação dos sulfetos liberava mais ouro. Era uma característica intrigante para os garimpeiros, acostumados com o ouro aluvionar, o fato de que o minério pudesse ser repassado até 9 vezes com teores às vezes crescentes, até alcançar um limite em que a recuperação era sub-econômica.

Em meados da década de 80, já em um período de arrefecimento da atividade garimpeira, surgiram em todo o Estado pequenas empresas de capital privado internacional (Junior Companies), buscando oportunidades de exploração de ouro.

Após diversos tentativas de se descobrir, a partir dos trabalhos de lavra garimpeira, reservas exploráveis por processos de extração em regime empresarial de mineração organizada na região de Peixoto de Azevedo e Pontes e Lacerda, foi iniciada, em 1996, a avaliação por sondagem, rotativa a diamante, da fonte primária da Serra do Expedito pela companhia canadense Ambrex Mining Company, em uma área de pesquisa de 2.000 hectares.

De imediato, no primeiro furo de sonda, localizado ao lado do Buraco do Expedito, orientado para alcançar a mineralização aurífera por baixo da área explotada, foi interceptado um nível sulfetado com esfalerita e galena, insuspeitado até aquele momento, em termos de modelo prospectivo. A mineralização aurífera, alvo preliminar da campanha exploratória, demonstrou-se restrita e sub-econômica e foi relacionada a fenômenos epigenéticos de mobilização do ouro dos sulfetos maciços e enriquecimento em zonas de falhas.



Figura 3. Em primeiro plano, trabalhos de rebaixamento executados pelos garimpeiros até 1992. Em segundo plano, no vale, o aluvião lavrado margeado pelo Gossan Hill.

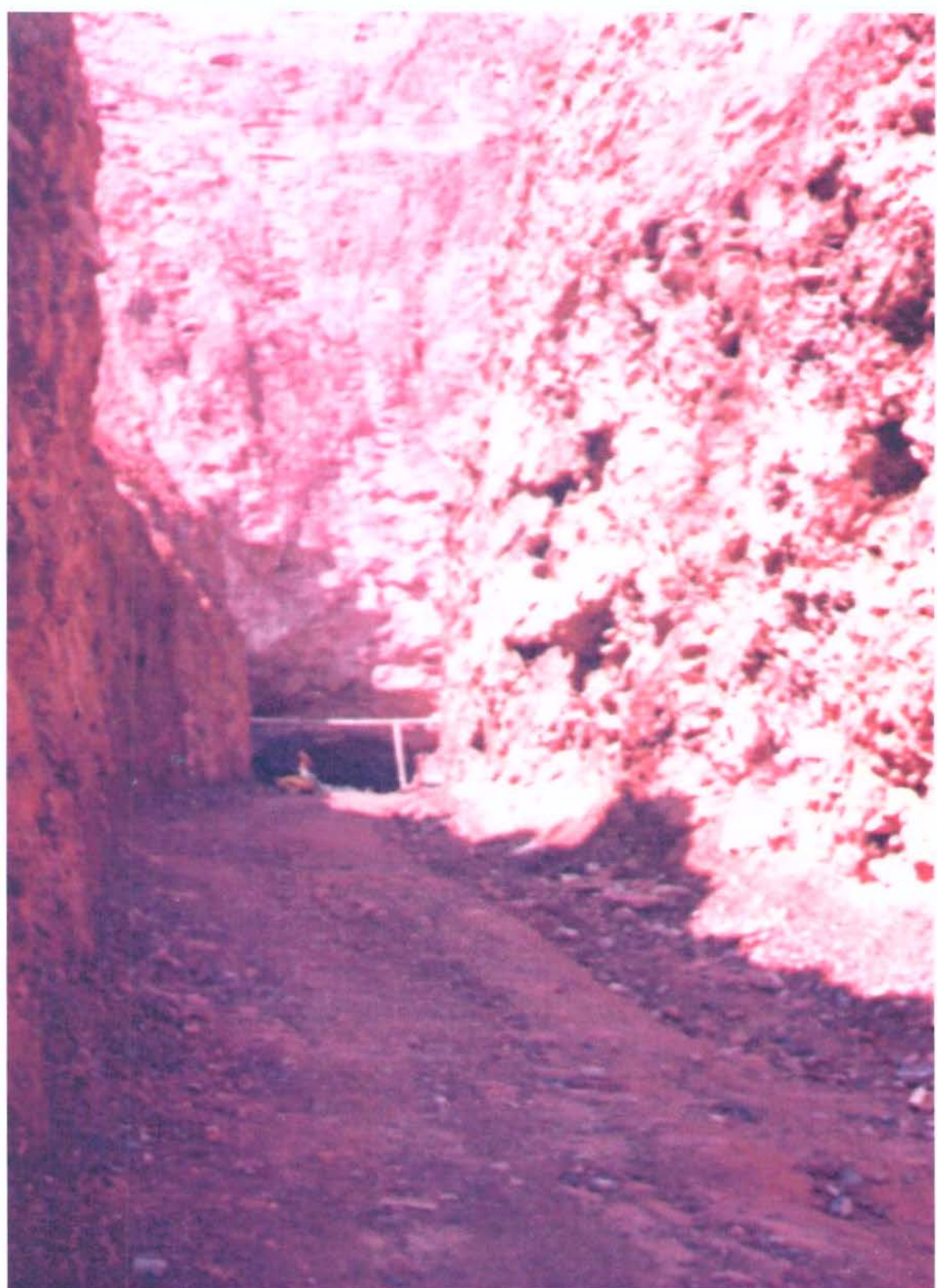


Figura 4. Trincheira de acesso à Cava do Expedito vista no último plano .



Figura 5. Vista geral do Gossan Hill. No primeiro plano a drenagem(Grota do Maranhão), mineralizada em ouro a partir da represa, à esquerda .



Figura 6. Vista a partir do vale dos trabalhos de rebaixamento executados pelos garimpeiros.

A possibilidade de se tratar de um depósito VMS (Volcanogenic Massive Sulfide) fez com que a Ambrex se associasse com a Noranda Mining and Exploration Inc., empresa líder mundial em experiência nesse tipo de depósito.

No período Junho/1997-Março/1998 foram realizados trabalhos de campo, incluindo abertura de malha topográfica, mapeamento geológico, amostragem geoquímica de solo e rochas, geofísica terrestre (EM e magnetometria), além da execução de 9.051 metros de sondagem com “down hole pulse-EM” em furos selecionados.

Os valores preliminares de cubagem obtidos ficaram aquém do necessário para os interesses da Noranda, que, em estudo preliminar de viabilidade econômica, fez projeções de necessidades mínimas de 20 Mt de minério, em função das dificuldades de infra-estrutura regional.

A seguir, numa tentativa de dar continuidade aos trabalhos, a Ambrex executou mais seis novos furos e re-analisou alguns já executados. Estes serviços, incluindo o furo DDH – 19, identificaram uma potente mineralização aurífera que não havia sido verificada, em função de não terem sido analisados os testemunhos das partes superiores da zona de oxidação nas etapas anteriores.

Posteriormente, em 2000, ocorreu uma associação da Ambrex com a Anglo American, detentora de diversos alvarás de pesquisas limítrofes, possibilitando a integralização de uma área de exploração de aproximadamente 20.000 hectares.

As diversas mineralizações no âmbito da Serra do Expedito, anteriormente definidas pela Anglo American e englobadas nesse acordo, incluem as continuações a Este e a Oeste dos depósitos descobertos pela Ambrex e Noranda, denominados Valley, Maçaranduba e Babaçu, possivelmente englobando toda a área de extensão da mineralização.

Os trabalhos, no momento em execução pelas empresas associadas, incluindo geoquímica, geofísica aérea e terrestre e intensa campanha de sondagem, têm alcançado resultados promissores em termos de descobertas de diversos novos alvos e corpos mineralizados e as informações disponíveis permitem supor que, independentemente de novas descobertas, os depósitos da região da Serra do Expedito, englobando as áreas de pesquisa da Ambrex e Anglo American, alcançam volumes superiores aos 20 Mt requeridos pela Noranda.

O quadro atual favorece a perspectiva de rápido aproveitamento das jazidas, independentemente dos problemas de infra-estrutura regionais e das instabilidades econômicas em escala mundial.

É relevante relatar que embora este projeto de doutorado tenha se iniciado no ano de 1997, o autor tem acompanhado a história desta descoberta desde março de 1990, quando foi desenvolvida as atividades de lavra no Buraco do Expedito. A seguir, depois da paralisação das atividades garimpeiras, o autor realizou o acompanhamento das atividades das diversas empresas interessadas na avaliação preliminar da área que visavam a aquisição da propriedade mineral, incluindo a Anglo American, WMC e TVX.

Depois negociações com a Ambrex foi possível acompanhar todos os passos da pesquisa realizada pela Ambrex e Noranda, incluindo as campanhas de sondagem e descrição dos testemunhos.

### 1-3. DEPÓSITOS VULCANOGÊNICOS DE SULFETOS MACIÇOS

Classificações genéticas e listagens de critérios diagnósticos de depósitos de sulfetos maciços vulcanogênicos são disponíveis em diversos trabalhos, incluindo Solomon (1976), Franklin et al. (1981), Lydon (1984) e Large (1992).

Lydon (1984) considera que depósitos de sulfetos maciços vulcanogênicos (VMS) pertencem a uma grande classe de depósitos de sulfetos maciços concordantes que inclui todos os depósitos de sulfetos maciços e semi-maciços formados pela descarga de soluções hidrotermais no assoalho oceânico. Propõe a subdivisão desta classe em dois grupos principais que incluem os depósitos de sulfetos maciços: (1) - Sedimentar-exalativos (sedimentary-exhalative, sediment-hosted or shale hosted) e (2) - Vulcanogênicos (volcanogenic), associados a vulcânicas (volcanic-associated), ou encaixado em vulcânicas (volcanic-hosted or volcanophile). Conclui que depósitos maciços vulcanogênicos são acumulações de sulfetos contemporâneas ao vulcanismo (sinvulcânicas) que ocorrem em domínios geológicos caracterizados por rochas vulcânicas submarinas.

A partir deste modelo, as caracterizações de depósitos como Volcanogenic Massive Sulfide ou Volcanic Associated Massive Sulfide ou Volcanic Hosted Massive Sulfide têm dominado a discussão sobre a origem de um grande número de depósitos em todo o mundo. Muitas controvérsias são geradas pelas imposições de que os depósitos apresentem

características concordantes (com as rochas encaixantes) e singenéticas (mesma filiação genética e contemporaneidade com as rochas encaixantes) e ainda a restrição ao uso do termo “Volcanogenic” para as acumulações de sulfetos como parte integral do processo vulcânico, induzindo à interpretação de que os sulfetos propriamente ditos sejam produtos do vulcanismo.

Contudo, os aspectos mais importantes a serem levados em conta na caracterização dos depósitos parecem ser os relacionamentos espacial e temporal entre a encaixante e minério, estas, as questões principais a serem considerados na classificação de depósitos vulcanogênicos. A gênese em si pode englobar os processos vulcânicos, os exalativos (deposição no assoalho oceânico) ou os de substituição (abaixo do assoalho oceânico). Estes aspectos são discutidos a seguir:

1) – O problema espacial relativo ao sítio da deposição do minério:

A descoberta de depósitos do tipo ‘mound-chimney’, formados em assoalhos oceânicos atuais, não só demonstrou o modelo hidrotermal exalativo como deu um novo impulso para o entendimento dos processos de formação de depósitos vulcanogênicos. O modelo morfológico clássico, em forma de monte ou cogumelo (‘mound style’), fortemente baseado nas observações dos depósitos recentes (atuais), tem salientado a parte concordante correspondente à acumulação de sulfetos em assoalho oceânico, por ser a parte dos depósitos passível de observação direta, relevando a um segundo plano a parte discordante, considerada como a zona de canais e venulações alimentadoras que funcionaram como dutos para as soluções hidrotermais mineralizadoras (zona de stringers ou stockwork), que sem dúvida são partes integrantes destas mineralizações, porém de acesso difícil por sondagem em condições submarinas sob espessa lámina de água.

2- O problema temporal, ou seja, se o minério foi depositado simultaneamente (singenético) ou posteriormente à deposição das encaixantes (epigenético):

Há o reconhecimento, na atualidade, de grandes acumulações de sulfetos em ambientes de sub-superfície de assoalho oceânico, claramente relacionadas à falhas sin vulcânicas, e associadas temporalmente e espacialmente com depósitos VMS típicos. Essas descobertas provocaram o aumento da abrangência desta classificação para englobar depósitos totalmente discordantes incluindo Ansil –Noranda (Galley et al., 1995, Galley et al., 2000), Les Mines Selbaie no Quebec – Canadá (Larson e Hutchinson, 1993), Atlantis II

no Mar Vermelho (Zierenberg e Shanks, 1983), Middle Valley na cordilheira oceânica, Juan de Fuca (Goodfellow e Blaise, 1988), Mount Morgan e Highway-Reward em Queensland - Austrália (Doyle e Huston , 1999).

Verifica-se em todos esses trabalhos que o conceito singenético assume uma conotação menos restrita e passa a ser atribuído à contemporaneidade e relação com o processo vulcânico. Em outras palavras, se o depósito mineral, mesmo discordante, foi formado contemporaneamente com, e essencialmente pelo mesmo processo que as rochas vulcânicas encaixantes, então ele pode ser considerado singenético.

A partir da década de 60 tornou-se consensual a utilização do modelo exalativo para explicar a formação de sulfetos (VMS) precipitados a partir de fluidos hidrotermais. Esses depósitos apresentam normalmente uma parte concordante em forma de lente, manto ou monte (lens, blanket or mound) de sulfetos maciços sobreposta à uma zona discordante de stringers e stockworks.

Recentemente, a partir do final da década de 80, diversos depósitos considerados como VMS têm sido interpretados como formados a partir de processos de substituição estruturalmente controlada, ao longo de falhas sin vulcânicas contíguas a corpos plutônicos. (Arnold e Sillitoe, 1989; Beams et al., 1989; Galley et al., 1995)

Da mesma forma, lentes de sulfeto maciço no Middle Valley, na crista oceânica Juan de Fuca e na fossa Escanaba, apresentam boas evidências de substituição em porções abaixo do assoalho oceânico de material pobramente consolidado (Goodfellow e Blaise, 1988; Franklin, 1990).

Esse mecanismo é considerado por Bodon e Valenta (1995) para o deposito Siluriano Zn-Pb-Cu de Currawong, no sudeste da Austrália, por explicar convenientemente descontinuidades laterais e a ciclicidade na zonação de metais. Sugerem esses autores que parte da mineralização daquele depósito foi produzida pela entrada de fluidos hidrotermais em rochas epiclásticas, brechas vulcânicas, hialoclastitos e turbiditos inconsolidados devido à alta porosidade e permeabilidade primária dessas rochas, o que ocorreu simultaneamente a manifestações de vulcanismo e sedimentação no assoalho oceânico.

Galley et al. (2000) salienta que a consideração dos depósitos formados em ambientes abaixo do assoalho oceânico é importante para o estudo dos depósitos vulcanogênico modernos. Demonstra que, embora os processos de formação sejam

análogos aos dos depósitos antigos, o tamanho médio dos depósitos recentes é significativamente menor. Considera a possibilidade deste fato ser resultante da desconsideração de acumulações na parte subterrânea em substratos altamente permeáveis, considerando que o que se observa nos depósitos recentes seria somente a 'ponta do iceberg', e a parte discordante incluiria a maior parte da mineralização.

Um fator importante, que deve ser considerado, é que a profundidade da lâmina de água é o principal fator que controla a ebulação (boiling) de fluidos hidrotermais antes de sua descarga no assoalho oceânico. Tem sido sugerido em diversos trabalhos (Haas, 1971, Finlow-Bates e Large, 1978) que em ambientes rasos a ebulação origina brechação e precipitação de sulfetos em sub-superfície e que são necessárias espessuras de lâmina de água superiores a 1.000-1.500 m (Henley e Thornley, 1979) para impedir a ebulação e portanto concentrar a deposição dos metais sob o assoalho oceânico.

Assim sendo, é importante na caracterização dos depósitos vulcanogênicos que o aspecto singenético deva ser considerado em relação ao processo vulcânico, salientando que o caráter discordante não impede a origem singenética de depósitos.

Nesse sentido, objetivando alcançar maior consenso na classificação destes depósitos vulcanogênicos, observa-se como uma tendência na literatura mais específica, a utilização da terminologia Volcanic-Hosted Massive Deposit (VHMS) para todos os depósitos singenéticos hospedados em seqüências vulcânicas submarinas, independente da consideração de serem formados por descargas hidrotermais em assoalho oceânico, substituição de encaixante ou preenchimento de falhas em subsuperfície.

#### **1-4. OBJETIVOS**

Com a realização desta pesquisa pretendeu-se contribuir para o entendimento geológico do distrito metalogenético Pb-Zn de Aripuanã lançando mão de estudos de campo e laboratório, com ênfase na obtenção de dados químicos e isotópicos que permitissem entender os mecanismos geradores da mineralização e a evolução temporal do depósito de Pb-Zn do Expedito.

O projeto foi orientado para que fossem alcançados os objetivos específicos a seguir:

- 1- Sugerir um modelo genético para a mineralização de Pb-Zn da Serra do Expedito, a partir de estudos geológicos, mineralógicos e geoquímicos, isotópicos e geocronológicos;
- 2- Definir critérios que possam ser usados como subsídio para a elaboração de modelos exploratórios para depósitos de ouro e de sulfeto maciço na região norte mato-grossense.

## **1-5. METODOLOGIA**

A seguir são apresentados os métodos utilizados no desenvolvimento dos trabalhos de pesquisa. O tratamento sucinto dos métodos e técnicas empregadas se deve à existência de apresentações mais detalhadas nos trabalhos publicados ou em preparação para publicação que constam nos capítulos seguintes.

### **1-5-1. Mapeamento**

A região estudada apresenta, além das dificuldades de infra-estrutura já relatadas, base cartográfica única, na escala 1:250.000, elaborada a partir de imagens de radar, ausência de levantamento aerofotogramétrico, intensa cobertura florestal, malha viária precária e incipiente e pequena taxa de ocupação humana. Nesse sentido, o caminhamento geológico objetivando a definição de limites entre as diversas unidades litológicas é bastante prejudicado. Entretanto, por serem as unidades litológicas orientadas E-W e as grandes drenagens, às quais geralmente apresentam as melhores exposições de rochas, de direção N-S, foi possível obter uma quantidade satisfatória de dados de afloramentos.

Assim, preliminarmente, foi executado um levantamento geológico de barco pelo Rio Aripuanã, a partir da cidade homônima, até a desembocadura do Rio Branco, quando se conseguiu observar uma grande quantidade de afloramentos, representativos de todos os litotipos da área.

A partir destas informações, a definição das unidades geológicas foi possível pela utilização de imagem de satélite e pela integração com os dados de afloramentos localizados às margens de estradas e caminhos aos quais se somaram alguns pontos em que foi possível o acesso ao leito do Rio Branco.

As dificuldades relatadas acima não permitiram a delimitação de importantes faixas de basaltos e cherts, cujo relacionamento com as rochas vulcânicas ácidas pode ser interpretado somente em escala de maior detalhe.

Em escala de detalhe foi utilizado um mapa efetuado pela Noranda que foi elaborado a partir da coleta de dados geológicos, obtidos de caminhamentos em linhas NE com espaçamento variável (50-100-200 metros), informações geofísicas e grande massa de informação extraída da descrição de testemunhos de sondagem.

### **1-5-2. Análise de Testemunhos de Sondagem**

Foram executados, em diversas etapas, trabalhos de descrição de testemunhos, com disponibilização pela Noranda dos resultados de análises químicas do minério, da zona de alteração e da encaixante não alterada (1200 resultados de análises).

As regiões sondadas que mostraram melhores feições da mineralização e da alteração hidrotermal foram analisadas petrográficamente por luz transmitida e refletida (25 amostras).

### **1-5-3. Análises Isotópicas**

Foram realizadas 20 análises com utilização de diversas metodologias isotópicas incluindo U-Pb em zircões de vulcânicas e intrusivas, Pb-Pb em galena, feldspato e rocha total, Sr-Sr em carbonato e sulfetos e Rb-Sr em sulfetos.

Na Tabela I consta a descrição das amostras estudadas e especificações sobre o material analisado e métodos isotópicos utilizados.

Um grande trabalho de preparação das amostras e separação dos diversos minerais foi realizada pelo autor utilizando-se das facilidades dos laboratórios da Unicamp e USP.

Todas as análises isotópicas foram executadas no Centro de Pesquisas Geocronológicas do IG-USP, com exceção das análises U-Pb em zircões realizadas no SHRIMP II da Universidade of Western Austrália.

As amostras utilizadas para determinações Sr/Sr incluindo calcita e sulfetos foram analisadas semi-quantitativamente por fluorescência de raios-X para determinação da razão  $Rb_{Total} / Sr_{Total}$ .

A análise K/Ar de anfibólio da zona de alteração não foi possível devido ao fato de

ser este uma tremolita com teor de  $^{40}\text{K}$  no limite inferior de detecção do espectrômetro utilizado.

Tabela I – Relação de amostras e sistemáticas isotópicas utilizadas.

Nº Lab	Nº Campo*	Descrição	Material	R X	Rb/ Sr	Sr/ Sr	K/ Ar	Ar/ Ar	Pb/ Pb	U/ Pb
	16/219	Minério Maciço	Galena						X	
	19/257	Minério Maciço	Galena						X	
	25/207	Minério Maciço	Galena						X	
34168	24/445.7	Minério Maciço	Galena						X	
34169	8/322.9	Veio de galena	Galena						X	
34170	19/231	Minério Maciço	Galena						X	
34171	19/220.5	Minério Disseminado	Galena						X	
34172	16/219	Carbonato	Calcita	X		X				
34173	19/220.5	Carbonato	Calcita	X		X				
34174	49/367	Carbonato	Calcita	X		X				
34175	8/144	Carbonato	Calcita	X		X				
34176	25/165	Minério Disseminado	Pirita	X		X				
34177	19/220.5	Minério Disseminado	Pirita	X		X				
34178	49/470.5	Minério Disseminado	Pirita	X		X				
34179	49/470.6	Zona de Alteração	Anfíbólio							
34180	20/355	Esfalerita	Esfalerita		X					
34183	Granito Paraibão	Granito	Pó-RT						X	X
34183	Granito Paraibão	Granito	Feldspato						X	
34184	Dacito Maçaranduba	Dacito								X
34455	19/267	Minério Disseminado	Galena						X	

\* O número de campo quando utilizando a barra significa nº do furo / profundidade.

#### 1-5-4. Análises Químicas

Trinta e oito amostras de rochas, representativas das litologias da região, e de testemunhos de sondagem da zona de alteração e do minério foram preparadas e analisadas quimicamente no Laboratório de Geoquímica da Unicamp por fluorescência de raios X e espectrometria de absorção atômica. Os resultados completos referentes a estas análises são apresentados nas Tabelas II e III em Anexo no final deste trabalho.

Um programa de análise química de minerais por microssonda eletrônica foi executado no laboratório do IGc-USP e os resultados integrais também são apresentados nas Tabelas IV, V, VI e VII em Anexo.

#### **1-5-5. Conteúdo da Tese**

A presente dissertaçãodissertaçao encontra-se estruturada da seguinte forma:

- 1- No **Capítulo 1** é apresentada uma *Introdução* com um histórico da descoberta do depósito, considerações sobre estado do conhecimento e relevância do tema, objetivos e um relato sucinto dos métodos e materiais utilizados.
- 2- No **Capítulo 2** é apresentado o artigo intitulado: *The Expedito massive sulfide deposit, Mato Grosso*, R.D.Neder, B.F. Figueiredo, C. Beaudry, C. Collins., J.A.D. Leite, publicado na Revista Brasileira de Geociências, v. 30(2) de junho de 2000.
- 3- No **Capítulo 3** encontra-se o artigo denominado: 1.76 Ga volcano-plutonism in the southwestern Amazonian craton, Aripuanã-MT, Brasil: tectono-stratigraphic implications from SHRIMP U-Pb zircon data and rock geochemistry, R. D. Neder, J.A. D. Leite, B. R. Figueiredo, N.J. McNaughton, submetido em março de 2001 para publicação no IGCP-426 Special Issue do periódico internacional Precambrian Research.
- 4- No **Capítulo 4** é apresentado o artigo: Mineralogy, Isotopic Data and Mineralization Styles of the Volcanic - Hosted Massive Sulfide Zn - Pb Expedito Deposit in Aripuanã, Mato Grosso-Brazil, R.D. Neder, C. C. G. Tassinari, B. R. de Figueiredo and Jayme Alfredo Dexheimer Leite a ser submetido também a um periódico especializado.
- 5- No **Capítulo 5** são apresentadas as Considerações Finais com a principais conclusões do presente trabalho e recomendações para estudos futuros no distrito metalogenético de Aripuanã e região amazônica.
- 6- Em *Anexo* são apresentadas descrições de testemunhos de sondagem e tabelas completas de dados químicos e isotópicos, que não constam dos artigos.

## CAPÍTULO 2

### The Expedito massive sulfide deposit, Mato Grosso

#### ABSTRACT

The Expedito massive sulfide Pb-Zn deposit is located 14 Km north of the Aripuanã town, in the northwestern portion of the State of Mato Grosso, western Brazil. The deposit occurs within a thick pile of acid to intermediate volcanic rocks and co-genetic intrusions of the Uatumã Group. These rocks are believed to be related to Mesoproterozoic intracontinental rift, supported by U-Pb zircon age of dacitic volcanics ( $1,762 \pm 6$  M.y.) and of a granite ( $1,755 \pm 5$  M.y.). The deposit is hosted by a horizon of dacitic lapilli and crystal tuff interlayered with massive dacitic porphyritic flows and carbonate and chert layers. The deposit consists of several discordant and discontinuous lenses of massive to semi-massive pyrrhotite, pyrite, sphalerite, galena, chalcopyrite, and arsenopyrite. Sulfides also occur disseminated or in veins. There are two types of ores: sphalerite-rich, more prominent, and chalcopyrite-rich with high Cu-Au grades. These deposits are enveloped by a hydrothermal alteration halo consisting of chlorite, biotite, and a peculiar assemblage of calc-silicate minerals associated with carbonate. Magnetite-rich zones overprint the massive sulfides and suggest post-depositional sulfide replacement. The ore lenses are intimately associated with the volcanic rocks, suggesting an exhalative origin. However, the absence of typical exhalative textures, intense calc-silicate alteration, and syn-deformational character of the deposits do not fit the classical VMS model. Therefore, an intrusion-related, epizonal hydrothermal replacement model is proposed.

#### INTRODUCTION

The Expedito Deposit is located in the Aripuanã District, western Mato Grosso State, Brazil, approximately 700 km northwest of Cuiabá (Fig. 1). The deposit was discovered through the drilling of a gold quarry worked since the early '80s by *garimpeiros*. It includes three orebodies named Valley , Massaranduba e Babaçu, set along a 4 km long NW-SE trending sigmoidal fold belt, plunging northwestwards. The orebodies crop out as gossans formed by oxidation of the primary sulfide lenses (Fig. 2). Total resources of the Valley

Deposit are 11.65 million metric tons @ 6.29% Zn, 2.25 wt% Pb, 0.07 wt% Cu, 65 g/t Ag, 0.25 g/t Au. (Ambrex, Public News Release 1998).

The deposit occurs at the western portion of the Guaporé Shield, and is related to plutonic and volcanic rocks of the Uatumã Group, which possibly accumulated in an intra-continental rift (Almeida, 1974). Volcanic activity was accompanied and followed by the deposition of a thick shallow marine to fluvial sedimentary sequence.

U-Pb Shrimp dating of zircon from volcanic and intrusive rocks, both related to the mineralization, yield ages of  $1,762 \pm 6$  Ma and  $1,755 \pm 5$  Ma respectively.

The Expedito deposit consists of an unique economic concentration of Zn-Pb-(Cu-Ag-Au) hosted by the acid volcanic rocks of the Uatumã Group. The purpose of this study is to describe the geologic environment and main features of the Valley Deposit orebody.

## LOCAL GEOLOGY

The Expedito deposit is hosted by unmetamorphosed acid volcanic rocks and minor chemical and epiclastic sediments of the Iriri Formation, which belongs to a part of the Uatumã Group. The volcanic succession is dominantly pyroclastic, and includes rocks of rhyolitic, dacitic and rhyodacitic composition.

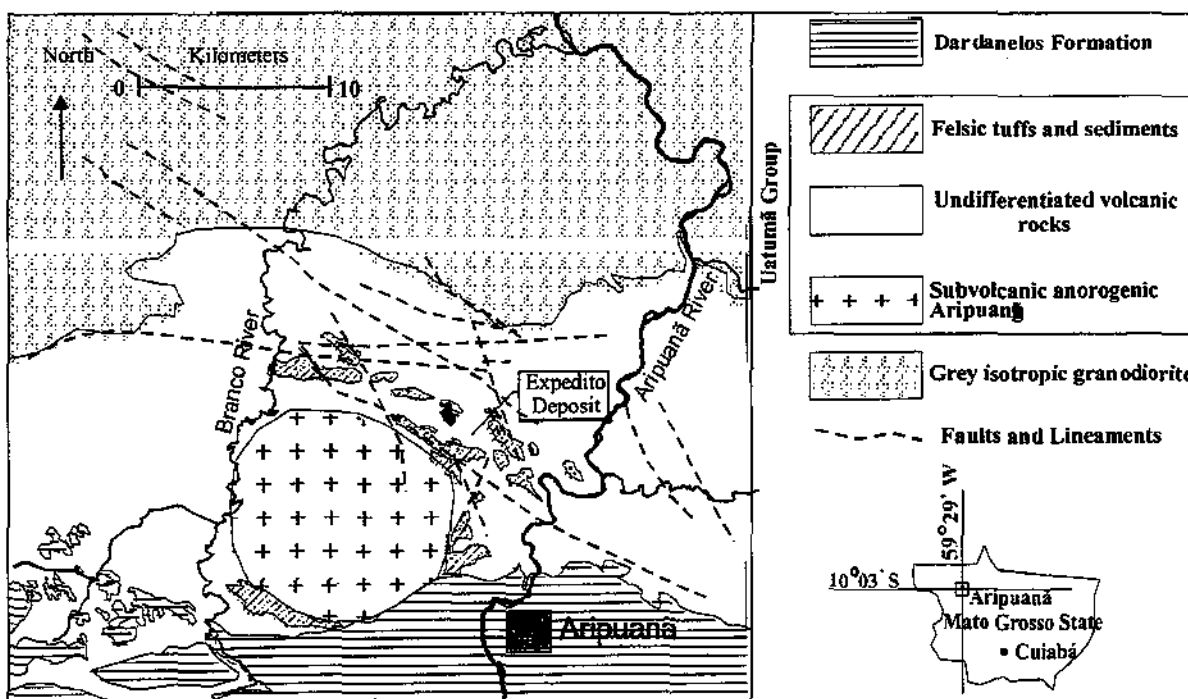


Figure 1. Location map and regional geology of the Aripuanã Region.

Towards the northwest of the deposit, the host sequence strikes N55W, inflecting to N15W in the southeastern portion, and dips usually moderate to steep to southwest. Minor folds have an axial plane trending EW and dipping moderately to the north, with axis plunging moderately to northwest. Only one phase of deformation is evident in the area and its intensity increases towards the proximity of the major faults that host the deposit. Although orebodies and host rock have similar strike, the former dip crosscutting the host rocks. This discordant relation is better observed at the contact between ore and less deformed laminated rocks.

Table 1- Average chemical composition of least altered rocks. (n) = number of samples

	Basalt (5)	Dacite (25)	Rhyolite (30)
SiO <sub>2</sub>	48.68	68.71	73.40
TiO <sub>2</sub>	0.80	0.43	0.19
Al <sub>2</sub> O <sub>3</sub>	15.29	13.77	11.10
Fe <sub>2</sub> O <sub>3T</sub>	12.94	4.03	2.05
MnO	0.24	0.21	0.08
MgO	8.50	1.44	1.14
CaO	11.26	1.32	0.86
Na <sub>2</sub> O	2.01	1.92	2.23
K <sub>2</sub> O	0.81	4.45	3.81
P <sub>2</sub> O <sub>5</sub>	0.08	0.10	0.04
LOI	1.52	1.28	1.08
Total	100.22	99.26	99.53
Ba	273	1057	890
Rb	55	135	97
Sr	205	72	31
Nb	1.3	14.5	11.4
Zr	40	264	169
Y	23	39	35
Th	1.14	4.54	5.19
Cr	267	2	1
Ni	1	2	0
V	5	19	1
Cu	12	3	4
Pb	15	2	3
Zn	10	11	3

The dominant host-rock of the orebodies is a fine to coarse-grained ash, lapilli, and crystal tuffs with minor intercalation of sericitized feldspathic siltstone. All rock types are grayish-green to brownish-red and are composed mainly of quartz and feldspar with rare lithic fragments, ranging from fine grained to lapilli. Rounded quartz are frequent and may have formed by filling vesicles of pumice fragments. Crystal tuffs are porphyritic, with millimetric euhedral feldspar crystals and centimetric rounded quartz set in an ash size and sericitized groundmass, occasionally with microspherulites.

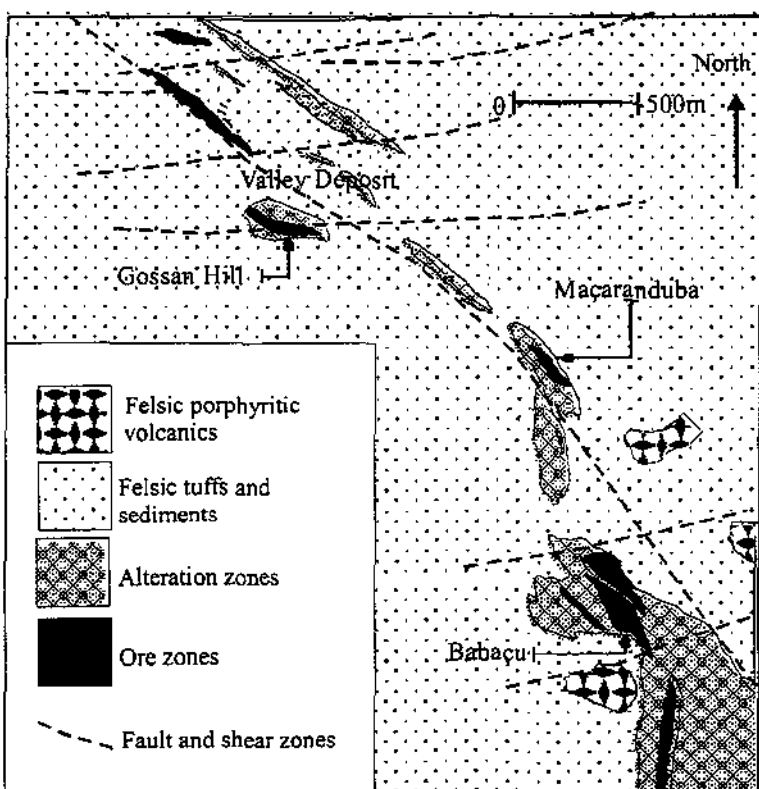


Figure 2. Simplified Geology of the Area of the Expedito Deposit (modified from Collins et al. 1998)

A chemical sedimentary unit occurs along the strike of the Expedito deposit. The horizon consists of chert and carbonate with subordinate silty and clayey laminae suggesting subaqueous deposition. The extension of this unit outside the prospect area is still unknown.

The felsic massive volcanic rocks are silicified and their composition falls within the range of rhyolite and dacite. They are characteristically yellow and porphyritic.

Phenocrystals include corroded and euhedral quartz, sericitized orthoclase, plagioclase and chloritized biotite within a sericitized and recrystallized quartz-feldspar groundmass.

Sub-alkaline (tholeiitic) basalts occur regionally in close association with quartz and feldspar porphyry and rhyolitic volcanics, suggesting a bimodal volcanism.

Geochemical data of local and regional rocks indicate the immobility of Ti, Zr, Nb and Y as predicted in literature (e.g. Pearce and Cann 1973, Floyd and Winchester 1975). Chemical classification of weakly altered rocks ( $LOI < 2\%$ ) based on the relationships between these elements (Table 1, Fig.3), corroborates the presence of a bimodal volcanic pile. Figure 4 indicates that these rocks are not only sub-alkaline but also co-magmatic.

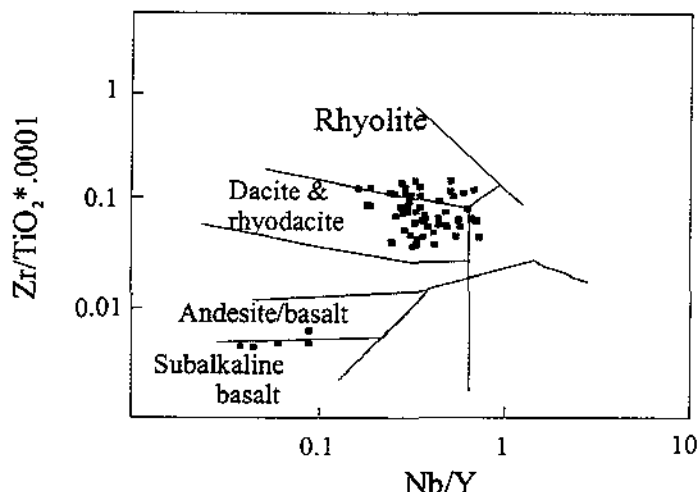


Figure 3-Winchester and Floyd 1977, discriminant plots for representative volcanic rocks of the Expedito District.

### THE VALLEY DEPOSIT

The Gossan Hill is an exposure of oxidized ore more than 40m thick. The soil anomalies have more than 500 ppb Au and 0.5% of Pb. Underground, deposit consists of several discordant tabular bodies enveloped by shear and breccia zones. In general, the most significant ore zones are rimmed by a breccia, suggesting that a fault controlled the mineralization. Unlike barren and unaltered country-rocks, the orebodies and the alteration zone are intensely deformed.

The massive sulfide bodies consist of pyrite, sphalerite, pyrrhotite, and galena, disseminated or in bands, together with minor amounts of chalcopyrite. Semi-massive

bodies have a compositional banding given by the alternation of zones rich in pyrite or pyrrhotite and sphalerite-rich levels. Although resembling a syngenetic feature, no primary sedimentary textures or structures were observed within the sulfide zones. Disseminated sulfides occur as veinlets, stringers, and open-space filling, including boxwork and crustiform veins.

Selected ore samples with Zn > 3% and Cu > 0.3%, show that there is a high positive correlation between Pb and Ag, a moderate positive correlation between Zn and Pb and Au and Cu, and a negative correlation between Cu-Zn, Cu-Pb and Cu-Ag. This suggests a metallogenetic relationship common to Archean VMS deposit (Knuckey et al. 1982, Piché and Guha 1991) (Table 2).

In decreasing order of abundance, the ore minerals are pyrite, pyrrhotite, sphalerite, galena, chalcopyrite, carbonates, magnetite, arsenopyrite, and cassiterite. Fine-grained sphalerite presents a distinct metallic luster, while less frequent coarse-grained crystals are brown with a glassy luster and suggest two generations. Galena occurs in veins, segregation, or inclusion in sphalerite. The majority of the galena crystals are fine-grained, but coarse crystals also occur in veinlets or in cavity-fillings. Electron microprobe analysis indicated that galena contains trace amounts of silver. Chalcopyrite is rare in the Zn-rich ore. In the Cu-rich zones, chalcopyrite occurs associated with pyrrhotite, filling dilatational fractures and rimming pyrite. Pyrite is fine-grained and subhedral, and when euhedral, displays corroded boundaries. Pyrrhotite occurs either as granular crystals or as linear blebs in sphalerite. Magnetite is subhedral and replaces sulfides in a characteristic "porphyroblastic" texture. Carbonates fill fractures and post-ore veins. Cassiterite is rare and occurs as microcrystalline grains recognized only in SEM analyses.

Table 2 – Correlation matrix of ore samples (288 Samples)

	Cu	Pb	Zn	Ag
Au	0.42	-0.07	-0.12	-0.03
Ag	-0.14	0.92	0.41	
Zn	-0.29	0.53		
Pb	-0.24			

Table 3 – Isotopic composition of galena crystals

Sample	$^{206}\text{Pb}/^{204}\text{Pb}$	$^{207}\text{Pb}/^{204}\text{Pb}$	$^{208}\text{Pb}/^{204}\text{Pb}$
F16/219	15.861	15.414	35.575
F19/257	15.835	15.440	35.685
F25/207	16.004	15.652	36.302

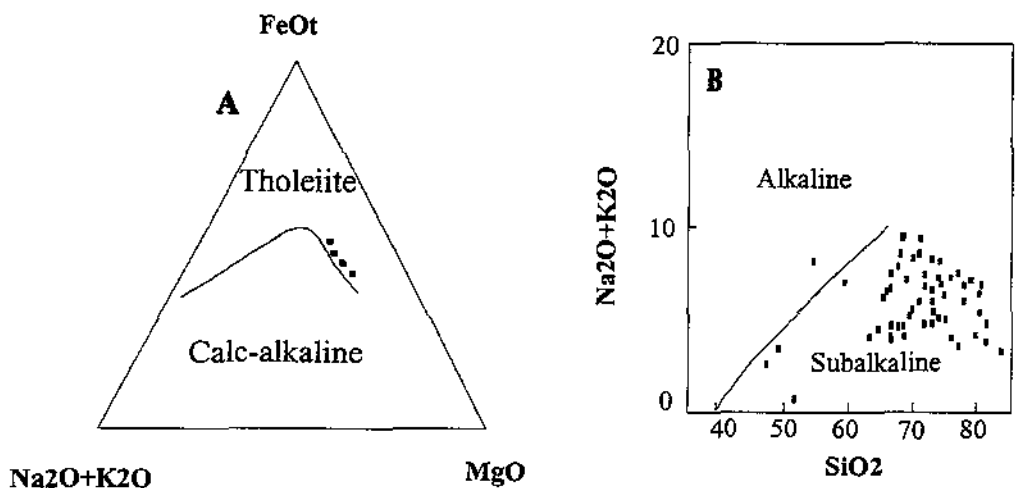


Figure 4 - Magmatic affinity of volcanic rocks: (A) AFM diagram for basalts and (B) Total Alkali X SiO<sub>2</sub> diagram of basalts and felsic rocks (Fields according Irvine and Baragar 1971)

A widespread alteration zone, reaching up to 200 m, resulted from the channeling of hydrothermal fluids through the shear and fault zones (Fig.5). The zones are concordant with the sulfide lenses, and consist of chlorite with variable proportions of biotite, tremolite-actinolite, magnetite, and carbonates. Alteration is zoned and consists of:

- 1)-An outer shell with porphyroblastic biotite in a fine grained chlorite-biotite groundmass;
- 2)-Calc-silicate alteration (tremolite-actinolite) coupled with carbonatization and silicification. In hand specimens, this zone is mottled, occasionally brecciated, and contains granoblastic and acicular amphibole. Rocks from this zone have locally a talc-like appearance;
- 3)-A distinctive chlorite-magnetite halo with porphyroblastic magnetite, partially replacing sulfides;

4)-A core of breccia hosting the major Zn-(Pb) lenses.

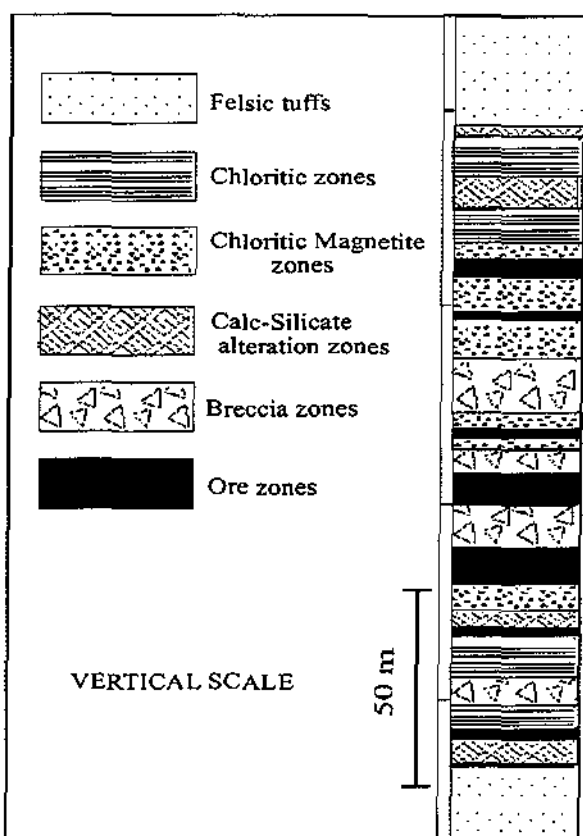


Figure 5 - Sketch of relationship of mineralization and alteration zone

Lead isotopes of galena from the Valley deposit (Table 3), when interpreted under the Stacey and Kramers (1975) two-stage model, yield model ages of 1.76, 1.82 and 1.99 M.y. The first two agree with the ages of zircon from barren igneous country rocks. These data adhere to the upper crust evolution curve of Zartman and Doe (Version II) (1981) (Fig.6).

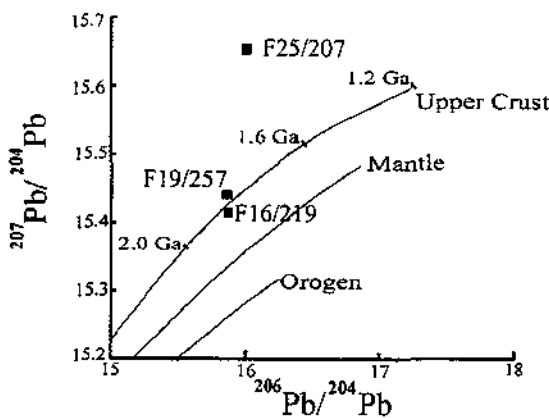


Figure 6- Pb isotopic reservoir growth curves of the plumbotectonic model (Zartman and Doe 1981) (Version II), applied to the Expedito sulfide deposits

## DISCUSSION

The general lack of detrital sedimentary structures and the widespread occurrence of cherts suggest that the host rock accumulated in a sub-aqueous environment. The intercalation of thinly and rhythmically laminated tuffs within thick homogeneous intervals of pyroclastic rocks may have resulted from oscillating intensity of the volcanic activity. Laminated intervals may represent reworked tuffs and exhalites.

The clear association of the orebodies with a brittle deformation zone and the lack of consistent evidence of sea-floor discharge of sulfides, preclude the syngenetic models. The filling of the breccia matrix by hydrothermal minerals is characteristic of hydraulic explosion breccias, formed during fluid expansion triggered by underground phase separation (Hedenquist et al. 1985). Likewise, crustiform veins and veinlets are typical of the same conditions. This evidence suggests that the mineralization took place at shallow crustal levels, possibly connecting to the surface.

Satellite image interpretation together with regional mapping and field and petrographic observation show that the circular structure (Fig.1) represents a multiphase granitic intrusion emplaced in epizonal conditions. The deposition and preservation of a thick tuffaceous sequence requires topographic depressions, which could represent subsidence structures resulting from magmatic evacuation. The structure could possibly represent a caldera intruded by shallow pluton(s) during the resurgent stages, as suggested by the intimate spatial and chronological association of the volcanic pile with granites.

The orebodies are associated with zones of hydrothermal alteration controlled by syn-deformational faults, which, together with the isotopic data, indicates that accumulation of the host volcanic sequence deformation, granite emplacement, mineralization, alteration, and the fault system was contemporaneous. The overprinting of distinct alteration assemblages could be explained by successive reactivation of the synvolcanic faults, which in their turns would control the variable intensity of the hydrothermal alteration indicated by different styles of metassomatic replacement.

Under this interpretation, one single volcanic episode could, during early stages, chloritize and develop carbonate open-space filling during faulting, in a typical propylitic process. Later stages would be represented by a more intense reactivation and high temperature reactions, resulting in a calc-silicate assemblage, typically stable at temperatures above than 350°C (Winkler 1974). High-temperature alteration could also explain the magnetite-chlorite association that replaces the sulfides.

The calc-silicate alteration assemblage is intimately associated with the orebodies, as indicated by their simultaneous occurrence at the intersection of syn-volcanic faults with a carbonate-rich chemical-sedimentary unit. In spite of being volcanic-related deposits, they are probably not exhalative. They may have formed by reaction of acid magmatic-hydrothermal fluids released from a coeval granite and flushed along faults formed by accommodation of the country rocks during the final stage of emplacement of the intrusion. Even not being exhalative, the Valley Deposit, the synchronism between volcanism, sedimentation, granite emplacement, faulting, alteration, and mineralization in a subaqueous environment favors the occurrence of syngenetic volcanic-associated deposits in this region.

### Acknowledgements

To Noranda Exploração Mineral Ltda. For the permission to publish its private data. To Mineração Aripuanã Ltda, especially to geologist Mario Jorge Costa. To CNPQ and the Multi User SEM laboratory (IG-UNICAMP) funded by FAPESP (Fundação de Amparo a Pesquisa do Estado de São Paulo) for grant #95/06401-7

## References

- Almeida F.F.M. 1974. Evolução Tectônica do Cráton do Guaporé Comparada com o Escudo Báltico. *Rev. Bras. Geosc.*, 4:191-204.
- Collins C. and Monteiro H. 1998. Technical report on the Exploration Work on The Aripuanã property. Noranda Mineração. Intern Report Floyd P. A. and Winchester J. A.
1975. Magmatic type and tectonic setting discrimination using immobile elements. *Earth Planet. Sci. Letters.*, 27:211-218.
- Hedenquist J. W. and Henley R. W. 1985, Hydrothermal eruption in the Waiotapu geothermal system, New Zealand: Their Origin, associated breccias and relation to precious metal mineralization. *Econ. Geology*, .80:1640-1668
- Irvine T.R. and Baragar W.R.A. 1971. A guide to the chemical classification of the common volcanic rocks. *Canad. Jour. Earth Sci.*. 8. 523-548
- Knuckey M.J., Comba C.D.A., Riverin G. 1982, Structure, metal zoning and alteration at the Millenbach deposit, Noranda, Quebec., in Hutchinson, R.W., Spence, C.D. and Franklin, J.M., Precambrian sulphide deposits, Geological Association of Canada, Special Paper 25: 255-295.
- Pearce J. A . and CANN J. R. 1971, Ophiolite origin investigated by discriminant analysis using Ti, Zr, and Y. *Earth Planet. Sci. Letters.*, 12: 339-349.
- Piché M., Guha, J., Bouchard G., Bonenfant A. 1991. Metallogenetic and exploration significance of the deformation affecting the ore host stratigraphy and the VMS deposits of the Matagami Camp, Quebec. In: Program with Abstracts – Geological Association of Canada; Mineralogical Association of Canada; Canadian Geophysical Union, Joint Annual Meeting. 16: 99
- Stacey J. S. and Kramers J. D. 1975. Approximation of terrestrial lead isotope evolution by a two-stage model: *Earth. Planet. Sci. Lett.*, 26:207-221
- Winchester J.A. and Floyd PA. 1977. Geochemical discrimination of different magma series and their differentiation products using immobile elements. *Chem. Geology*. 20. 325-342
- Winkler H. G. F. 1974. Petrogenesis of metamorphic rocks, in Froese.,ed., Petrogenesis of metamorphic rocks, Springer-Verlag, .74-80.
- Zartman R. E. and Doe B. R., 1981. Plumbotectonics- the model: *Tectonophysics*,. 75. 135-162.

## CAPÍTULO 3

### 1.76 Ga volcano-plutonism in the southwestern Amazonian craton, Aripuanã-MT, Brasil: tectono-stratigraphic implications from SHRIMP U-Pb zircon data and rock geochemistry.

#### Abstract

Paleoproterozoic felsic and mafic volcanic rocks, extrusive and hypabyssal quartz porphyry, and high-K, A-type epizonal granites dominate the Aripuanã region (northwestern Mato Grosso State, Brazil), in the southwestern Amazonian Craton. The extrusive and intrusive felsic rocks display similar major and trace elements abundances and equivalent SHRIMP U-Pb ages of 1762 to 1755 Ma; contacts between them in the field occur gradually. The felsic volcanic activity occurred predominantly as explosive sub aqueous volcanism.

Various features such as absence of plate collision evidences, lack of any sign of oceanic crust, lack of complete trends of magmatic differentiation, and bimodal characteristics suggest that the magmatism was intracratonic. The characteristically undeformed felsic igneous rocks were formed by extensional events, probably triggered by mantle activation in an intracratonic ‘anorogenic’ or post-collisional environment. Throughout the entire Amazonian craton there are wide areas displaying similar magmatism responsible for the generation of distinctive A-type granites. These rocks and the associated volcanics yield ages of 1.75 Ga, suggesting that they are genetically linked and that there is a unique tectonic mechanism of widespread action in this craton.

**Keywords:** Paleoproterozoic; felsic volcanics; geochronology; geochemistry, Brazil, Amazonian craton.

## **1. Introduction**

The largest Precambrian craton in South American is the Amazonian craton. The Phanerozoic Amazon basin divides this craton into two blocks: the Guiana Shield in the north and the Central Brazil Shield in the south. Ages obtained from isotopic data become progressively younger westward from the Archean areas of the Central Amazonian Province into the Paleoproterozoic areas of Mato Grosso and Rondonia States. This is especially well illustrated by the great number of magmatic episodes with similar characteristics but of different ages and spatial environments. One of the main features of this craton is the presence of large and widespread occurrences of felsic volcanism. Trompette et al. (1994) estimated that this type of volcanism covers an area of more than 3,000,000 km<sup>2</sup>.

The Aripuanã region, in northwest Mato Grosso State, is located in the southwestern portion of the Amazonian craton, within the realm of the Rio Negro-Juruena geochronological province described by Tassinari et al. (1996), or alternatively, within the Juruena Block of Costa and Hasui (1997) or in the Juruena-Rondonia belt more recently described by Santos (2000). In this region, volcanic and plutonic products of Paleoproterozoic age predominate. The metallogenetic potential of this volcano-plutonic environment was highlighted during the last decade, after the discovery of the Expedito massive sulfide deposit, of singular characteristics, in the geological context of the Amazonian Craton.

Most of the current geological knowledge was the result of the RADAMBRASIL project (Silva et al., 1980) which produced a regional geological map (1:1,000,000) based on the interpretation of lateral view radar images and Rb/Sr and K/Ar geochronological data. More recent works about the region are documented by Tassinari (1996) and Tassinari and Macambira (1999) and consist mainly of geochronological studies and compilation of the isotopic results. The aim of this paper is to present new U-Pb zircon and geochemical data with the purpose of characterizing the geological and geochemical aspects of the volcano-plutonic episode of Aripuanã. As well, some of the stratigraphic and tectonic implications of these new results are discussed.

## **2. Regional geology**

The tectonic, physiographic and stratigraphic features of the Aripuanã region are shown in Figure 1. A better understanding of the stratigraphy of this region is hampered by the lack of

The crystal tuffs have a gray to yellow-green color with a well-developed fragmental texture. Locally they are porphyritic, with sub-millimetric, euhedral K-feldspar crystals, sub-centimetric felsite clasts, and rounded quartz clasts; the clasts are 2 to 3 mm in size, with all of them set in a fine, foliated and sericitized tuffaceous groundmass with a microspherulitic appearance.

The massive felsic volcanics are rhyolite-dacite-rhyodacite in composition, varying from green to yellowish gray and showing well-developed porphyritic textures. The Massaranduba dacite exemplifies this textural facies. Phenocrysts of quartz, plagioclase and rare orthoclase are set in a microcrystalline, sericitized and recrystallized groundmass. Quartz phenocrysts are usually anhedral and rounded, showing corrosion effects. More rarely some tabular sections, possibly representing tridymite paramorphous with undulating extinction, are present. The plagioclase is generally euhedral, but in some cases corroded and ragged edges are also observed. The rare euhedral orthoclase crystals are sericitized on the edges. Green biotite is the dominant mafic phase and is sometimes partially transformed to chlorite.

The suite represented by granitoid rocks displays textural variations between plutonic and subvolcanic environments. The plutonic units occur as stocks and as minor sills intruded in felsic volcanics and as a larger, circular shaped batholith; these have been informally described as the Aripuanã and Paraibão granites. Based on field relationships and characteristics such as the lack of foliation and textural features, this granite is interpreted as an epizonal, 'anorogenic' and (or) post-collisional pluton. The granite varies gradually from coarse-grained with microcline phenocrysts to porphyritic with microcline, quartz and plagioclase phenocrysts. In several good exposures it appears that the plutonic texture goes without transition to subvolcanic or volcanic tuffaceous rocks, suggesting normal faulting and (or) a caldera collapse environment. In the granites, as in the volcanics, biotite is the mafic phase. Granophytic and micrographic textures are common.

Chemical sediments represented by cherts are frequent and occur with variable thickness from millimetric to metric scales. A grayish color is predominant, and the metasedimentary rock mainly consists of cryptocrystalline silica that may be erroneously mistaken in diamond drill core samples for aphanitic, fine-grained volcanic rocks. Fine-grained clastic sedimentary rocks of grayish, greenish, to red colors are common and may represent sub-aquatic deposition of ashes

interlayered with the cherts. These rocks are well stratified and finely laminated (<1mm), with exhalitic appearance; they are always intensely sericitized.

The mafic rocks are phaneritic and green to black in color. They have a basaltic composition, consisting of fine-grained augite and andesine to labradorite feldspar.

#### 4. Major and Trace Element Chemistry

Geochemical data were determined by X-ray fluorescence in the Analytical Geochemistry Laboratory of University of Campinas for representative samples of the plutonic and volcanic rocks (Table 1). Samples considered to be the least hydrothermally altered were used for this study. In general, the rocks from Aripuanã show a  $\text{SiO}_2$  content ranging from 47% to 81% with a gap between 50% and 67%, which attests to the bimodal character of the suite. The dominant felsic members, dacite to rhyolite in composition, are geochemically related to the granitic rocks and display similar differentiation and compositional trends, with  $\text{SiO}_2$  ranging from 67% to 81%. The mafic members display  $\text{SiO}_2$  contents ranging from 47% to 50% (Fig.2a, Table 1).

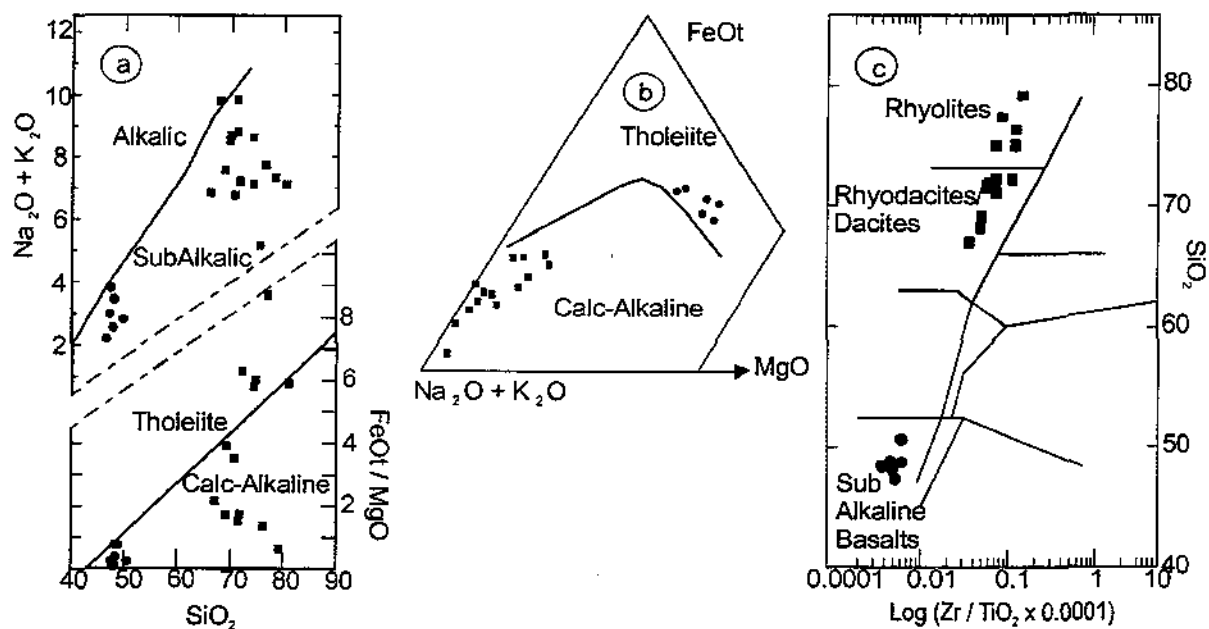


Figure 2. Bivariate plots for felsic (squares) and mafic (circles) rocks of the Aripuanã district (Table 2): a) total alkalies (Irvine and Baragar, 1971) and  $\text{FeOt} / \text{MgO}$  versus  $\text{SiO}_2$  (Miyashiro, 1974); b) AFM (Irvine and Baragar, 1971) diagram; and c) modified Winchester and Floyd (1977) petrographic discriminant diagram.

The felsic igneous rocks, including plutonic, volcanic, and subvolcanic counterparts, are classified as granites, dacites, rhyodacites, rhyolites, and quartz porphyries. Their high  $K_2O/Na_2O$  ratios categorizes these rocks as high-K, peraluminous and metaluminous (Fig. 3). They are corundum-normative and show total alkalies ranging from 6 to 10 percent. They are poor in CaO and very poor in MgO, resulting in high Fe/(Fe+Mg) ratios. They exhibit high abundances of large, highly charged cations such as Nb and Y and are rich in Zr.

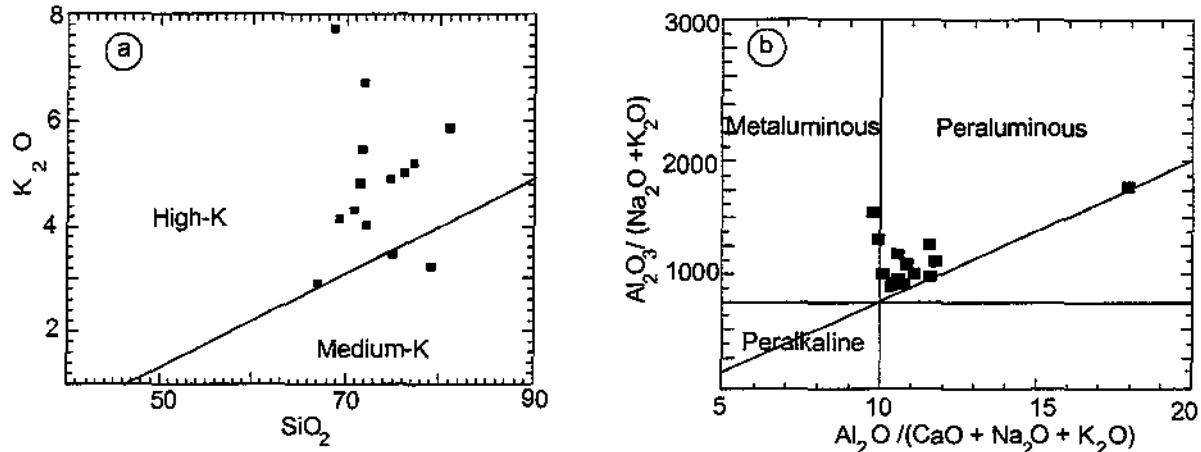


Figure 3. Discriminant diagrams for the felsic rocks of the Aripuanã district: a)  $K_2O$  vs. silica diagram showing the subdivisions of Le Maitre et al. (1989) and b) ratios between molar values diagram of Maniar and Piccoli (1989).

Major and trace element contents were also used in order to define a possible tectonic environment in which the suite evolved. In the  $Al_2O_3$  vs.  $SiO_2$  plot of Maniar and Piccoli (1989) (Fig. 4a), all but two samples plot in the field of post-orogenic granitoids. Their  $Al_2O_3$  contents also decrease with increasing differentiation, which can be interpreted as due to plagioclase fractionation. Within the Nb vs. Y discrimination diagram (Pearce et al., 1984; Fig. 4b), the data straddle the fields of volcanic-arc and within-plate granites; this was considered as a common feature of A-type magmatism by Eby (1990). A-type granites with similar geochemical characteristics have also been reported throughout the Amazonian craton (Dall'Agnoll et al., 1994; Tassinari et al., 1999; Santos, 2000 and Vasquez, 2001) and they might be correlated to the Uatamã volcanism.

Mafic rocks of the suite are chemically classified as subalkaline basalts. These rocks are silica-saturated basalts (Ol and Hy in the norm) which plot in the tholeiitic fields of the  $\text{FeO}_t$  /  $\text{MgO}$  versus  $\text{SiO}_2$  diagram (Fig. 2a). These rocks can also be classified as low-K tholeites based on the Pearce and Cann (1973) Zr-Ti diagrams (Fig. 5a) and  $\text{Ti}/100-\text{Y}^*3-\text{Zr}$  diagram (Fig. 5b).

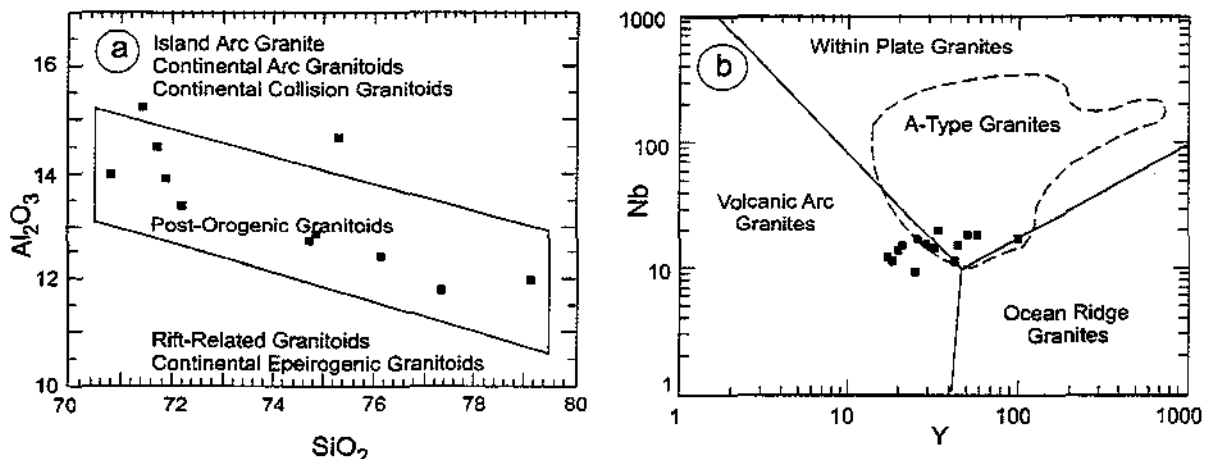


Figure 4. Tectonic setting discriminant diagrams for felsic rocks of the Aripuanã district. Boundaries are from: a) Maniar and Piccoli (1989) and b) Pearce (1984).

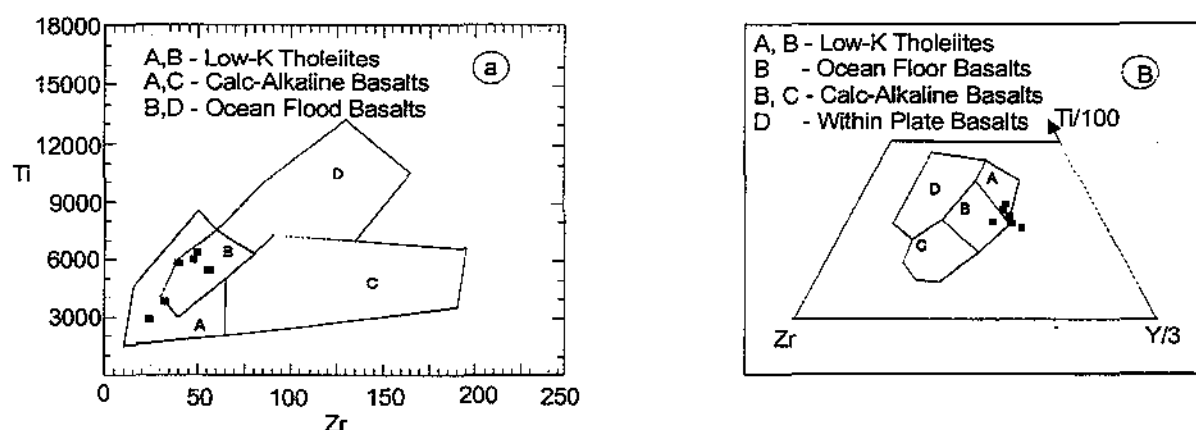


Figure 5. Tectonic setting discriminant diagrams for the basalts of the Aripuanã district. Boundaries are from Pearce and Cann (1973).

Table 1 Representative Analyses of Plutonic and Volcanic Rocks from the Aripuanã District.

Sample	RJ34	RJ95	RJ62	RJ18	RJ22	RJ36	RJ110	RJ117	RJ21	RJ98	RJ125	RJ118	RJ101	RJ115	RJ35	GrPb	RJ57	RJ77	DMass	RJ99
Weight percent																				
SiO <sub>2</sub>	47.50	47.99	48.24	48.41	48.97	50.55	67.03	68.70	69.29	70.82	71.48	71.76	71.92	72.26	74.79	74.89	76.14	77.31	79.13	81.06
Al <sub>2</sub> O <sub>3</sub>	15.05	15.96	15.84	15.30	14.40	15.74	15.60	13.13	14.47	13.95	15.22	14.46	13.86	13.43	12.73	12.88	12.46	11.82	11.97	9.49
Fe <sub>2</sub> O <sub>3</sub>	11.61	9.86	12.21	11.65	12.95	9.06	4.40	4.57	4.30	2.81	2.65	2.47	3.45	4.00	2.41	2.31	2.97	1.35	0.44	1.65
MnO	0.21	0.38	0.206	0.20	0.24	0.14	0.10	0.03	0.08	0.06	0.03	0.04	0.03	0.03	0.02	0.02	0.05	0.01	0.01	0.02
MgO	9.61	9.22	6.96	8.56	7.61	7.52	1.40	1.68	0.89	0.62	1.05	0.92	0.06	0.55	0.35	0.33	1.28	0.14	0.27	0.24
CaO	11.52	11.56	9.85	11.23	9.97	12.02	3.53	0.27	2.51	1.13	0.07	0.55	0.54	1.12	0.53	1.33	0.03	0.40	0.06	0.35
Na <sub>2</sub> O	1.72	1.30	2.09	2.15	2.41	2.47	3.90	2.05	3.35	4.33	1.92	3.27	3.04	3.15	3.69	3.60	0.08	2.59	4.07	1.23
K <sub>2</sub> O	0.54	1.55	1.75	0.48	1.12	0.37	2.90	7.71	4.15	4.28	4.81	5.45	6.69	4.02	4.88	3.47	5.01	5.18	3.23	5.84
TiO <sub>2</sub>	0.62	0.47	0.99	0.96	1.06	0.90	0.51	0.62	0.63	0.58	0.34	0.37	0.39	0.56	0.30	0.23	0.14	0.18	0.09	0.21
P <sub>2</sub> O <sub>5</sub>	0.05	0.05	0.08	0.10	0.09	0.09	0.18	0.11	0.15	0.06	0.05	0.07	0.06	0.12	0.04	0.05	0.01	0.02	0.01	0.03
LOI	1.59	2.40	2.69	0.81	1.54	1.26	0.75	0.49	0.53	0.75	2.50	1.00	0.72	0.90	0.62	0.53	2.48	0.68	0.68	0.67
Total	100.05	100.75	100.89	99.87	100.36	100.12	100.30	99.35	100.35	99.40	100.11	100.38	100.77	100.13	100.36	99.66	100.66	99.69	99.96	100.79
Parts per million																				
Ba	341	517	295	35	407	67	1106	1966	984	1501	666	1076	1023	1181	707	1193	1249	717	574	1235
Cr	78	421	163	323	229	283	5	16	6	4	20	2	4	10	4	<2	<2	7	4	10
Cu	93	93	95	150	71	49	17	4	14	5	2	3	5	2	5	3	2	3	32	23
Nb	<1	<1	<1	<1	<1	2	9	14	15	18	16	15	20	18	17	11	15	13	15	12
Ni	126	167	80	145	80	98	3	8	4	4	5	3	8	5	2	<2	0	<2	<2	5
Pb	<2	<2	<2	<2	8	<2	9	4	14	2	2	6	3	5	1	4	4	7	4	3
Rb	32	119	115	16	88	20	86	245	139	167	183	130	206	76	108	82	185	172	49	156
Sr	197	170	238	122	231	304	394	45	188	123	39	83	54	97	53	108	9	62	19	44
Th	<2	<2	<2	<2	<2	2	9	16	13	13	21	16	19	20	19	13	18	17	18	13
V	208	219	309	285	339	255	58	38	42	9	22	23	9	24	3	10	5	6	<3	7
Y	20	17	28	23	27	25	25	32	45	59	26	21	35	51	100	42	31	20	29	17
Zn	74	103	82	68	114	53	56	21	53	33	21	23	14	28	15	17	21	9	0	24
Zr	33	24	48	40	50	56	187	304	327	438	200	228	441	410	367	169	174	159	136	262

## **5. U-Pb methodology**

Two samples, one from the Paraibão granite and the other from the Massaranduba dacite, were chosen for U-Pb geochronology. Samples were crushed in a ring mill with subsequent separation, using nylon sieves, of the less than 60-mesh fraction. This material, after being duly washed and decanted, was treated with density liquids (LST and diiodomethane) and magnetically separated. The resulting higher density fraction was hand-picked for zircon grains under a binocular microscope. These grains were mounted on epoxy discs along with fragments of the zircon standard CZ3 (564 Ma) and polished by abrasion through to approximately the center of each grain. Microphotography of each grain was performed with reflected and transmitted light and their internal morphologies were observed by scanning electronic microscope (back-scattered electrons and charge contrasting imaging). The epoxy discs and their zircons were then metallized with gold to perform the SHRIMP analyses.

The isotopic composition of the zircons was determined by the use of SHRIMP II, using the more recently modified version (de Laeter and Kennedy 1998; Smith et al. 1998) of the methods originally published by Compston et al. (1984). Circular and oval areas, from 20 to 30  $\mu\text{m}$ , were analyzed in different zircon grains and several times on the CZ3 standard within the same epoxy disc. Corrections for common lead were been made using the Pb isotopic composition of Pb from Broken Hill galena. The common lead values from the samples were very similar to those observed in the CZ3 standard and the discrepancies were considered as coming from the gold film. The uncertainties of all the determined ages were within the 95 percent confidence level.

## **6. Geochronology results**

### 6.1. Sample 01 - Massaranduba dacite

The zircons of this sample consist of short prisms with well-defined pyramidal terminations. Some crystals show corroded borders and embayments that are interpreted as results of corrosion during the late stages of the magmatism or even during the late hydrothermal event previously characterized. They vary from colorless through brownish-yellow and to almost black.

consistently recognized basement. On a local scale, a suite of volcanic and associated intrusive rocks predominate. Of these, the Aripuanã granite occurs as a round structure, showing the characteristics of an epizonal multiphase intrusion. Layered chemical sedimentation is found locally, in the northern area of the Expedito Deposit and at the southern limit of the Dardanelos Plateau. The chemical sedimentation includes exhalites, cherts, and fine volcanogenic sedimentation, which characterize the final stages of the volcano-plutonic episode under sub-aquatic conditions. Later, clastic sediments of the Dardanelos Formation covered parts of the region, filling the Caiabis Graben. The exhalative environments are presumed to be more widespread in this area, but their recognition is still hampered by the poor regional geological knowledge.

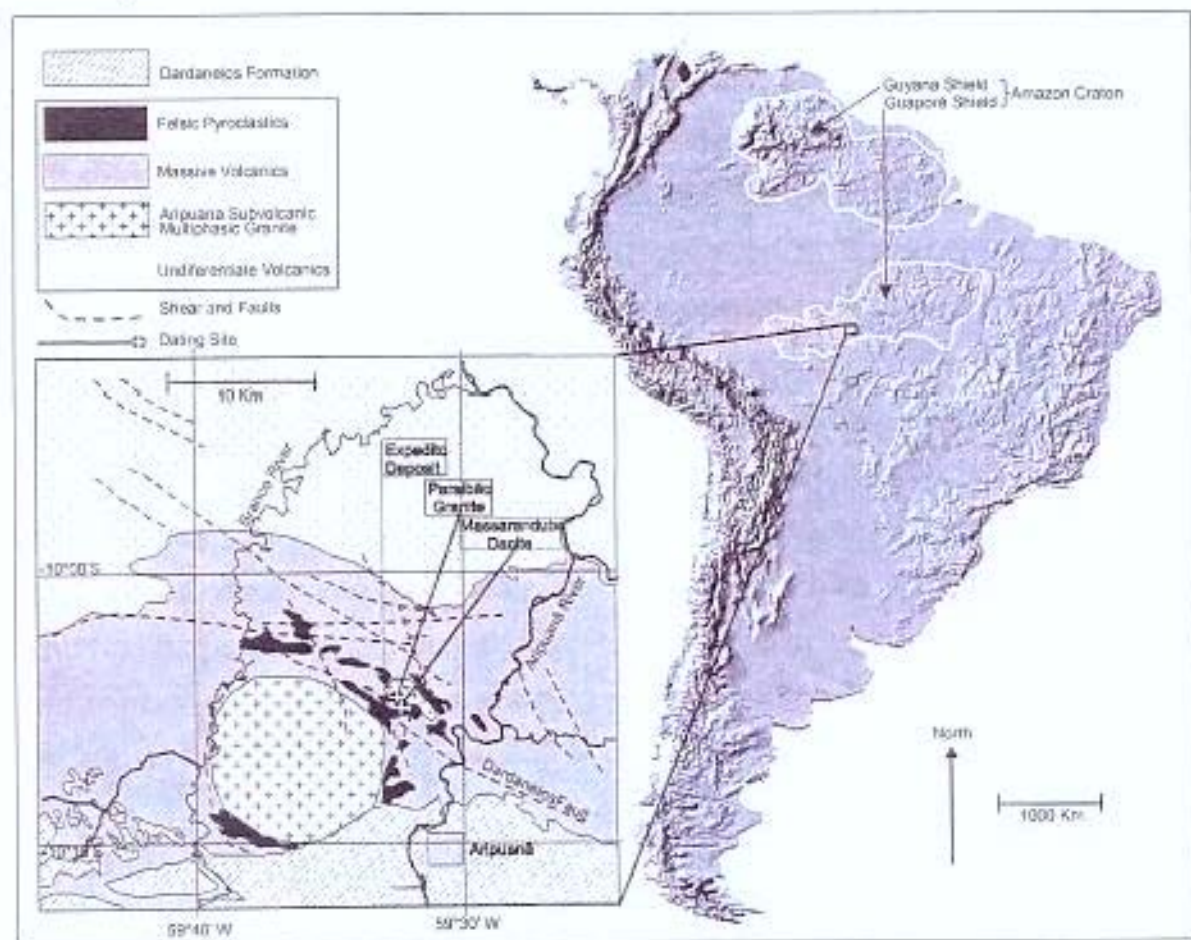


Figure 1. Simplified geology of the Aripuanã district. The locations of the samples dated in this paper are also shown.

These igneous associations have been considered related to the Uatumã Group (Silva et al. (1980), as defined by Oliveira and Leonardos in 1943 (Almeida, 1974). New U/Pb geochronological data have demonstrated a hiatus of about 100 m.y. between the various units of the Uatumã Group and there is, at the moment, a debate whether to subdivide this unit (e.g. Santos, 2000; Pinho et al., 2001). The sedimentary and volcanic rocks do not show regional metamorphism features. However, wide hydrothermally altered bands generally associated with fault zones are frequently recognized, as exemplified by the Zn-Pb-Ag Expedito massive sulfide deposit. (Neder et al., 2000).

From the structural point of view, there are domains in which ductile deformation prevails along narrow zones; these are characterized by a steep dipping foliation. Outside the high strain areas, both volcanic and plutonic units are undeformed and preserve their original characteristics. Overall, the tectonic behavior is characterized by rupture of the crust and the formation of horsts and grabens along previously weakened zones generally represented by dextral transcurrent, NW oriented faults, as exemplified by the Dardanelos, Canamã and Peixe faults in the so-called "Lineamento Arinos-Aripuanã" (Silva et al., 1980). This structural trend was considered by Tassinari (1981) to define the Rio Negro-Juruena mobile belt.

### **3. Characterization of the volcanic-plutonic association of Aripuanã**

The Aripuanã volcanic-plutonic association is characterized by the dominance of unmetamorphosed and undeformed pyroclastic rocks, massive felsic volcanics with subvolcanic and plutonic co-magmatic associated bodies, and subordinate occurrences of basalts and exhalites. The felsic volcanic units consist of massive porphyritic and pyroclastic rocks, including crystal and lapilli tuffs and ashes. Flow structures are frequent in the pyroclastic rocks; the flow structures are interpreted as sub-aqueous, volcanogenic turbidity deposits that were intercalated within the felsic pyroclastic layers.

The lapilli tuffs are fine-grained (0.1 mm on average), greenish-gray colored rocks with partially sericitized felsitic groundmass. They show a well-developed fragmental texture with sub-angular to oval shaped polymitic felsitic clasts of about one centimeter size. Locally the clasts reach up to 5 cm, making up 50 to 70 per cent of the rock. The holocrystalline groundmass is composed of quartz and feldspar.

Observations of back-scattered images reveal zircon structures consisting of nuclei with relict euhedral zoning surrounded by massive and structureless borders (Fig. 6). This zoning is similar to that displayed by zircons generated by magmatic crystallization (Vavra, 1996). The overgrown borders might be considered as resulting from late processes (annealing) that may be attributed to hydrothermal processes.

For this sample 20 areas were analyzed in one single analytical section. The reproducibility of the U/Pb ratio for the CZ3 standard was  $\pm 1.03\%$ . The results are presented in Table 2 and U/Pb ratios are plotted in a concordia diagram (Figure 7).

Table 2 -Shrimp data of Sample 1 zircons - Massaranduba Dacite

#### Magmatic Zircons

Spot N°	U ppm	Th/U (ppb)	Pb (ppb)	f20 6	$\frac{^{207}\text{Pb}}{^{206}\text{Pb}}$	$\pm$	$\frac{^{208}\text{Pb}}{^{206}\text{Pb}}$	$\pm$	$\frac{^{208}\text{Pb}}{^{238}\text{U}}$	$\pm$	$\frac{^{207}\text{Pb}}{^{235}\text{U}}$	$\pm$	Age (Ma)	$\pm$	Conc %
32-1	85	0.51	28	0.01	0.1129	0.0032	0.1338	0.0070	0.298	0.004	4.64	0.16	1847	51	91
17-1	491	0.56	131	0.01	0.1106	0.0014	0.1655	0.0032	0.233	0.002	3.56	0.06	1809	24	75
36-1	295	0.45	85	0.00	0.1102	0.0009	0.1227	0.0013	0.272	0.003	4.14	0.06	1802	15	86
13-1	185	0.58	58	0.00	0.1100	0.0018	0.1380	0.0039	0.285	0.003	4.33	0.09	1799	30	90
18-1	319	1.04	110	0.00	0.1095	0.0013	0.2064	0.0029	0.300	0.003	4.53	0.08	1791	21	95
2-1	123	0.68	42	0.00	0.1089	0.0013	0.1768	0.0028	0.303	0.004	4.54	0.08	1781	21	96
25-1	126	0.58	41	0.00	0.1083	0.0025	0.1331	0.0055	0.303	0.004	4.53	0.13	1770	42	96
37-1	281	0.59	93	0.00	0.1082	0.0009	0.1495	0.0019	0.303	0.003	4.53	0.07	1769	16	97
7-1	563	1.34	124	0.00	0.1078	0.0010	0.1674	0.0022	0.198	0.002	2.95	0.04	1762	17	66
42-1	187	0.51	65	0.00	0.1075	0.0012	0.1458	0.0025	0.319	0.004	4.73	0.08	1757	21	102
1-1	279	0.31	88	0.00	0.1072	0.0005	0.0889	0.0008	0.306	0.003	4.53	0.06	1752	8	98

#### Recrystallized zircons "Annealed Hydrothermals"

Spot N°	U ppm	Th/U (ppb)	Pb (ppb)	f20 6	$\frac{^{207}\text{Pb}}{^{206}\text{Pb}}$	$\pm$	$\frac{^{208}\text{Pb}}{^{206}\text{Pb}}$	$\pm$	$\frac{^{208}\text{Pb}}{^{238}\text{U}}$	$\pm$	$\frac{^{207}\text{Pb}}{^{235}\text{U}}$	$\pm$	Age (Ma)	$\pm$	Conc %
33-4	293	0.34	90	0.00	0.1061	0.0012	0.0952	0.0023	0.293	0.003	4.29	0.07	1734	20	96
9-1	605	0.60	205	0.01	0.1058	0.0011	0.1877	0.0025	0.295	0.003	4.30	0.06	1728	19	96
3-1	276	0.74	99	0.00	0.1055	0.0005	0.2134	0.0012	0.315	0.003	4.58	0.06	1722	9	103
6-1	79	0.31	27	0.00	0.1044	0.0022	0.0797	0.0044	0.324	0.005	4.67	0.13	1704	39	106
14-1	2455	0.01	739	0.00	0.1037	0.0003	0.0022	0.0002	0.316	0.003	4.52	0.04	1691	5	105
10-1	28	0.56	10	0.02	0.1029	0.0072	0.1163	0.0158	0.311	0.008	4.41	0.34	1678	129	104
15-1	1812	0.65	289	0.01	0.0987	0.0008	0.1809	0.0018	0.142	0.001	1.93	0.02	1599	15	54
8-1	89	0.43	29	0.00	0.0986	0.0024	0.1276	0.0052	0.305	0.005	4.15	0.13	1598	45	107
9-1	731	0.06	180	0.00	0.0982	0.0007	0.0182	0.0011	0.254	0.003	3.44	0.05	1591	14	92

The data spread from 1847 to 1591 Ma with a well-defined cluster at ca. 1750 Ma. If all data are taken to calculate the  $^{207}\text{Pb}/^{206}\text{Pb}$  age, a chi-square value  $>>1$  is found. This value is much higher than the expected value ( $\sim 1$ ) for one single age population, therefore, two age populations are proposed which, is supported by the BSE imaging studies.

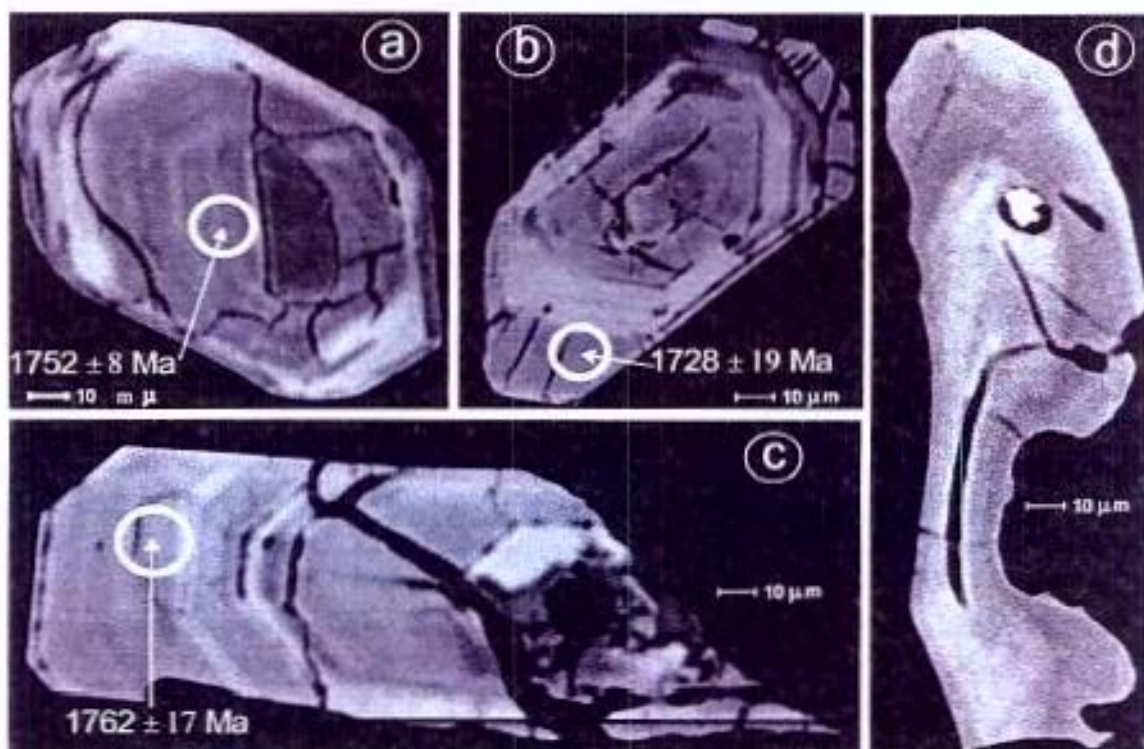


Figure 6. Back-scattered electron image of zircons of the Massaranduba dacite with analytical spots marked by white circles (see text for explanation). (A), euhedral short prismatic crystal showing faint euhedral zoning; (B), zircon displaying a similar habit with well defined euhedral zoning and overgrowth by magmatic crystallization; (C), zircons with overgrowth features; and (D), crystal showing corrosion features in borders and embayments.

The older age population was obtained on cores showing faint euhedral zoning, similar to those found in magmatic-derived zircons (Vavra, 1996). Eight spots considered to be the least altered isotopic site (Nutmann et al., 1991 i.e. low  $f_{206}$  and concordance degree  $>90$  and  $<110\%$ ) were used for age calculations which yielded a weighted mean

$^{207}\text{Pb}/^{206}\text{Pb}$  age of  $1762 \pm 6$  Ma. This age is considered to represent the crystallization age of the studied sample.

The younger age population was obtained on rims showing massive overgrowth and encompassed four analyses. These analyses yielded a weighted mean  $^{207}\text{Pb}/^{206}\text{Pb}$  age of  $1701 \pm 10$  Ma (chi-square = 1.5), and we suggest that it represents the age of the hydrothermal event that affected parts of the volcanic sequence and probably promoted the sulfide ore deposition in the nearby Expedito deposit.

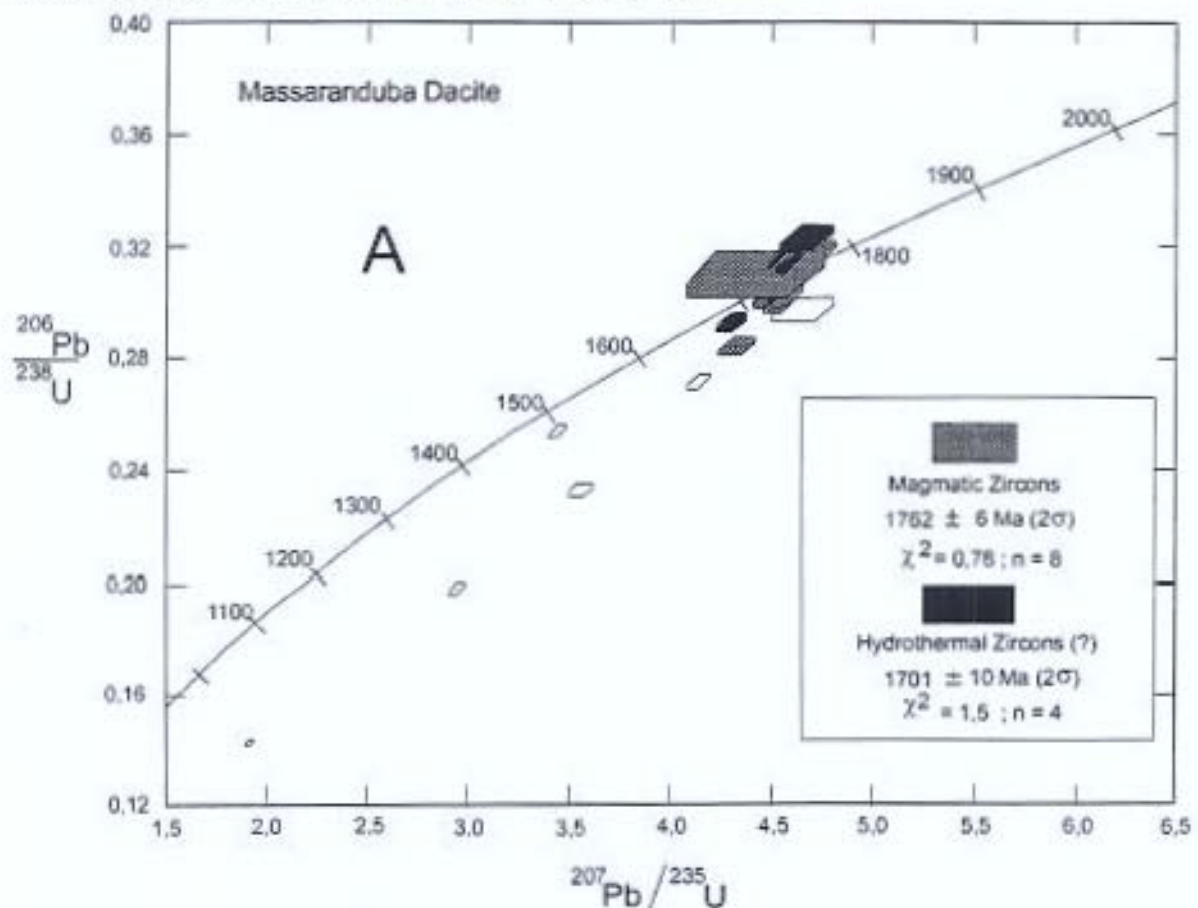


Figure 7. U-Pb concordia diagram for zircons from the Massaranduba dacite.

One single analysis yielded a  $^{207}\text{Pb}/^{206}\text{Pb}$  age of 1847 Ma (spot 32-1) and is considered to represent a xenocryst of metamorphic zircon. Its low U content of 85 ppm supports this. Other zircons were considered disturbed isotopic sites. This is corroborated by their degree of discordance ( $> 10\%$ ) and their tendency to form a chord in which the upper intercept is close to 1.80 Ga and the lower intercept is close to 0 Ga. This might

suggest recent lead loss from part of the magmatic and inherited metamorphic zircons. These zircons were not used for age calculation.

### 6.2. Sample 02 - Paraibão granite

The sample is an undeformed, coarse-grained porphyritic granite. The zircons from this sample consist of euhedral to subhedral short prisms with well-defined pyramidal terminations. They vary from pale yellow to dark caramel brown. The euhedral zoning is present in the majority of the zircons studied. Back-scattered electron observations reveal distinct patterns of zoning (Fig. 8). The most common is euhedral zoning, similar to that occurring in zircons crystallized from magmatic liquids (Vavra, 1996). The uncommon pattern is sector zoning. Elongate prismatic inclusions and fractures are common features in these zircons.

Table 3 SHRIMP data of the zircons of the Sample 2 - Paraibão Granite

Spot N°	U ppm	Th/U (ppb)	Pb (ppb)	$\delta^{206}_{\text{Pb}}$	$\frac{^{207}\text{Pb}}{^{206}\text{Pb}}$	$\pm$	$\frac{^{208}\text{Pb}}{^{206}\text{Pb}}$	$\pm$	$\frac{^{206}\text{Pb}}{^{238}\text{U}}$	$\pm$	$\frac{^{207}\text{Pb}}{^{235}\text{U}}$	$\pm$	Age (Ma)	$\pm$	Conc %
<hr/>															
5-1	221	0.55	58	0.00	0.1087	0.0013	0.1237	0.0026	0.247	0.003	3.71	0.07	1778	22	80
49-1	423	0.58	146	0.00	0.1084	0.0007	0.1645	0.0016	0.313	0.003	4.68	0.06	1772	12	99
7-1	655	0.62	232	0.00	0.1081	0.0005	0.1779	0.0012	0.320	0.003	4.77	0.05	1768	9	101
18-1	218	0.44	74	0.00	0.1080	0.0009	0.1237	0.0019	0.319	0.003	4.75	0.07	1767	16	101
50-1	593	0.78	220	0.00	0.1079	0.0007	0.2221	0.0015	0.323	0.003	4.80	0.06	1764	11	102
16-1	408	0.48	132	0.00	0.1077	0.0008	0.1391	0.0016	0.299	0.003	4.44	0.06	1761	14	96
19-1	331	0.5	122	0.00	0.1076	0.0007	0.1409	0.0014	0.343	0.003	5.09	0.06	1759	12	110
42-1	259	0.49	87	0.00	0.1073	0.0010	0.1422	0.0021	0.311	0.003	4.59	0.07	1753	18	99
50-4	274	0.46	94	0.00	0.1067	0.0010	0.1333	0.0019	0.321	0.003	4.73	0.07	1745	17	103
58-1	294	0.51	102	0.00	0.1064	0.0010	0.1481	0.0018	0.319	0.003	4.68	0.07	1739	17	103
43-1	283	0.67	90	0.00	0.1064	0.0012	0.1963	0.0028	0.281	0.003	4.12	0.07	1739	22	89
6-1	452	0.57	161	0.00	0.1063	0.0007	0.1570	0.0014	0.326	0.003	4.77	0.06	1738	11	105
43-2	229	0.67	83	0.00	0.1063	0.0010	0.1869	0.0023	0.323	0.004	4.74	0.07	1738	18	104
50-2	265	0.58	84	0.00	0.1061	0.0011	0.1531	0.0024	0.291	0.003	4.26	0.07	1734	19	95
18-2	206	0.46	71	0.00	0.1060	0.0011	0.1270	0.0021	0.323	0.004	4.72	0.07	1732	19	104
61-1	254	0.52	80	0.01	0.1060	0.0016	0.1577	0.0035	0.282	0.003	4.12	0.08	1731	27	88
51-1	434	0.6	103	0.00	0.0918	0.0010	0.1674	0.0024	0.216	0.002	2.74	0.04	1464	21	82

In this sample, 17 spots in 14 crystals were analyzed in a single analytical session in which the reproducibility of the U/Pb ratio for the CZ3 standard was  $\pm 1.03\%$ . The results are presented in Table 2 and the U/Pb ratios are plotted in a concordia diagram (Figure 9).

The majority of the analyses are concordant, with the  $^{207}\text{Pb}/^{206}\text{Pb}$  ages varying between 1778 to 1464 Ma and clustering around 1750 Ma. With the exception of 6 sites considered isotopically disturbed (concordance  $<96\%$  or  $>105\%$ ), the weighted mean  $^{207}\text{Pb}/^{206}\text{Pb}$  age for the 11 concordant analyses suggests one single population of  $1755 \pm 5$  Ma (Chi-square = 1.04) that we consider to be the sample's crystallization age. This age is indistinguishable from the crystallization age of  $1762 \pm 6$  Ma determined for the Massaranduba dacite (Sample 01).

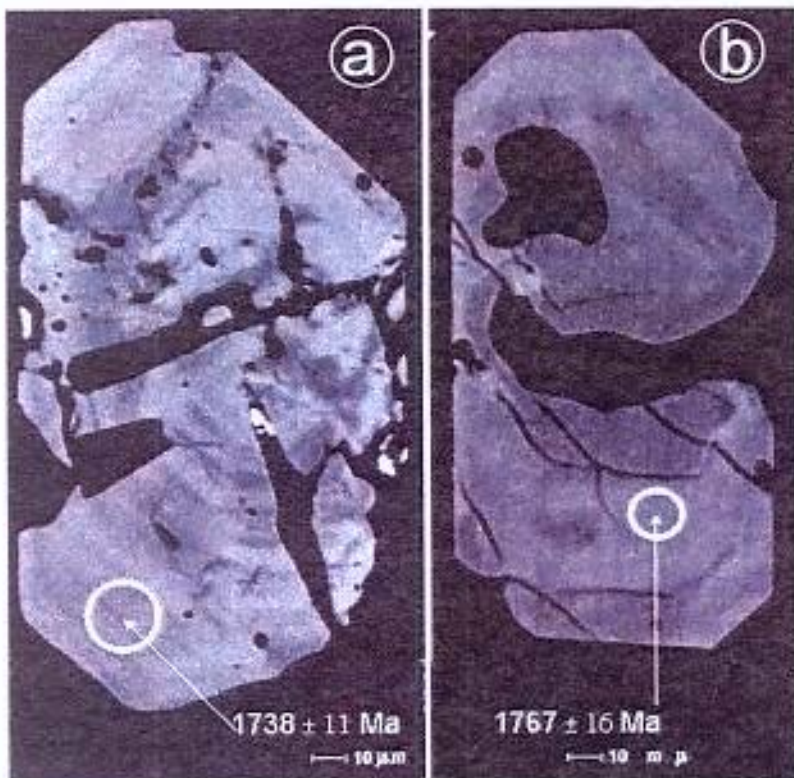


Figure 8. Back scattered electron image of zircons of the Paraibão Granite. (A), euhedral short prismatic crystal showing faint euhedral zoning; and (B), crystal showing sector zoning and corrosion features in borders and embayments.

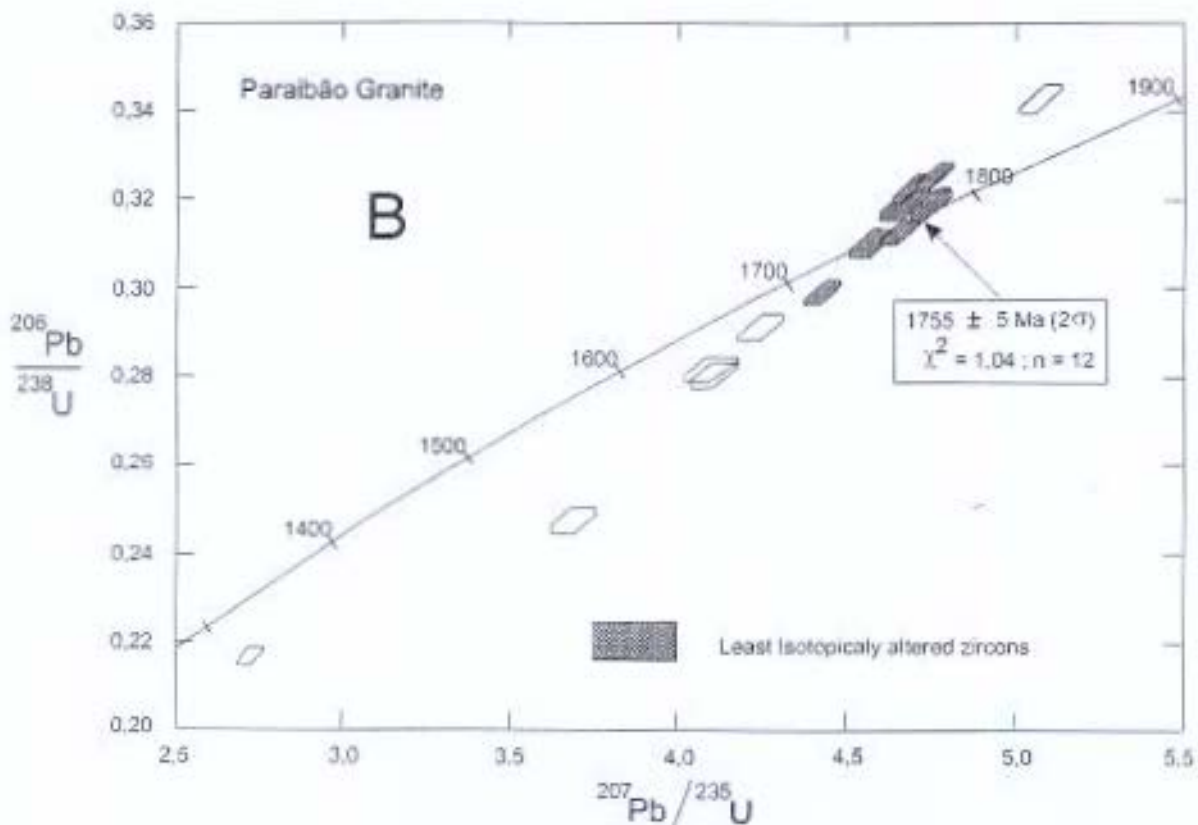


Figure 9. U-Pb concordia diagram for zircons from the Paraibão Granite.

## 7. Discussion

The Amazonian craton has large areas where volcano-plutonic rock associations are encountered. These bodies are similar in composition, being mostly felsic with intraplate affinity. In the northern portion of the craton, in the Guiana Shield, the Surumu Formation is a representative of volcano-plutonism for which the U-Pb age is  $1966 \pm 9$  Ma (Schobbenhaus et al., 1994). Recently, a distinctly younger age of  $1753 \pm 3$  Ma was obtained for the Waiapi granites, which are interpreted as an A-Type granite (Vasquez, 2001). This granite has characteristics similar to the Aripuanã granite of this study. In the southern part of the craton, two other volcano-plutonic associations are recognized. The first occurs in the south of Pará State and is known as the Iriri Formation; it yields an age of  $1888 \pm 2$  Ma (Vasques et al., 1999).

The second association in the southern part of the craton is located in the southwestern Amazonian craton. It ranges over most of the boundary region between Mato

Grosso and Pará States and between Mato Grosso and Rondonia States, covering the Teles Pires, Juruena, Aripuanã, and Roosevelt river basins in the southern part of the Amazon River basin. In this formation, the following U-Pb ages have been reported:  $1740 \pm 8$  Ma in the Roosevelt dacite (Santos, 2000),  $1760 \pm 12$  Ma in the Teles Pires Suite (Santos, 2000), and  $1761 \pm 12$  Ma in the Moriru River district (Pinho et. al., 1999). Finally, ages of  $1755 \pm 6$  Ma and  $1762 \pm 6$  Ma were found in the volcanic and plutonic rocks of Aripuanã (this work). These U-Pb ages around 1.76 Ga suggest that the Paleoproterozoic felsic magmatism of the Amazonian Craton may be due to a widespread genetic process acting in various areas.

One hypothesis for the southwestern Amazonian craton is magma generation by underplating and rifting. This is supported by similar magmatic manifestations in spatially distinct districts, absence of compressional orogenic evidence such as deformation features, widespread rifting in the Southwestern Amazonian craton, and the lack of evidence of processes characteristic of continental. Another hypothesis, collision-related rifting, is hampered by the absence of immature clastic sedimentation and the occurrence of large volumes of extrusive rock. Keavey and Vine (1992) consider these criteria as characteristic of rifting by continental rupture.

A last hypothesis is that the magmatism under study might be an intracratonic reflex of the "Alto Jauru" orogen (Geraldes et al., 2000), which has U/Pb ages of 1.79 to 1.74 Ga. Several lines of evidence have been reported which indicate that alkaline granites generated in a rift environment and/or above mantle plumes are related to continental margin orogenies. This lead Karlstrom et al. (1999) to interpret intracraton events generating A-type granites in the southwestern United States as distant reflexes of subduction and transcurrent tectonism near plate margins.

## 8. Tectonic Model

Montalvão et al. (1984) proposed a tectonic evolution model where rifting via crustal rupture triggers the sequence of events and in which the Uatumã Group is associated with a rifting stage in an environment subject to slow subsidence rates. These authors consider that in the initial stages a crustal thinning occurred, favoring the formation of an intermediate or even oceanic crust. The extraction of lower crust material would

presumably generate an event where the vertical displacements predominate. The rising mantle material would be counterbalanced by subsidence phenomena forming an environment of rifts and collapsed volcanic structures. These would both be filled by ascending diapirs as well as by volcanic and sub-volcanic co-magmatic rocks.

A model compatible with the available data suggests that underplating of mafic magma and upwelling of hot asthenosphere (Fig.10) triggered partial melting in the lower crust under several areas of the southwestern Amazonian Craton. Extensive volcanism and plutonism was generated by this mechanism, with the building of very large volcanic structures (diameter  $>> 100$  km). The collapse of these volcanic complexes formed caldera structures, the diameter of which is many times greater than the original volcanoes along with their multiple included vents. As the magmatic event vanished, the continuation of the vertical adjustments generated environments for the accumulation of huge amounts of pyroclastic material. These basin shaped volcanic traps were also favorable structures for deposition of thick accumulations of chemical sediments including exhalites, cherts, and fine-grained volcanogenic sedimentats, which mark the final stages of volcanism. Under these conditions, the conjunction of active volcanism, synvolcanic faults, and the availability of hydrothermal fluids probably combined to make favorable environments for exhalative deposits. High rates of subsidence in sub-aquatic depositional environments and concomitant deposition of the clastic sedimentary unit (Dardanelos Formation) lead to conditions of tectonic quiescence necessary for the formation of the exhalative deposits. Almeida (1974) considered Dardanelos Formation deposition simultaneous with igneous activity of the Uatumã Group. Finally, a rift stage occurred, generating block-faulting structures by dextral transtensional kinematics and characterized by vertical movements in a broadly extensional setting, probably reflecting collision phenomena anywhere in the cratonic environment.

The widespread preservation of the transition zones between volcanic and plutonic rocks suggests that subvolcanic and shallow intrusives have risen resurgently into the roofs of calderas or other volcanic structures, and therefore do not represent the volcanic supply chambers.

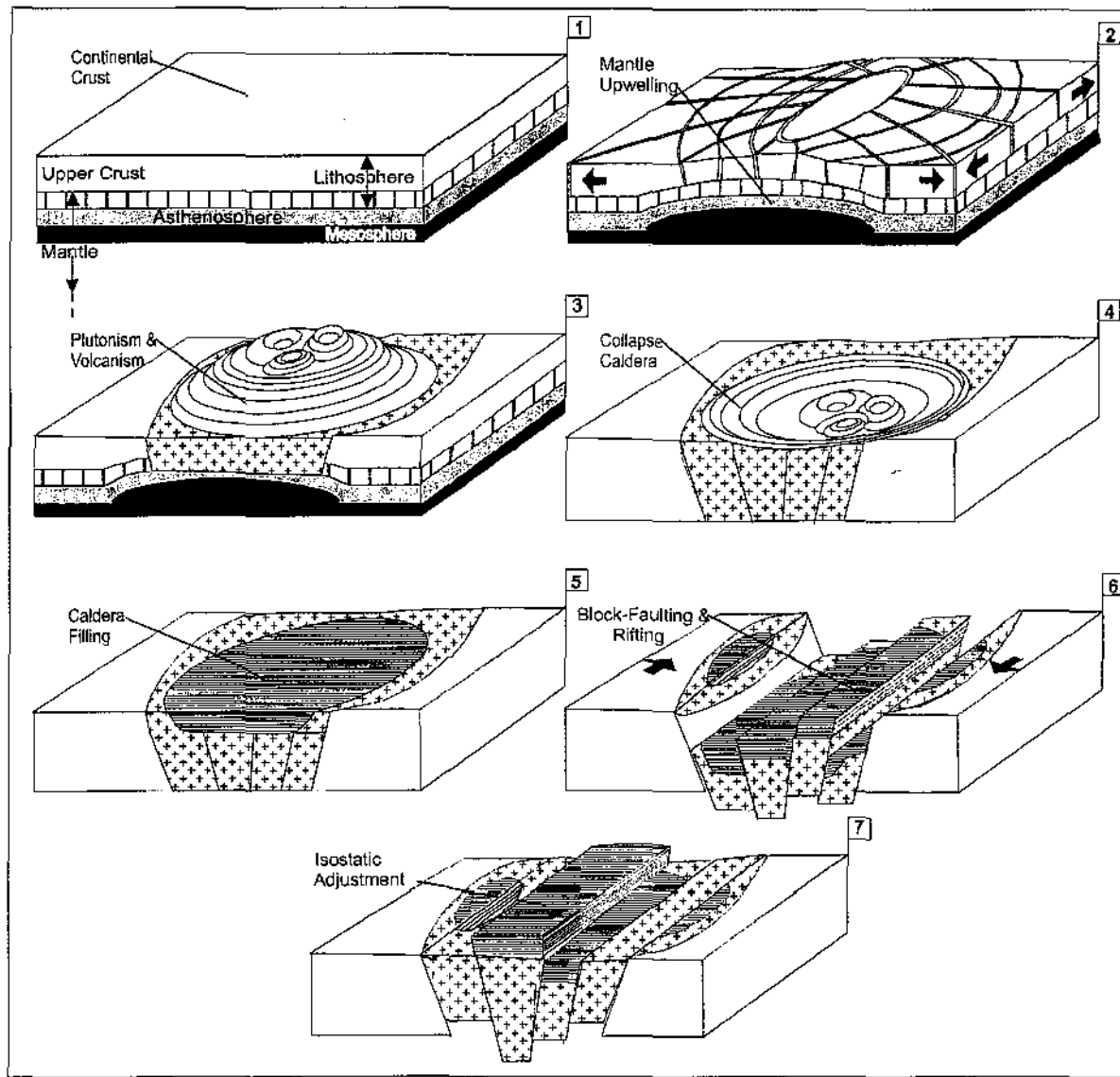


Figure 10. Series of block diagrams showing the sequence of tectonic episodes in the Aripuanã region. (1), initial configuration; (2), mantle underplating of mafic magma and upwelling of hot asthenosphere; (3), extensive plutonism and volcanism with predominance of massive felsic flows; (4), caldera subsidence originating a large basin-shaped volcanic depression; (5), caldera initially filling with huge amounts of pyroclastic, followed by chemical sedimentation and by detritic material in the vanishing stages of volcanism; (6), rifting stage and block faulting by crustal extension in response to dextral transtension; and (7), isostatic adjustments.

## **9. Conclusions**

The Aripuanã volcano-plutonism is dominated by epizonal granitoid rocks intruded into a sequence of felsic volcanics along with its explosive products. Uncommon interlayering of basalts also happens in this sequence. These events occurred during the interval 1762 to 1755 Ma. Its evolution is marked by the absence of evidence of an orogenic event and by the undeformed character of the associated granitic plutonism. This suggests that the cratonic evolution has taken place by mantle activation in an intracontinental environment, through broadly extensional events and a long duration of rifting, which prevailed during the late Paleoproterozoic and early Mesoproterozoic.

Thick preserved tuffaceous sequences, nearly circular structures in intrusive granitoids, close association between pyroclastic, subvolcanic and intrusive rocks, and the absence of effects of contact metamorphism are frequent and notable features at several sites. These features are surface geological evidence that we interpret as indicative of passive emplacement of plutonic bodies in epizonal levels.

We believe that the absence of marked stratigraphic discordance, persistence of the geochemical features of the volcanic rocks, geochemical bimodality of the volcanics without any noticeable compositional trends, and absence of folding are evidence that the Aripuanã district was stabilized during the Mesoproterozoic, after intense magmatic activity in an ensialic extensional setting. This stabilization was temporally followed by, or even culminated with, the deposition of wide sedimentary basins in a rifting environment, suggesting that the magmatism of the district accompanied an extensional deformation phase.

The wide area of similar magmatism with the generation of similar rocks in the whole of the Amazonian craton suggests that these additions of crustal material happened during magmatic episodes which, although discreet in occurrence, were derived from similar tectono-magmatic mechanisms.

## **Acknowledgements**

The authors are grateful to Dra. Jacinta Enzweiler for technical support in geochemistry. Early versions were substantially improved by reviews by M. C. Geraldes, A. Choudhuri, K. C. Condie, and W. R. Van Schmus.

## References

- Almeida, F.F.M., 1974. Evolução Tectônica do Cráton do Guaporé Comparada com o Escudo Báltico. *Revista Brasileiro de Geociencias* 4, 191-204.
- Compston, W., Williams, I.S., Meyer, C., 1984. U-Pb geochronology of zircons from lunar breccia 73217 using a sensitive high mass-resolution ion microprobe. *J. Geophys. Res.* 89, 525-534.
- Costa, J.B.S., Hasui, Y., 1997. Evolução geológica da Amazônia. In: Costa, M.L. and Angélica, R.S., (Eds.), *Sociedade Brasileira de Geologia, Contribuições à Geologia da Amazônia*, p. 15-90.
- Dall'Agnol, R., Lafon, J.M., Macambira, M.J.B., 1994. Proterozoic anorogenic magmatism in the Central Amazonian Province, Amazonian Craton: geochronological, petrological and geochemical aspects. *Mineral Petrology* 50, 113-138.
- de Laeter, J. R., Kennedy, A . K., 1998. A double focusing mass spectrometer for geochronology. *International Journal of Mass Spectrometry* 178, 43-50.
- Eby, G. N., 1990. The A-Type granitoids: a review of their occurrence and chemical characteristics and speculations on their petrogenesis. *Lithos* 26, 115-134.
- Geraldes, M.C., Teixeira, W., Van Schmus, W.R., 2000. Isotopic and chemical evidence for three accretionary magmatic arcs (1.79-1.42 Ga) in the SW Amazon Craton, Mato Grosso State, Brazil. *Revista Brasileira de Geociências* 30(1), 99-101.
- Irvine, T.R., Baragar, W.R.A., 1971. A guide to the chemical clasification of the common volcanic rocks. *Canadian Journal of Earth Sciences* 8, 523-548.
- Karlstrom, K.E., Harlan, S.H., Williams, M.L., McLelland, J., Geissman, J.W., Ahäll, K.I., 1999. Refining Rodinia: Geologic Evidence for the Australia – Western U.S. connection in the Proterozoic. *GSA Today* 9 (10), 4-7.
- Kearey, P., Vine, F.J., 1994. Global tectonics. Oxford, Blackwell Scientific Publications, 302 pp.
- Le Maitre, R.W., Bateman, P., Dudek, A., Keller, J., Lameyre Le Bas, M. J., Sabine, P. A., Schmid, R., Sorensen, H., Streickeisen, A., Wooley, A.R., Zanettin, B., 1989. A classification of igneous rocks and glossary terms. Oxford, Blackwell Scientific Publications, 193 pp.

- Maniar, P.D., Picolli, P.M., 1989. Tectonic discrimination granitoids. Geological Society of America Bulletin 101, 635-643.
- Miyashiro, A., 1974. Volcanic rock series in volcanic arcs and active continental margins. American Journal of Science 274, 321-355.
- Montalvão, R.M.G., Bezerra, P.E.L., Drago, V.A., Cunha, B.C.C., 1984. Cobertura de plataforma da Amazônia sua sedimentação e evolução tectônica. Anais do XXXIII Congresso Brasileiro de Geologia, Rio de Janeiro, 2101-2123.
- Neder, R.D.N., Figueiredo, B.R., Beaudry, C., Collins, C., Leite, J.A.D., 2000. The Expedito Massive Sulfide deposit, Mato Grosso. Revista Brasileira de Geociências 30(2), 222-225.
- Nuttmann, A., Kinny, P.D., Compston, W., Willian, J.S., 1991. Shrimp U-Pb zircon geochronology of the Narrier Gneiss Complex, Western Australia. Precambrian Res. 52, 275-300.
- Pearce, J. A., Cann J. R., 1973. Tectonic setting of mafic volcanic rocks determined using trace element analyses. Earth and Planetary Science Letters 19, 290-300.
- Pearce, J. A., 1982. Trace element characteristics of lavas from destructive plate margins. In: Thorpe, R. S. (Ed.), Andesites, orogenic andesites and related rocks. Chichester, Wiley & Sons, 525-548.
- Pearce, J.A., Harris, N.B.W., Tindle, A. G., 1984. Trace element discrimination diagrams for the tectonic interpretation of granitic rocks. J. Petrol., 25, 956-983.
- Pinho, M.A.S.B., Lima, E.F., Chemale Jr., F., 1999. Geologia da região do Moriru - Dados preliminares da Formação Iriri-Aripuanã - Mato Grosso. Boletim de Resumos, Programa VII Simpósio de Geologia do Centro-Oeste e X Simpósio de geologia de Minas Gerais, Brasília, p. 14.
- Pinho, M.S.A.B., Pinho, F. E. C., Quadros, A. P., Chemale Jr., F., 2001. Discussao do Termo Uatumã-Iriri, Região Norte do Estado de Mato Grosso – Brasil. Resumos Expandidos –VII Simpósio de Geologia da Amazônia, Sociedade Brasileira de Geologia, Belém, 15-18.
- Santos, J.O.S., 2000. Os terrenos paleoproterozóicos da Província Tapajós e as mineralizações de ouro associadas. Ph. D. thesis, Univ. Federal do Rio Grande do Sul, Porto Alegre-RS, 209 pp.

- Schobbenhaus, C., Hoppe, A., Lorke, A., Baumann, A., 1994. Idade U/Pb do magmatismo Uatumã no norte do Cráton Amazônico. Escudo das Guianas (Brasil): primeiros resultados. Sociedade Brasileira de Geologia, XXXVIII Congresso Brasileira de Geologia Extended Abstracts 2, 395-397.
- Silva, H.A., Leal, J.W.L., Montalvão, R.M.G., Bezerra, P.E.L., Pimenta,O.N.S., Tassinari, C.C.G., Fernandes, C.A.C., 1980. Geologia. In: Projecto RADAM-BRASIL, Folha SC-21 Juruena, DNPM/MME, Rio de Janeiro, 21-116.
- Smith, J.B., Barley, M.E., Groves, D.I., Krapez,B., McNaughton, N.J., Bickle,M.J., Chapman, H.J., 1998. The Scholl shear zone, West Pilbara: evidence for a terrane boundary structure from integrated tectonic analyses, SHRIMP U/Pb dating and isotopic and geochemical data of granitoids. Precambrian Research 88, 143-171.
- Trompette, R., Carozi, A.C. 1994. Geology of Western Gondwana. A.A.Balkema, Rotterdam, 350 p.
- Tassinari, C.C.G., 1996. O Mapa Geocronológico do Cráton Amazônico no Brasil: Revisão dos dados isotópicos. Tese de livre Docência, Instituto de Geociências, Universidade de São Paulo, 139 p.
- Tassinari,C.C.G., Cordani, U.G., Nutman, P., Van Schmus, W.R., Bettencourt, J.S., Taylor, P.N., 1996. Geochronological systematics on basement rocks from the Rio Negro-Juruena Province (Amazonian Craton) and tectonic implications. Intl. Geol. Review 38, 161-175.
- Tassinari, C.C.G., Macambira, M.J.B., 1999. Geochronological provinces of the Amazonian Craton. Episodes, 22(3), 174 -181.
- Vavra, G., 1994. Systematics of internal zircon morphology in major Variscan granitoid types: Contributions to Mineralogy and Petrology 117, 331-44.
- Vasquez, M.L., Klein, E.L., Quadros, M.L.E., Bahia, R.B.C.; Santos, A., Ricci, P., Sachett, C.R., Silva, C.M.G., Macambira M.J.B. 1999. Magmatismo Uatumã na Província Tapajós – Novos dados geocronológicos. VI Simpósio de Geologia da Amazônia. Ext. Abst. Bull. 471-474.
- Vasquez, M.L., Klein, E.L., Ricci, P.S.F. 2001. Granitóides pós-colisionais da porção leste da Província Tapajós. VII Simpósio de Geologia da Amazônia. Ext . Abst. Bull. 46-54.

## CAPÍTULO 4

### THE VHMS Zn-Pb EXPEDITO DEPOSIT, WESTERN BRAZIL: MINERALOGY, MINERAL CHEMISTRY AND ISOTOPIC DATA

#### Abstract

The Expedito Zn-Pb deposit is located in the southwestern portion of the Amazonian Craton in the Aripuanã mining district. Mineralization is associated with a Paleoproterozoic volcano-plutonic predominantly felsic association correlated to the Uatumã Group.

Drill-core studies of the main ore body (Valley deposit) point to a model in which metal deposition occurred in a subsea-floor environment by replacement of high primary porosity and permeability volcanic rocks along a system of synvolcanic and hydrothermal fissure faults. In addition, the deposit displays some peculiar mineral and textural relations as part of the sulfides are substituted by massive and semi-massive magnetite in association with the development of an assemblage of calc-silicate minerals.

Replacement fronts in the deposit are difficult to interpret from drill core, but it is suggested that Ca-Na-Fe-CO<sub>2</sub> rich fluids were formed through interaction of magmatic and circulating seawater channeled by the same system of synvolcanic faults that controlled the formation of the original massive sulfide deposit.

Application of chlorite and arsenopyrite thermometers yielded temperatures of 300 to 350°C for ore formation consistent with the values for volcanogenic deposits. Deeper portions of the deposit may have undergone further heating at elevated oxygen partial pressure as suggested by arsenopyrite compositions and by the occurrence of the magnetite-bearing calc-silicate alteration assemblage.

Lead and strontium isotopic compositions of sulfides and carbonate are consistent with Upper Crust fluid and metal sources. A volcanogenic origin for the deposit is proposed here due to the similarity of galena Pb-Pb model age (1,75 Ga) with U-Pb zircon age of volcanic and plutonic rocks (1,76-1,75 Ga) along with the intimate association of the mineralization with host rocks. The deposit was formed during the last stages of a magmatic-tectonic-hydrothermal event that occurred in the interval 1,76-1,75 Ga. The lead isotopic data for K-feldspar and a Rb-Sr isochron for sphalerite leachates are consistent with a later tectonic event at 1,1 Ga with little influence on the Expedito deposit.

## **Introduction**

The Expedito Pb-Zn deposit is the largest ore deposit up to now described in the Amazonian Craton in association with the felsic volcanic, sub-volcanic and plutonic rocks of the Uatumã Group. It belongs to the Aripuanã ore district located 14 km north of Aripuanã town in Mato Grosso State, Brazil (Fig. 1). In the last years, several pipe and vein-style volcanic associated Zn-Pb massive sulfide deposits have been described in the Aripuanã district, however, the present report is focused only in the best investigated orebody locally known as the Valley deposit.

In the present study, the relationships between volcanism, hydrothermal alteration and mineralization processes have been approached by means of field evidences, drill-core examination, petrographic and chemical studies. Previous studies on the Expedito deposit have led to an interesting debate and divided opinions regarding the origin of the mineralization and about the metallogenetic potential of the Amazonian Craton for VMS or VHMS deposits.

Most research in the worldwide Archean to Cenozoic volcanic-associated massive sulfide deposits have concentrated on conformable deposits among which the common morphological type is of mound, lens and blanket, according to the classification of Large (1992). These deposits are considered to have formed on the sea floor where circulating hot seawater and bacterial activity play the main role during sulfide deposition.

On the other hand, vein and pipe-style, including crosscutting discordant deposits that form from well-focused hydrothermal fluids moving along faults and replacing the adjacent wall rocks, as recognized in the Aripuanã district, differ from the classical mound-style VMS in the sense that they are better explained in terms of predominance of sub sea-floor sulfide deposition.

The aim of this paper is to present a detailed mineralogical and chemical description of the metallic mineralization and hydrothermal alteration of the Expedito Zn-Pb deposit. Strontium and lead isotopic studies were carried out in support of the genetic model and tectonic evolution of the deposit.

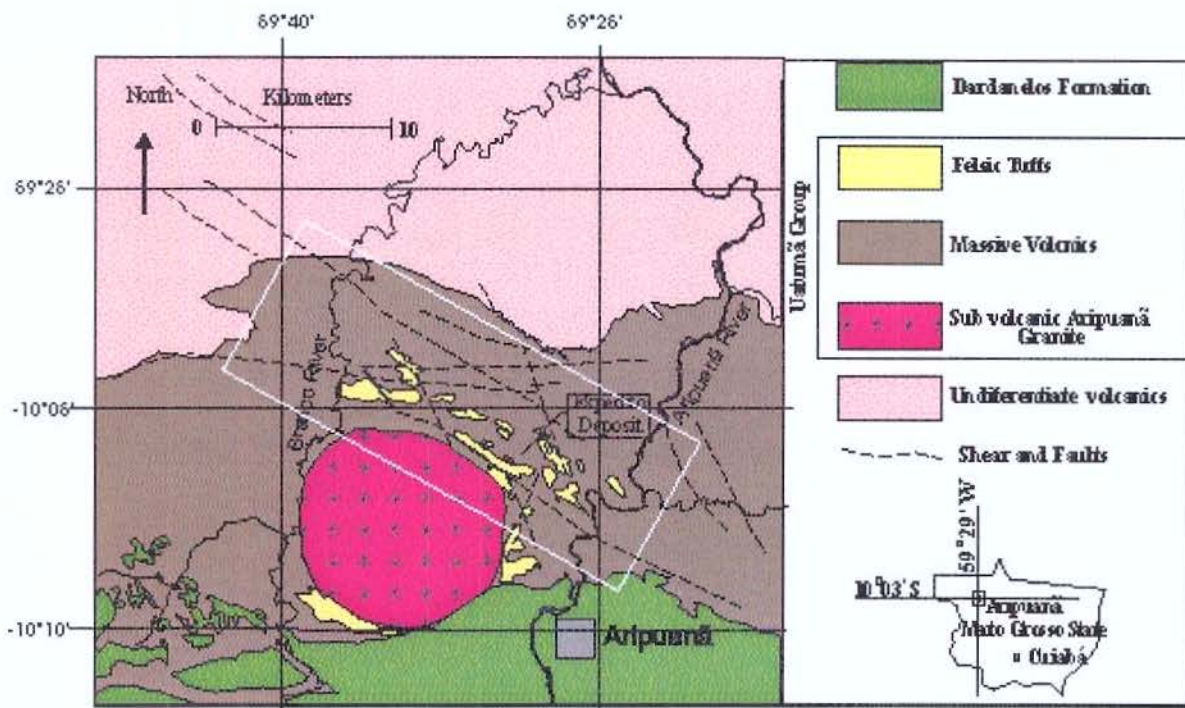


Fig. 1. Geologic map of the Aripuanã Area showing the location of the metallogenic district (rectangle) and of the investigated deposit.

## Background

The Expedito deposit was discovered in 1990 by a group of prospectors led by Expedito José Rodrigues. At that time, they were searching in the slopes of the mountains for the probable primary source of gold previously exploited from alluvial sediments. Subsequently, the Canadian mining company Rio Taboco made an attempt to assess the gold mineralization by diamond drilling which led to the discovery of an unsuspected massive sulfide mineralization. Later works, including geological mapping and soil geochemistry helped to identify various zones where sulfide bodies, including the so-called Valley and Gossan Hill, crop out.

Independent prospection in adjacent areas by Noranda Mines and Anglo American included extensive drilling, soil geochemistry and terrestrial and aerial geophysics which led to identification of other outcrops of gossans and underground extensions of the Zn-Pb mineralization.

The gold mineralization found at first by prospectors turned out to be a secondary enrichment zone associated with faults along which gold was re-mobilized from the primary sulfide ore.

The reported reserves of the Expedito deposit account for 11.65 millions metric tons @ 6.29 % Zn, 2.25 wt% Pb, 0.07 wt% Cu, 65 g/t Ag, 0.25 g/t (Ambrex, Public News Release, 1998). Presently, a re-assessment of the mineral district is being conducted by a joint venture led by the Anglo America company and the new results point to a substantial increase of measured reserves and to the characterization of an important base metal and gold metallogenic district in central-western Brazil.

### **Regional geology**

The geology of the Aripuanã district (Fig. 1) has been previously described by Neder et al. (2000). It comprises an area of some 30 km east west by 30 km north south, located near the eastern border of the Rio Negro–Juruena geochronological province of Tassinari (1981).

The district is dominated by a Paleoproterozoic supracrustal sequence comprising mainly pyroclastic and massive acid volcanics and subordinate volcanogenic sedimentary and basic rocks.

The volcanics are intruded by several shallow intrusive and subvolcanic plutons and form a roughly EW trending volcano-plutonic belt. Zircon U-Pb ages of volcanic and plutonic rocks fall in the time interval 1,768 - 1,750 Ga. This geologic unit was assigned by Neder et al. (2002) as the Volcanic-Plutonic Association of Aripuanã and includes volcanic and plutonic rocks, which display similar chemical compositions and clear cogenetic features.

These volcanic rocks and associated undifferentiated plutonic suite are informally considered as correlated to the Iriri Formation of the Uatumã Group, defined in 1943 by Oliveira & Leonardos (Almeida, 1974), of widespread occurrence in the Amazonian Craton. The volcanic rocks are acidic and grade from rhyolite to dacite with lesser amounts of basaltic rocks attesting the bimodal character of the sequence. Volcaniclastic rocks, chert and laminated siltstone and mudstone, interpreted as volcanogenic sediments, predominate in the study area. The plutonic and sub-volcanic rocks include anorogenic high-K, A-type

granites and equivalent porphyritic rocks.

The wide range and thick occurrence of pyroclastic rocks and intimate association with epizonal plutons suggest passive positioning of intrusions in the volcanic sequence by subsidence structures. This interpretation is also supported by the lack of metamorphism and folding, only present in fault and sheared zones, suggesting extensional environment where graben and caldera prevail.

Although welded structures were not observed in the acid pyroclastics, the common bedding and banding structures indicate that the volcanic rocks represent mainly subaqueous deposit. Other features that also suggest this are the fine interbedding of volcaniclastics and chemical sediments (cherts) as well as rapid changes of the different lithologic units.

Overlying the volcanic rocks, there occurs the Dardanelos Formation, a sedimentary unit formed by conglomerates and sandstones grading upwards to shale.

### **Geology of the ore deposit**

The Expedito deposit is hosted within a thick sequence of pyroclastic and volcanogenic sedimentary rocks weathered to depths in excess of 50 m and consists of massive and semi-massive Zn-Pb ores and minor disseminated Cu-Au mineralization.

The predominant volcanic host rocks include crystal and lapilli tuffs that are interpreted as submarine record of a distal volcanic center of unknown localization.

The base-metal sulfide are stratabound within the volcanic sequence, but do not show stratigraphic control in the scale of volcaniclastic layers.

The orebodies have been modified by deformation and in the Valley ore body occur as a continuous belt oriented toward northwest and inflecting southwards in the SE part of the area (Fig. 2).

This field evidence indicates that the orebodies form one single belt, representing the actual trace of a system of synvolcanic fault that channeled the hydrothermal fluids at the time of the mineralization. The tabular orebodies in the Expedito deposit dip to northeast and drill log data integration demonstrates a NW plunging in the Valley and surrounding area.

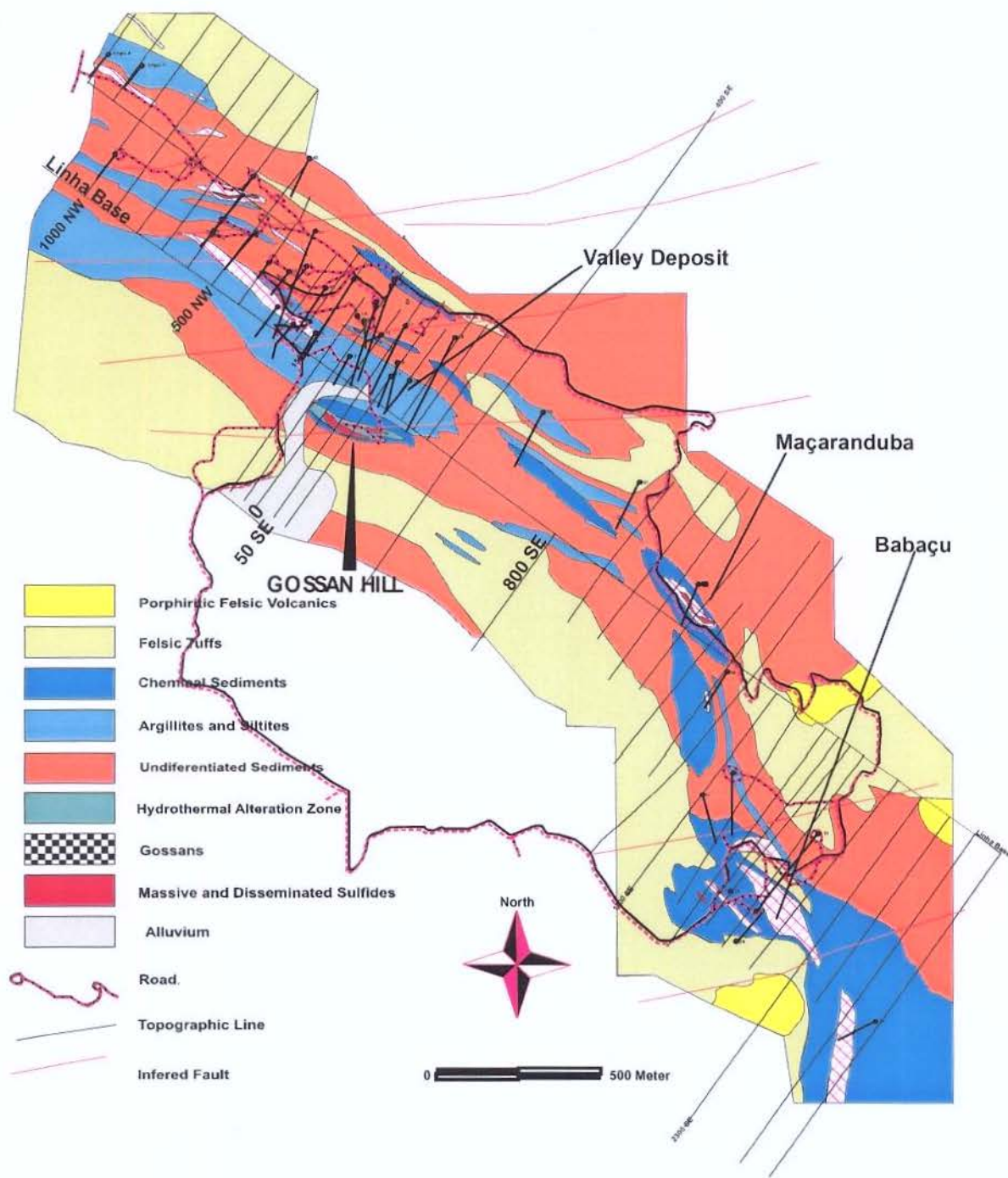


Fig. 2. Geologic map of the Serra do Expedito area modified of Collins and Monteiro (1998)

The hydrothermal alteration envelope is highly strained reflecting the significant phyllosilicate content of these lithologies in comparison to unaltered rocks. Furthermore, deformation textures of ores suggest that mineralization predates deformation.

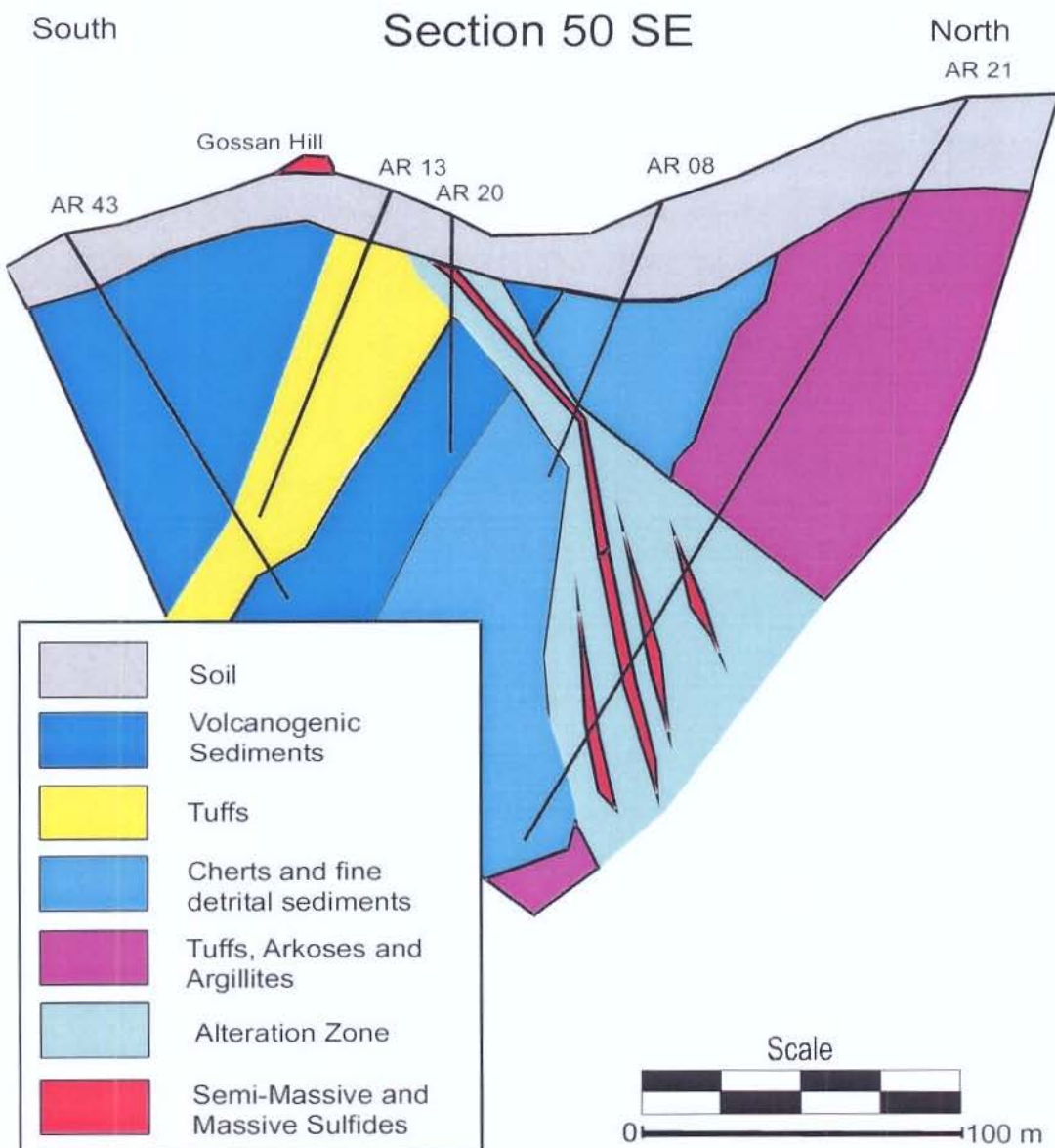


Fig. 3. Geological section at the Gossan Hill showing the relationship between mineralization, hydrothermal alteration zones and country rocks (localization indicated in Fig. 2).

The orebodies present normal sulfide mineralogy for volcanogenic deposits consisting of pyrite, pyrrhotite, sphalerite, galena, chalcopyrite and minor arsenopyrite. On the other hand, the alteration is atypical by presenting chloritic zones locally associated with actinolite and magnetite.

Presently, several gossan exposures are recognized, and the most prominent of which is the 'Gossan Hill', a 40 m thick oxidized ore zone that extends for more than 150 m along strike. A geologic section at this site indicates that sulfide mineralization and respective alteration and brecciation zones are discordant and formed by several vein and pipe-style ore bodies (Fig. 3).

### **Materials and analytical techniques**

Representative samples of all ore types, alteration zones and wall rocks were studied by optical petrography and electron microprobe techniques. The chemical compositions of minerals were determined in a Jeol - JXA - 8600S electron microprobe at the University of São Paulo using high quality mineral standards and routine experimental conditions as the take off angle of 40 degrees, accelerating voltage of 15 kV and a current of 26  $\mu$ A in the sample, integration time of 5-10 s and electron beam diameter of 1-10  $\mu$ m.

Furthermore, Pb and Sr isotopic studies were carried out for some samples. Galena and K-feldspar were selected for Pb isotopic analyses. The galena crystals were powdered in agate pestle and mortar to obtain 0.2 g of material and the powder was dissolved in hot nitric acid. After evaporation in filtered air environment the residue was loaded on Re filament with phosphoric acid and silica gel. Pb isotope compositions are normalized to NBS 981, analyzed repeatedly during the analytical work.

Determination of Sr isotopic compositions was performed for pure calcite and sphalerite, which were separated by handpicking and then powdered in agate pestle and mortar. The samples were also analyzed by X-ray fluorescence for the determination of the Rb and Sr concentrations. Afterwards, the samples were dissolved in a mixture of fluoridic, chloridic and perchloric acids and the Sr was concentrated by standard cation exchange. The product was deposited on Ta filament.

All the isotopic analyses were obtained on a VG-354 mass spectrometer at the Isotope Laboratory of the University of São Paulo.

## Results

### Petrographic studies

The sulfide ore of the Expedito deposit consists of large amounts of sphalerite and galena associated with pyrite and pyrrhotite with minor chalcopyrite and arsenopyrite. In massive sulfide layers, pyrite contributes with more than 50% of the sulfide mineral composition. Sulfides also occur disseminated in host rocks and forming veins and stringers. Gangue mineralogy consists predominantly of quartz, chlorite, calcite and actinolite.

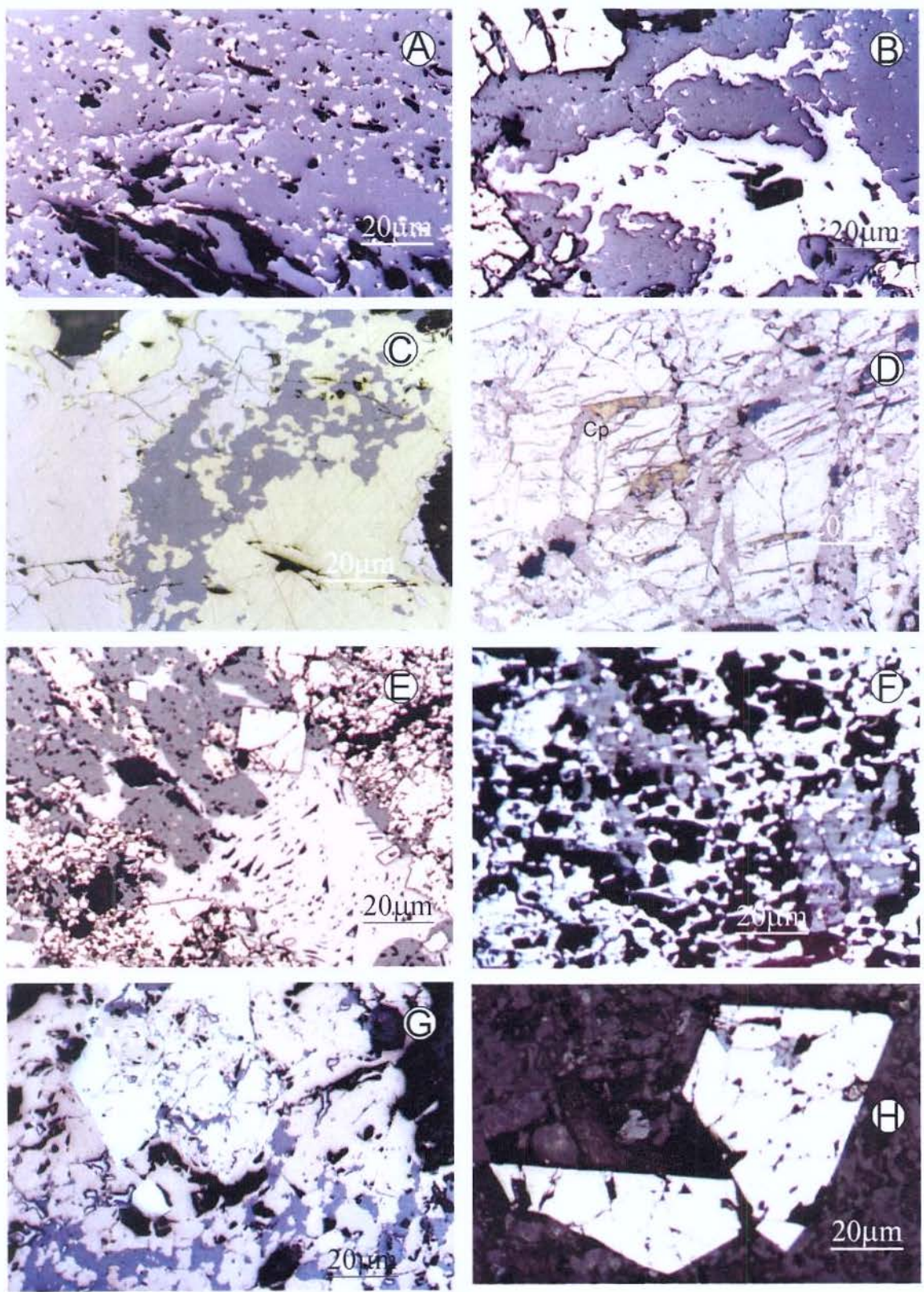
In the massive sulfide, the sphalerite is fine-grained and frequently displays chalcopyrite disease textures. Mostly, the sphalerite is opaque with its distinct metallic luster (Fig. 4A and 4B), but there were rarer occurrences as coarse-grained crystal with brown glassy luster in the transparent form. Galena occurs in vein and segregation in well defined levels associated with sphalerite, pyrite and pyrrhotite, in inclusions in sphalerite and filling open spaces in fractured sphalerites and pyrites (Fig. 4D), demonstrating its ductile behavior in the deformed zones of the orebodies. Chalcocite is rare and displays evidences of substitution by pyrrhotite and magnetite.

Pyrite occurs in euhedral and anhedral crystals (Fig. 4E) and are ubiquitous in ore and alteration halo involving the deposits. Magnetite occurs as subhedral porphyroblasts substituting sulfides, chlorites and actinolite (Fig 4F). Arsenopyrite occurs as idiomorphic (Fig 4H) grains disseminated in alteration zones and in restricted levels in the disseminated sulfides (Fig 4G). Pyrrhotite occurs as granular crystals and as linear blebs in sphalerites.

Calcite occurs always in association with actinolite filling fractures. Actinolite occurs in the tabular form and as acicular aggregates (Fig 4I). Veins with calcite, sphalerite, pyrite and pyrrhotite with crustiform features demonstrate its high level, near surface formation (Fig 4J).

The subsurface data obtained by diamond drill logs show that alternate zones of massive and semi-massive sulfides are symmetrically enveloped by an alteration zone in an undifferentiated felsic volcanic or/and volcanogenic sediment protholit. This alteration envelope shows the following general characteristics:

- 1- An outer zone marked by very strongly pervasive sericite alteration;



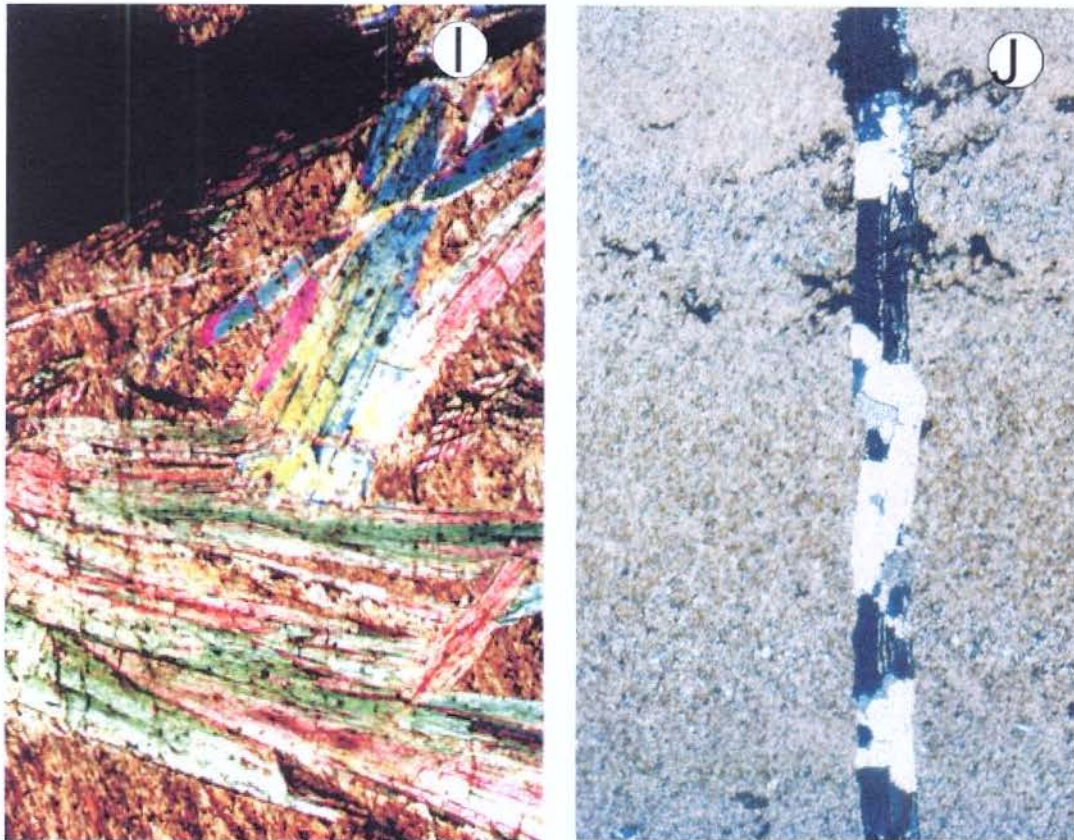


Fig 4. Microphotographs of representatives examples of ores. A. Sphalerite in massive sulfide ore with inclusions of galena and very fine chalcopyrite disseminated and euhedral pyrite. B. Galena intruding cavities in sphalerite groundmass. C. Pyrrhotite substituting sphalerite. D. Sphalerite and chalcopyrite filling fractures in pyritic ore. D.Euhedral and anhedral pyrites with sphalerite and galena displaying characteristic pits. E. Magnetite replacing sphalerite. F. Fractured arsenopyrite injected by arsenopyrite in pyrrhotite sphalerite groundmass. G.Fractured arsenopyrite with inclusion of sphalerite in chloritic groundmass. I..Aggregates of acicular actinolite in chloritic groundmass. J. Crustiform vein with quartz, calcite and sphalerite in tuff.

2- Followed inward by a silicified zone with millimeter sized disseminated pyrite grains;

3- An inner zone, approximating the massive and semi-massive sulfides orebodies, enriched by chlorite with very dull luster which is accompanied, in some places, by strong

calc-silicate alteration formed by acicular textured actinolite in ubiquitous calcite veining domains.

Recognized by its green to white colors, these rocks are strongly brecciated and carbonated indicating fault and shearing zones with fragments of chert in a matrix of very fine-grained massive granular chlorite. Black porphyroblastic magnetite occurs associated with the chlorite and calc-silicate alteration. The relationship between magnetite, calc-silicate alteration minerals and sulfides seems to indicate that magnetite assemblage overprinted sulfides and the calc-silicate alteration facies that itself had replaced the chloritic alteration, formed at the time of the sulfide deposition.

### **Mineral chemistry**

In spite of the facts that the study of the altered material is difficult due to the extreme variation in mineral composition over relatively short distances from the ore horizons and limitations imposed by drill core sampling, a mineral chemistry study of the alteration zones of the Expedito deposit was carried out.

The optical and chemical characteristics of chlorite with  $\text{Fe} / (\text{Fe} + \text{Mg})$  between 0.47 and 0.53 (Table I and Fig. 5) indicate that it is a magnesian ripidolite according to Hey's (1964) classification. The amount of ferric iron in chlorite was estimated using octahedral site valence charge imbalances and range from 4.47 to 5.02 wt %. These high ferric values and the presence of magnetite in the alteration zone clearly demonstrates a high oxygen fugacity environment, above the quartz-fayalite-magnetite buffer.

The amphibole found at the Expedito deposit consists of fibrous, fine to coarse-grained masses of porphyroblasts reaching 3 cm in length. They are Al-poor calcic amphibole classified as actinolite by its intermediate composition between ferroactinolite and tremolite according to the electron microprobe results (Table II). Furthermore, several carbonate grains of the alteration zone were analyzed and yielded an invariably calcitic composition.

### **Geothermometric and geobarometric determinations**

In the Expedito deposit, evidences of post-depositional re-equilibration makes the interpretation of mineral chemistry parameters for pressure and temperature estimations at

time of formation of the deposit very difficult. In spite of these restrictions, some geothermometry and geobarometry techniques were tentatively used.

### **Chlorite geothermometry**

Chlorite is generally the most abundant mineral in the alteration halo forming local massive zones and is also observed far from the ore zones. It is associated with sulfide aggregates and calc-silicate alteration spots and is rare in veins.

Cathelineau and Nieva (1985) and Cathelineau (1988) demonstrated that the  $^{[4]}Al$  of chlorites of hydrothermal altered rocks correlated positively with temperature and can be used as a geothermometer. In fact, the regression coefficient of 0.97 presented by Chatelineau (1988), favors a linear dependence of the Al tetrahedral occupancy with temperature in the range of 130-310 °C. Kranidiotis & Maclean (1987) introduced a correction for the influence of the Fe-Mg substitution in chlorite and applied that in temperature determination for the VMS Phelps Dodge Deposit in Abitibi. The modified geothermometer with the correction factor is given as:

$$T \text{ (°C)} = 106 \times ({}^{[4]}Al + 0.7 \times Fe/(Fe+Mg)) + 18$$

Using the above calibrated model for the Expedito deposit chlorite, temperatures in the range 300-325°C were obtained, which appears to be reasonable temperature interval for hydrothermal events related to volcanic hosted sulfide mineralizations.

### **Arsenopyrite geothermometry**

The theory behind arsenopyrite geothermometry can be found in several papers including Clarke (1960), Barton (1969), Kretshmar & Scott (1976) and Sharp et al. (1985). According to this theory, the composition of arsenopyrite is a function of temperature as well as of the sulfur fugacity with low influence of pressure. Commonly, determinations of arsenopyrite compositions are carried out on grains co-existing with pyrite and pyrrhotite which is supposed to have functioned as a buffer for S<sub>2</sub> partial pressure.

Several grains of arsenopyrite found in the ore of the Expedito deposit were submitted to electron microprobe analysis (Table III). Unfortunately, no mutual contact of the arsenopyrite with pyrite and with pyrrhotite was observed in the polished sections because

iron sulfides are rare in the arsenopyrite rich ore. The arsenopyrite compositions as depicted in Fig. 6 fall in the interval from 26 to 34 at % As clustering around 30,5 and 33,5 at % As.

Table I. Chemical composition of chlorite (n=25) from hydrothermal alteration zone in the Valley Deposit chlorites.

	Minimum	Maximum	Mean	St.Deviation
SiO <sub>2</sub>	25.16	27.14	25.94	0.46
TiO <sub>2</sub>	0.00	0.10	0.05	0.03
Al <sub>2</sub> O <sub>3</sub>	18.66	21.14	20.38	0.60
FeO	25.91	28.89	27.07	0.72
MnO	0.08	0.95	0.81	0.17
MgO	14.00	16.53	15.32	0.62
Si	5.32	5.65	5.41	0.08
Fe <sub>2</sub>	4.47	5.02	4.72	0.14
AlIV (8-Si)	2.35	2.69	2.59	0.08
AlVI	2.23	2.53	2.42	0.08
Fe/(Fe+Mg)	0.47	0.53	0.50	0.02

Assuming that the occurrence of pyrite and pyrrhotite is widespread in the deposit and considering the compatible S<sub>2</sub> fugacity levels for pyrite-pyrrhotite equilibrium, the arsenopyrite thermometer would yield temperatures in the intervals 300-350°C and 500-550°C (Fig. 6). The former temperature interval is consistent with values yielded by chlorite thermometer and may represent the temperature of sulfide deposition and, the latter is suggestive of localized heating that originated the calc-silicate alteration assemblage.

Table II. Electron microprobe results of calcic amphiboles of the Valley Deposit

Analysis	SiO <sub>2</sub>	TiO <sub>2</sub>	Al <sub>2</sub> O <sub>3</sub>	FeO	MnO	MgO	CaO	Na <sub>2</sub> O	K <sub>2</sub> O	F	Total
1	51.73	0.09	3.86	11.60	1.69	17.59	10.23	0.57	0.04	0.25	97.65
2	49.16	0.07	2.57	9.44	1.47	19.86	10.84	0.53	0.05	0.42	94.41
3	50.60	0.11	3.18	10.39	1.52	18.95	10.94	0.52	0.04	0.52	96.77
4	50.21	0.03	2.27	7.70	2.45	21.17	9.58	0.44	0.07	0.56	94.49
5	54.96	0.00	0.42	4.04	1.04	22.69	12.41	0.05	0.04	0.34	95.99
6	53.19	0.01	0.98	6.55	0.95	20.46	11.85	0.12	0.14	0.48	94.75
7	54.33	0.05	0.82	6.58	1.11	20.35	12.01	0.13	0.03	0.67	96.09
8	55.46	0.05	0.93	6.48	2.47	20.86	10.47	0.21	0.04	0.39	97.36
9	49.37	0.00	0.40	6.16	1.75	22.09	10.94	0.13	0.03	0.42	91.29
10	53.30	0.01	0.52	5.50	1.26	22.30	12.31	0.09	0.02	0.44	95.77
12	54.42	0.07	1.20	6.03	0.88	21.97	10.12	0.06	0.09	0.36	95.20
13	53.06	0.08	2.45	7.84	2.19	19.30	10.61	0.43	0.05	0.27	96.27
14	50.33	0.08	1.86	7.37	1.29	20.36	11.52	0.33	0.16	0.36	93.68
17	55.62	0.00	0.75	6.43	0.97	20.70	12.22	0.11	0.02	0.48	97.30
18	55.53	0.02	0.75	6.35	0.74	20.36	12.60	0.11	0.05	0.43	96.94
19	54.27	0.05	1.11	11.73	1.74	17.58	10.71	0.24	0.02	0.00	97.44
20	51.25	0.03	0.98	12.56	2.27	17.48	9.29	0.21	0.02	0.00	94.10
21	48.34	0.04	1.08	7.28	1.29	22.35	11.20	0.19	0.03	0.53	92.32
23	54.40	0.09	1.33	10.86	1.29	17.94	11.20	0.30	0.03	0.00	97.43
29	55.45	0.00	0.71	9.92	1.16	18.47	12.17	0.14	0.02	0.00	98.04

Table III. Compilation of electron microprobe results of 26 analyses of arsenopyrite of the Valley Deposit.

	S%	As%	Fe%	As (At%)
Maximum	24,08	47,15	36,23	33,93
Minimum	19,45	37,56	34,03	26,37
S.Deviation	1,25	2,59	0,50	1,94

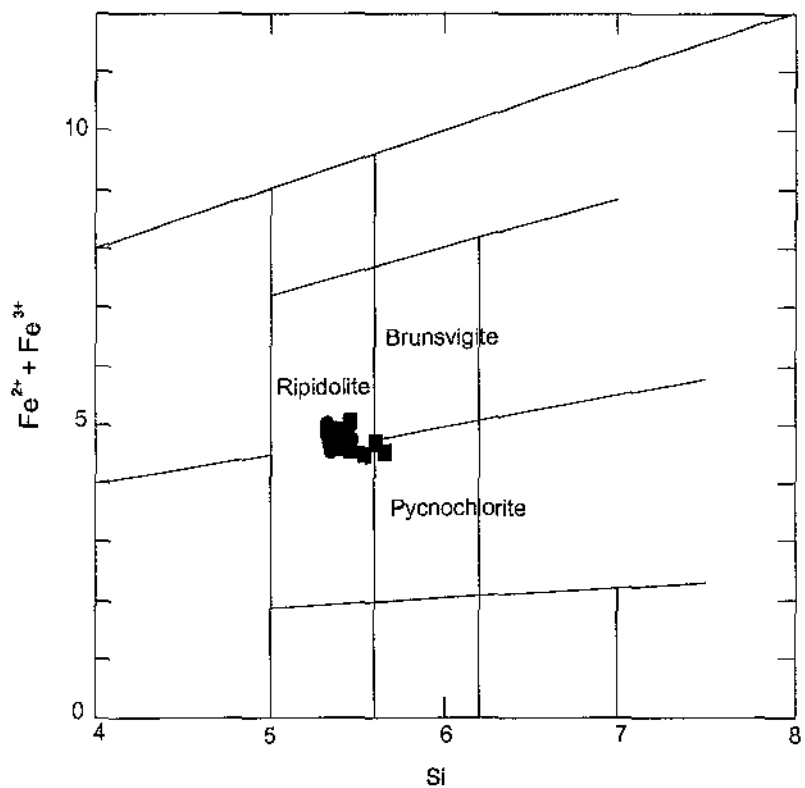


Fig. 5. Plots of the Expedito deposit chlorite compositions in the cationic diagram of Hey, (1964)

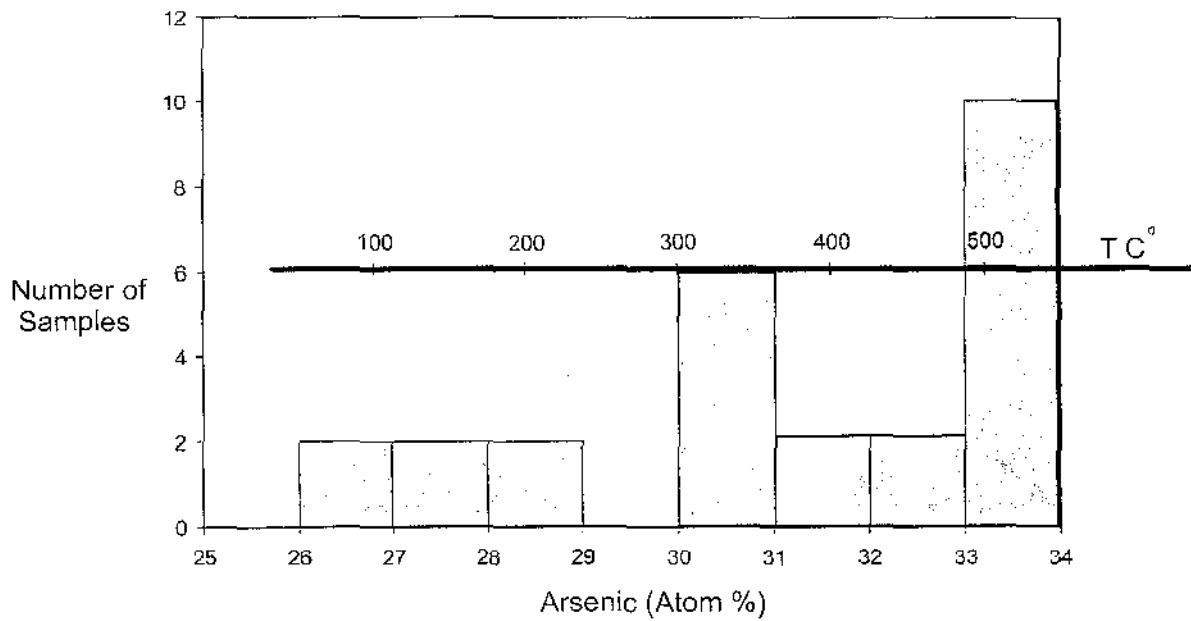


Fig. 6- As content (%) in arsenopyrite from the Expedito Deposit. Temperatures after Sundblad et al. (1984)

### Sphalerite geobarometry

The experimental and theoretical basis of geobarometry for the Fe-Zn-S system was reasonably established for temperatures of 500°C and above. Below 500°C, thermodynamic calculations diverge from experimental results for reasons that are not clear, perhaps due to low temperature re-equilibration, especially for temperatures below 300 °C. In this sense, studies carried out by Toulmin et al. (1991) at the Calloway mine in Ducktown, Tennessee, indicate that a low-temperature event has overprinted the high-temperature one, possibly destroying the high temperature record in the sulfide ore.

An attempt was made to apply the sphalerite geobarometer to the Expedito deposit ores. Firstly, several polished sections were examined under microscope for the co-existing sphalerite, pyrite and pyrrhotite and absence of chalcopyrite inclusions. Only the sphalerite grains that fulfilled this condition were analyzed by electron microprobe (36 point analyses) and the sphalerite compositions of 9 to 13 mol % FeS are shown in Table IV and Fig. 7.

According to the equation of Shimizu & Shimazaki (1981) which relates pressure and FeS content in sphalerite ( $P = 42.30 - 32.10 \times \log M_{FeS}$ ), the sphalerite geobarometer gives very high pressures (6 to 12 kbar) for the Expedito deposit. These pressure conditions are obviously inconsistent with the regional metamorphic facies indicating that the sphalerite geobarometry is not applicable to the Expedito ore deposit.

As mentioned before, the probable temperature of ore deposition lies in a 300 to 350°C interval. At these conditions a re-equilibration of sphalerite and monoclinic pyrrhotite and pyrite is likely to have occurred at the Expedito deposit leading to formation of iron-poor sphalerite to which the geobarometer can not be applied. Nevertheless, the occurrence of iron-poor sphalerite associated with pyrite and sulfur-rich pyrrhotite is suggestive of high S<sub>2</sub> partial pressure conditions during ore deposition at the Expedito deposit

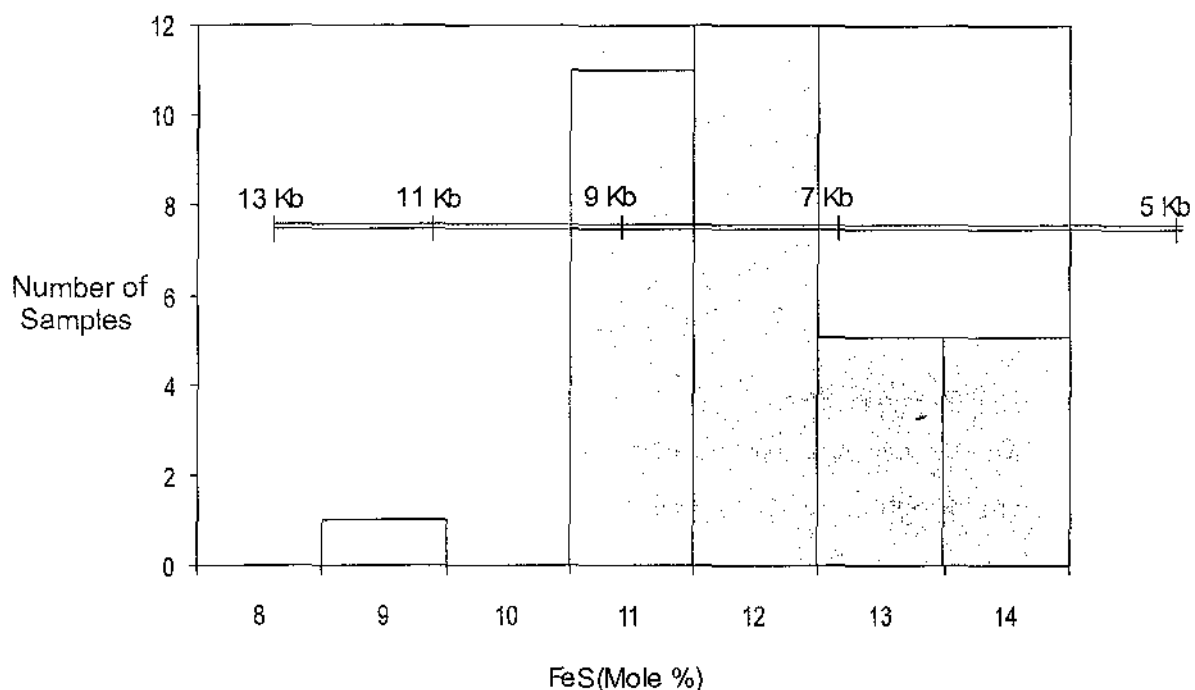


Fig. 7- FeS content (Mole%) in sphalerite from the Expedito Deposit. Pressures after Shimizu & Shimazaki, 1981.

Table IV. Compilation of electron microprobe results from sphalerites of the Valley Deposit ( $n=36$ ). Pressures in Kb were calculated using the equation  $P = 42.30 - 32.10 \times \log M_{FeS}$  (Shimizu & Shimazaki, 1981)

	%Fe	%S	%Zn	%Cu	Mole % FeS	P (Kb)
Maximum	7.70	34.21	61.39	1.22	13.41	11.71
Minimum	5.17	31.75	58.01	0.00	8.97	6.11
Mean	6.62	32.80	59.61	0.22	11.51	8.24
S. Deviation	0.65	0.57	0.91	0.39	1.12	1.51

### Isotopic studies

Radiogenic isotopes provide information both on the age of mineralization and the source of metals and fluids. Although valid age determinations are subjected to conditions of closed systems, and the deposit conditions are in general subjected to many post-ore

deposition transformations caused by differences in the physical parameters between the ore and country rocks, some assumptions and approaches can be used to put some constraints in ages and in mineralization sources tracing.

The genesis of massive sulfides involves volcanic, hydrothermal and sedimentary processes driven by the heat of sub-volcanic intrusions. Outstanding questions about the source of metals, age of the mineralization and age of disturbances can be solved by the use of Sr and Pb isotopes.

### Strontium Isotopes

The difference in mass between molecules of calcite containing the  $^{87}\text{Sr}$  or  $^{86}\text{Sr}$  is too low, c.a 1.2%, and because this, these isotopes are not fractionated during precipitation of calcite from aqueous solutions. Additionally, calcium carbonate permits  $\text{Sr}^{2+}$  to replace  $\text{Ca}^{2+}$  but excludes  $\text{Rb}^+$ . As a result, calcite has a very low Rb/Sr ratio and its  $^{87}\text{Sr}/^{86}\text{Sr}$  ratio is not significantly altered after deposition (Faure, 1991). Thus, the isotope composition of Sr in calcite, either hydrothermal or sedimentary in origin, records the composition of Sr in the oceans or of interacting hydrothermal fluids and supracrustal and basement rocks at the time of deposition ( $^{87}\text{Sr} / ^{86}\text{Sr}$  initial ratio).

Strontium contents as well as Sr-isotope compositions of calcite and sulfides sampled from the orebody are presented in Table V. Calcite shows a wide range in Rb and Sr isotopic compositions and very high values compared to the seawater at any time in the geological past. Thus the carbonate bearing rocks are unlikely to be sedimentary, as has been reported previously.

Although there is great variation in the  $^{87}\text{Sr}/^{86}\text{Sr}$  ratio of the calcite, the anomalous high values can be accounted for by the high Rb/Sr ratio in the country rocks (Table V) since the  $^{87}\text{Sr}/^{86}\text{Sr}$  ratio is proportional to the Rb/Sr of the system in which the Sr resides (Faure, 1986).

High Sr-isotope ratios are also present in the sulfides. The Sr-isotope compositions of sulfides encompasses the values of calcite as depicted in Fig.8, favoring the hypothesis of a common fluid source for sulfide minerals and carbonate against a sedimentary origin for the carbonate.

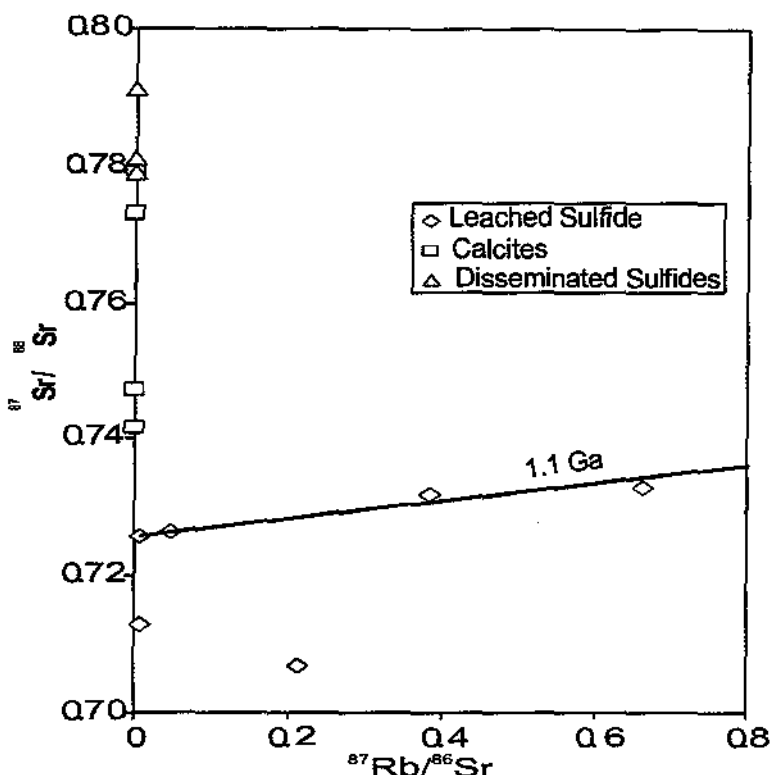


Fig. 8.  $^{87}\text{Sr}/^{86}\text{Sr}$  intermediate composition of calcites in relation to disseminated sulfides and one sphalerite lixiviate. One isochron referring to an event of 1.1 Ga in age is shown.

Sulfides are hard to date by the Rb/Sr method because they do not admit Rb in their crystalline structure. However, the presence of small quantities of Rb within sphalerite was used to measure isotopic ratios in sphalerite lixiviate as an attempt to obtain an isochronic age for the mineralization. As indicated in Fig. 8 a 1.1 Ga isochrone was obtained which can be interpreted as the result of a later remobilization event.

#### Lead isotopes

The Pb-isotope compositions were determined in galena (8 samples) of the sulfide ore and in K-feldspar separated from the Paraibão Granite localized few kilometers north of the Valley ore body.

Stanton & Russel (1959) first recognized that the patterns in Pb isotope composition of exhalative orebodies could be modeled in terms of source reservoir.

The use of Pb isotopes as a tool in mineral exploration was recognized by several authors including Cannon et al. (1961) and Delevaux et al. (1967) who introduced the concept of "Pb fingerprinting", which postulates that if the isotopic composition of a

mineral prospect can be matched with the Pb isotope ratios of a significant deposit, in a same particular metallogenic domain, there is an increased probability that the prospect is also a viable resource.

Table V. Rb and Sr isotopic data of sulfides and carbonate minerals

Sample	Rb (ppm)	Sr (ppm)	Rb/Sr	$^{87}\text{Rb}/^{86}\text{Sr}$	err	$^{87}\text{Sr}/^{86}\text{Sr}$	err
Pyrite /Sphalerite	0.05	3.21	0.015576	0.04930	0.0004	0.726240	0.000240
Pyrite /Sphalerite	0.33	135.80	0.002430	0.00700	0.0001	0.725760	0.000210
Pyrite /Sphalerite	0.47	3.55	0.132394	0.38370	0.0031	0.731780	0.000160
Pyrite /Sphalerite	0.15	0.68	0.220588	0.66180	0.0075	0.732800	0.000340
Pyrite /Sphalerite	0.03	0.36	0.083333	0.21370	0.0662	0.706960	0.001720
Pyrite /Sphalerite	0.02	5.29	0.003781	0.00820	0.0001	0.712850	0.000540
Calcite/Carb	6.00	88.70	0.067644	0.19640	0.0001	0.747084	0.000037
Calcite/Carb	3.40	160.90	0.021131	0.06134	0.0001	0.741541	0.000030
Calcite/Carb	3.00	138.90	0.021598	0.06289	0.0001	0.773207	0.000039
Calcite/Carb	89.00	97.50	0.912821	2.65956	0.0001	0.779441	0.000023
Pyrite/Diss. Sulf.	24.80	nd	nd	nd	nd	0.791300	0.000237
Pyrite/Diss. Sulf.	4.90	nd	nd	nd	nd	0.779170	0.000195
Pyrite/Diss. Sulf.	3.70	nd	nd	nd	nd	0.781290	0.000148
Rhyolite(RJ57)	185.00	9.00	20.7700	nd	nd	nd	nd
Dacite DMass	49.00	19.00	2.5700	nd	nd	nd	nd

Pb isotopes studies in galena yielded two sets of data characterized by their  $^{206}\text{Pb}/^{204}\text{Pb}$ ,  $^{207}\text{Pb}/^{204}\text{Pb}$  and  $^{208}\text{Pb}/^{204}\text{Pb}$  ratios (Table VI and Fig.9). Galena with higher  $^{206}\text{Pb}/^{204}\text{Pb}$  ratio plots near the linear array in the two stage Stacey-Kramers (1975) lead growth curve (Fig.9A) yields a model age around 1.75 Ga which is proposed here as the approximate age of sulfide deposition. In addition, some of the galena samples are roughly adjusted to the 1.75 Ga., consistent with U/Pb Shrimp ages of 1762-1755 Ma. for the volcanic and plutonic rocks of the Aripuanã district.

Furthermore, the galena isotopic compositions were plotted in the uranogenic and thoriogenic diagrams of Zartmann and Doe (1981) as depicted in Fig. 9B and 9C. The

obtained values plot systematically above the Upper Crust curve indicating that lead was provided by sources located in shallow and more radiogenic reservoirs in the Earth Crust.

An attempt was made to use K-feldspar to trace the probable source of lead. Feldspars of igneous rocks are enriched in lead and depleted in uranium and thorium. They contain lead concentrations up to several hundreds parts per million while their uranium and thorium content is usually less than 1 ppm. As a result, the bulk isotopic compositions of lead in feldspar are practically constant, thus maintaining the record of the lead originally incorporated from the melt.

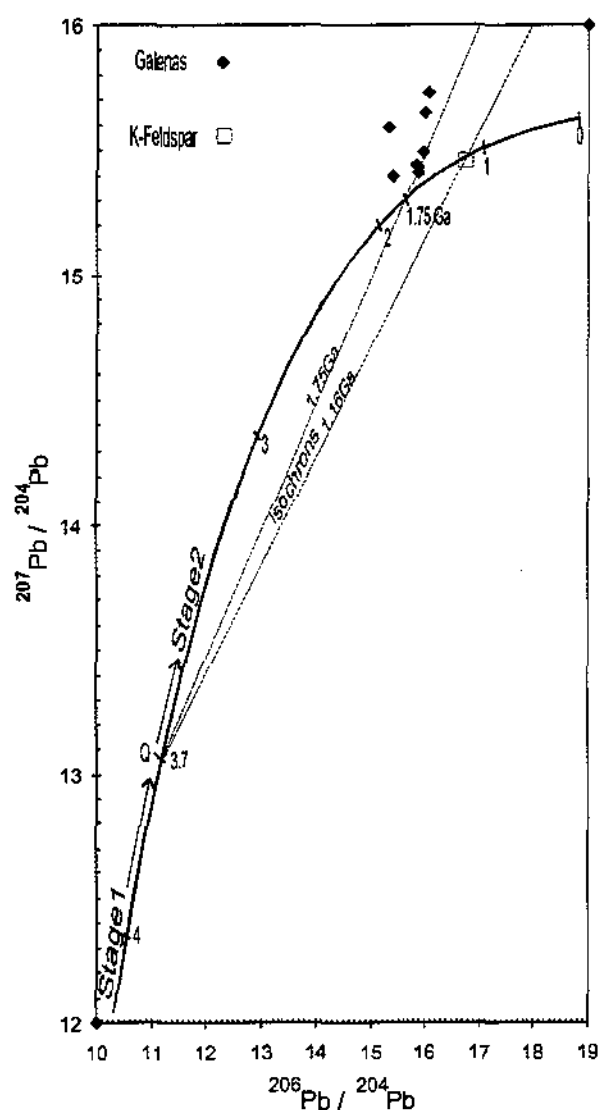


Fig. 9. Galena and K-feldspar lead isotopic data with reference to the average crustal growth curve of Stacey and Kramers (1975)

A centimeter-sized grain of potassium feldspar of the Paraibão Granite was analyzed for lead isotopes yielding an age of 1.160 Ma by the common lead method. The data when compared with galena show an enrichment in the  $^{206}\text{Pb}/^{204}\text{Pb}$ , probably implying an excess of U in relation to Th, acquired during crystallization of the feldspar or by scavenging of radiogenic lead during a late thermal event, similarly to what has found by Doe and Hart (1963) for potassium feldspar of Idaho Springs Formation of Colorado.

Several studies of Precambrian feldspar including that by Sinha (1969) showed that the lead isotopic composition tend to give somewhat young model ages compared to the related sulfide ores, as found here.

The  $\mu$  parameters ( $^{238}\text{U}/^{204}\text{Pb}$ ) obtained in galena are inconsistent with that of granite K-feldspar. These parameters for galena ( $> 10$ ) can be used as a criterion to identify the source of lead and indicate that the potential source of Pb in the Aripuanã district was not restricted to plutonic rocks and that part of lead was provided by fluid interaction with supracrustal rocks.

Finally, the obtained K-feldspar age is approximatively coincident with 1.1 Ga Rb/Sr age of sphalerite leachates, which again support the idea of occurrence of a later tectonic event affecting the area.

Table VI.- Lead isotopic data of galena from the Expedito deposit and of whole rock and K-feldspar of the Paraibão granite

Sample	$^{206}\text{Pb}/^{204}\text{Pb}$	Sigma	$^{207}\text{Pb}/^{204}\text{Pb}$	Sigma	$^{208}\text{Pb}/^{204}\text{Pb}$	Sigma	$\mu_2$	T (Ma) <sup>(1)</sup>
F16/219	15.861	0.020	15.414	0.024	35.575	0.03	10.23	1.766
F19/257	15.835	0.042	15.44	0.05	35.685	0.057	10.45	1.825
F25/207	16.004	0.016	15.652	0.011	36.302	0.014	11.76	1.995
513	15.955	0.012	15.492	0.012	35.833	0.012	10.64	1.810
514	16.057	0.030	15.731	0.025	36.607	0.031	12.29	2.059
515	15.846	0.010	15.432	0.011	35.692	0.013	10.38	1.805
516	15.304	0.051	15.592	0.045	36.202	0.047	13.13	2.425
517	15.407	0.114	15.396	0.121	35.603	0.124	10.98	2.098
K-feld	16.739	0.018	15.459	0.019	36.34	0.019	9.66	1.160

(1) Stacey-Kramers (1975)

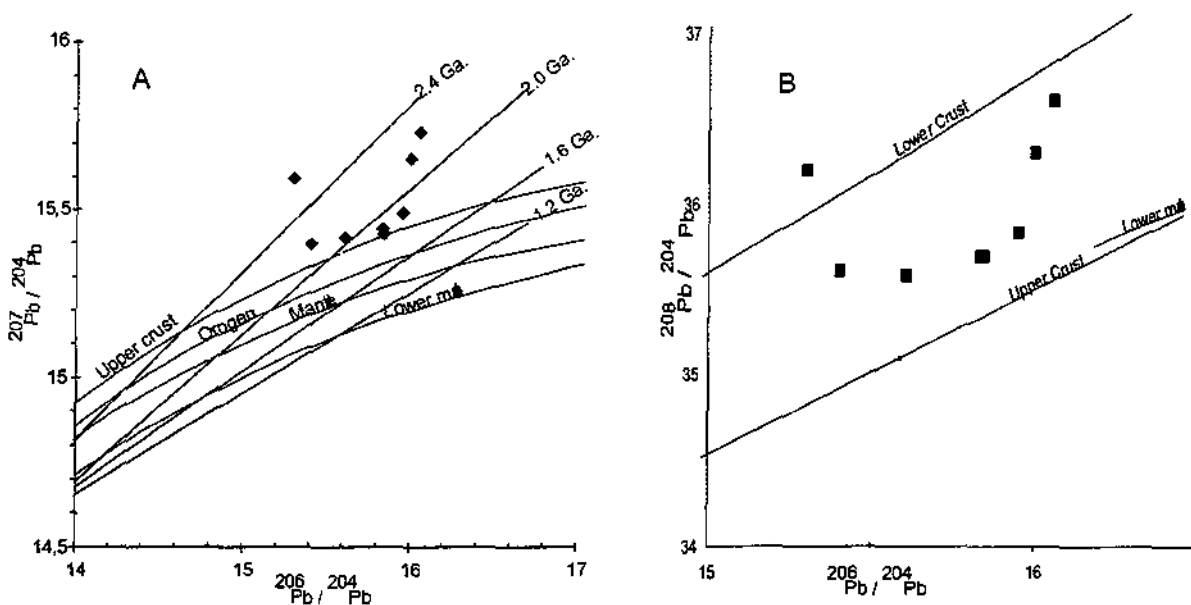


Fig. 10. Galena lead isotopic data with reference to the reservoir growth curves of Zartman and Doe (1981).

### Discussion and conclusions

The genesis of the Aripuanã massive sulfide deposits, whether on or under the ocean floor, involves hydrothermal processes driven by heat of plutonic and sub-volcanic intrusions. This fact is corroborated by the roughly equivalent galena Pb-Pb model age and U-Pb zircon ages of nearby volcanic and plutonic rocks indicating contemporaneity of volcanic process and sulfide deposition at around 1.75 Ga.

Little is known about the strontium isotopic composition of Precambrian seawater. Veizer and Compston (1976) presented values of the  $^{87}\text{Sr} / ^{86}\text{Sr}$  ratio of seawater in the range of 0.705-0.706 between 2.0 and 1.5 Ga. The occurrence of a carbonate sedimentary unit in the area was not recognized during geologic mapping and drill-core descriptions. The carbonate associated with the sulfide mineralization display high  $^{87}\text{Sr} / ^{86}\text{Sr}$  ratios probably due to random variations in strontium isotopic composition of the mineralizing fluids at the Expedito deposit. Hence, a process in which a pre-existing carbonated sedimentary horizon was metasomatized like the classic exoskarn model was unlikely to have occurred in the area.

The Rb/Sr isochron of  $\approx 1.1$  Ga. obtained for sphalerite lixiviate agree with the Pb/Pb model date of K-feldspar. This data leads us to consider the occurrence of a tectonic

perturbation of the pre-existing sulfide deposit related to a later event that activated the Dardanelos fault and locally reset the isotopic systems.

The calc-silicate alteration and the occurrence of magnetite in the Expedito sulfide deposit may be interpreted as superimposed alteration events along which sulfides and alteration minerals were affected by metassomatic substitution. In this sense Ca-Fe rich magmatic hydrothermal fluids might have contributed to modify the primary mineralization either through interaction with convecting seawater, or by chemical reaction with early formed minerals.

Hydrothermal alteration of this type was described in sub-surface environments in Atlantis II in the Red Sea where it was attributed to contact metamorphism induced by intrusion of a basic sill (Zierenberg & Shanks, 1983). Skarns also are reported, in Canadian and Swedish districts, with similar alteration mineral assemblages, including Snow Lake (Galev et al., 1993), Ansil (Galley et al., in prep.) and the Bergslagen base metal deposit (Vivallo, 1985). As a common characteristic the above authors consider this alteration as resulting from a high-grade regional or contact metamorphism with carbonate of hydrothermal origin.

It is widely accepted that magmatic fluids are responsible for the skarn type mineralization and that interaction of these with external fluids played a major role during retro metamorphism and formation of associated magnetite.

In the region, the low metamorphic grade of the rocks and the absence of a carbonate unit suggest that this uncommon hydrothermal alteration assemblage is not the product of reactions associated to regional temperature increase. Conversely, it is suggested that syn-volcanic faulting functioned as natural channels for Ca, Na, Mg, and Fe rich fluids leading to formation of this atypical alteration assemblage and sulfide deposition in epizonal environment.

Thus, the formation of the deposit may have occurred in a sub-surface environment by influx of hydrothermal fluids while submarine volcanism and sedimentation were occurring on the seafloor. The hydrothermal fluids were selectively focused on rocks that were more porous and permeable along faults originated by collapsing and subsidence phenomena during the evolution of the volcanic and plutonic emplacement event in the area. The Expedito sulfide deposit experienced local heating and suffered the action of

magmatic fluids that would then form the calc-silicate mineral assemblage. This hypothesis could be corroborated as more core-drilling data become available.

As mentioned before, diagnostic features of a typical VMS mineralization, in the sense of a sea floor massive sulfide deposition has not been observed in the Aripuanã ore district. However, the intense metasomatism in the studied area could have hampered some features indicative that part of this deposit had been generated in the water-ocean floor interface.

The present study leads to the conclusion that the Expedito deposit is a singenetic, replacement-type, structurally controlled, volcanic-hosted massive deposit (VHMS). This classification is in agreement with the convention adopted by Solomon (1976), Franklin et al. (1981), Lydon (1984) and Large (1992) in which sulfide deposition is considered to have roughly the same age as the host volcanics.

## References

- Almeida F.F.M. 1974. Evolução Tectônica do Cráton do Guaporé Comparada com o Escudo Báltico. *Rev. Bras. Geosc.*, 4:191-204.
- Cannon, R.S., Pierce, A.P., Antweiler, J.C., Buck, K.L. 1961. The data of lead isotope geology related to problems of ore genesis. *Economic geology*. v.56.p1-38.
- Chatelineau M. 1988. Cation site occupancy in chlorites and illites as a function of temperature. *Clay minerals*. 23, p.471-485.
- Chatelineau M., Nieva, D. (1985). A chlorite solid solution geothermometer The Los Azufres (Mexico) geothermal system. *Contrib. Min. Petrol.* 91, p.235-244.
- Collins C. and Monteiro H. 1998. Technical report on the Exploration Work on The Aripuanã property. Noranda Mineração. Intern Report
- Delevaux, M.H., Doe, B.R. Brown, G.F. 1967. preliminary lead isotope investigations of brine from the Red Sea, galena from the Kingdom of Saudi Arabia, and galena from the United Arab Republic (Arabia): *Earth and Planetary Science Letters*. v.3. p-139-144.
- Doe, B.R., Hart, S.R. 1963. The effect of contact metamorphism on lead in potassium feldspar near the Eldora Stock, Colorado. *J. Geophys. Res.*, 68, p.3521-30.
- Faure, G. 1986. *Principles of Isotope Geology*. 2<sup>nd</sup> ed. Wiley, New York. 589 pp.

- Faure,G.1991. Principles and applications of inorganic geochemistry: a comprehensive textbook for geology students. Macmillan Publishing Company. New York. 626 pp.
- Franklin, J.M., Lydon, J.W. and Sangster, D.F. 1981. Volcanic-associated massive sulfide deposits: Economic Geology, 75 th Anniversary Volume, p. 485-627.
- Galley, A. G. , Bailes, A . H., Kitzler, G. 1993. Geological setting and hydrothermal evolution of the Chisel lake and North Chisel Zn-Pb-Ag-Au massive sulfide deposit. Snow lake, Manitoba. Expl. Min. Geol (2). 271-295.
- Galley, A.G.,Jonasson, I.R., D.H.Warkinson. 2000. Magnetite-rich calc-silicate alteration in relation to synvolcanic intrusion at the Ansil volcanogenic massive sulfide deposit, Rouyn-Noranda, Quebec, Canada. Mineralium Deposit. (35). 619-637.
- Hey, M.H. 1964. A review of chlorites. Mineral Mag. 30. 277-292.
- Lydon, J. W. 1984. Volcanogenic massive sulphide deposits Part I: A descriptive model: Geosci. Canada, 15. p.195-202.
- Kranidiotis, P.,MacLean, W.H. 1987. Systematics of Chlorite Alteration at the Phelps Dodge Massive Sulfide Deposit, Matagami, Quebec. Economic Geology. 82. pp.1898-1911.
- Large, R. 1992. Australian Volcanic-Hosted Massive Sulfide Deposits: Features, Styles, and Genetic Models. Economic Geology. 97. p.471-510
- Neder, R.D.N., Figueiredo, B.R., Beaudry, C., Collins, C, Leite, J.A. D. 2000.The Expedito Massive Sulfide Deposit, Mato Grosso. Revista Brasileira de Geociências, 30(2); 222-225.
- Riverin, G., La Brie, M. ,Salmon, B.,Cazavant, A., Asselin, R., Gagnon, M. 1990. The geology of the Ansil Deposit. Rouyn-Noranda. Quebec. Inn: Rive M. Gagnon PVY. Lulin J.M. Riverin G. , Simard A . (eds). The Northwest Quebec polymetallic belt. Can. Inst. Min. Metall. Spec. Vol 43: 143-152.
- Solomon, M. 1976. “Volcanic” massive sulphide deposits and their host rocks – a review and an explanation, in Wolf, K.H., ed. , Handbook of Stratabound and Startiform Ore Deposits: Elsevier, Amsterdam, 2,p.21-50.
- Stanton, R.L., Russel,R.D.1959. Anomalous lead and the emplacement of lead sulfide ores. Economic Geology. v.54.p.588-607.

- Sunblad,K., Zachrisson, E., Smeds, S. A., Berglund, S. , Alinder, C. 1984. Sphalerite geobarometry and arsenopyrite geothermometry applied to metamorphosed sulfide ores in the swedish caledonides. Economic Geology. V.79. pp1660-1668.
- Tassinari, C.C.G., 1981. Evolução tectônica da Província Rio Negro-Juruena na região Amazônica. São Paulo, (Dissertação de MSc.) Instituto de Geociências, Universidade de São Paulo. 2v.,pp.99.
- Toulmin, P., Barton, P.B., Wiggins, L.B. 1991. Commentary on the sphalerite geobarometer. American Mineralogist. 96. p.1038-1051.
- Veizer, J., Compston, W. 1976.  $^{87}\text{Sr}/^{86}\text{Sr}$  in Precambrian carbonates as an index of crustal evolution. Geochim. Et Cosmochim. Acta, v. 40, p. 905-914.
- Vivallo, W. 1985. The geology and genesis of na Early proterozoic massive sulfide deposit at Garpensberg, Central Sweden. Economic Geology. (80). 17-32.
- Zierenberg, R.A., Shanks, W.C.III. 1983. Mineralogy and geochemical epigenetic features in metalliferous sediment. Atlantis II Deep, Red Sea. Econ. Geol. 57-72.

## CAPÍTULO 5 - CONSIDERAÇÕES FINAIS

### 5-1. Estratigrafia

A região de Aripuanã é caracterizada pela ocorrência de uma unidade plutono-vulcânica não metamórfica Paleoproterozóica constituída de rochas félscicas e máficas, incluindo dacitos, riadacitos, riolitos, basaltos, quartzo pôrfitos, cherts, sedimentos vulcanogênicos e granitos potássicos epizonais anorogênicos.

A seqüência vulcânica é caracterizada pela dominância de rochas ácidas piroclásticas e vulcânicas maciças e por ocorrências subordinadas de rochas básicas e exalitos. O inter-acamamento de rochas sedimentares e vulcânicas, as mudanças bruscas laterais e verticais entre diferentes unidades litológicas, somadas às texturas observadas nos tufos (embora não tenham sido observadas na área estudada ‘welded structures’, comuns na região) são feições que sugerem que as rochas vulcânicas foram depositadas em ambiente sub-aquático (cf. Vivallo, 1985).

As rochas plutônicas ocorrem como stocks e sills intrusivos nas rochas vulcânicas ácidas. Na região são representadas pelo Granito Paraibão correlacionável ao Granito Aripuanã. As vulcânicas e intrusivas ácidas apresentam características químicas similares e idades equivalentes dentro dos erros analíticos (idades SHRIMP U-Pb em zircões  $1762 \pm 6$  Ma e  $1755 \pm 6$  Ma).

Sobrepondo-se a esta unidade vulcâno-plutônica um espesso pacote de conglomerados e arenitos que constitui a Formação Dardanelos.

As rochas vulcânicas e corpos intrusivos associados da região Norte e Noroeste do Estado de Mato Grosso têm sido correlacionadas por diversos autores à Formação Iriri do Grupo Uatumã, às vulcânicas Teles Pires e à Formação Roosevelt.

Essa nomenclatura controversa tem sido motivo de discussões, que sem dúvida decorrem do pouco conhecimento geológico e da falta de integração dos dados regionais.

Pinho et al. (2001) propõem a substituição do termo Formação Iriri pelo termo Magmatismo Teles Pires, sugerido por Basei (1977), para as rochas formadas no intervalo 1.80 Ga e 1.74.Ga.

Atualmente existe uma única determinação de idade U-Pb para a Formação Iriri na área tipo (1,88 Ga.) discrepante das obtidas neste trabalho, a partir de datações U/Pb em

zircões (em torno de 1,75 Ga). É possível porém que com o aumento do número de datações fique demonstrada a coincidência de idades, conduzindo à conclusão de que o Magmatismo Teles Pires corresponde, na realidade, à fase final do Evento Iriri, não tratando-se, portanto, de eventos magmáticos distintos.

No presente trabalho, buscou-se manter a coerência com a literatura mais atual (Pinho et al., 2001) e considerou-se a unidade plutono-vulcânica de Aripuanã correlacionável ao Grupo Teles Pires.

## 5-2. Ambiente Tectônico

Na área de Aripuanã, a ausência de feições colisionais e de 'trends' de diferenciação, somado ao caráter bimodal do vulcanismo e à predominância de rochas félscicas, sugerem condições de magmatismo intracratônico, gerado por eventos extensionais decorrentes de ativações mantélicas.

Os processos petrogenéticos envolvidos na formação de grandes seqüências de vulcânicas félscicas e seu relacionamento com os diversos ambientes geotetônicos têm sido estudados por diversos autores, incluindo Lesher et al (1986), Barrie et al. (1993) e Lentz (1998), que chamaram a atenção principalmente para o relacionamento desses ambientes com mineralizações vulcanogênicas.

Esses autores demonstraram que depósitos de sulfetos maciços, relacionados a vulcanismo félscico, têm sido formados do Arqueano ao Cenozóico, geralmente associados com episódios extensionais, existindo um relacionamento geoquímico-metalogenético empírico evidente entre ambientes com depósitos desse tipo e magmatismo intraplaca do tipo A ou de cordilheira oceânica anômala (Tipo OR).

Neste sentido, Lentz (1998) postulou que, no Fanerozóico, rochas vulcânicas félscicas submarinas ocorrem em quatro tipos distintos de ambientes: (1) cordilheira oceânica, compreendendo também ilhas oceânicas; (2) arcos de ilhas intracratônico e intracontinental; (3) retro-arcos e (4) riftes ensiálicos e hot spots.

O padrão estrutural regional, com desenvolvimento de grabens e bacias, bem como a ampla distribuição areal do magmatismo ácido, com geração de rochas similares em todo Craton Amazônico, tudo sugere que adição crustal, por geração de magmas félscicos em zonas de rifteamento intracratônico, tenha sido o processo dominante durante o

Paleoproterozóico na região.

Interpreta-se que a estabilização final do episódio plutono-vulcânico foi seguida pela deposição de amplas bacias sedimentares, sugerindo que o magmatismo e a deposição da Formação Dardanelos se deu provavelmente em função de uma única fase extensional de longa duração.

Um modelo possível para este processo seria a fusão parcial da Crosta Inferior, em diversas zonas da porção sudoeste do Craton, em resposta a perturbações na astenosfera provocadas por intrusão de magmas máficos que teria assim dado origem a esse extenso magmatismo ('mantle underplated').

O desequilíbrio ocasionado pelo posicionamento supracrustal de grandes quantidades de magma, durante os eventos vulcano-plutônicos, favoreceu a geração de estruturas de colapso, incluindo riftes e caldeiras.

Estas estruturas se constituíram em locais favoráveis para formação de bacias sub-aquáticas em ambiente de crosta continental o que favoreceu a deposição e preservação de espessos níveis de chert, sedimentos e tufos aquagênicos e ainda a sedimentação clástica do tipo da Formação Dardanelos.

Embora esta seja a conclusão que se chegou neste trabalho, devem ser considerados os modelos tectônicos que propõem para a região uma evolução crustal durante o Proterozóico relacionada a eventos episódicos de acreção crustal por amalgamação de arcos magmáticos, modelos que implicariam na existência de feições tectônicas colisionais que não foram observadas na presente pesquisa.

### **5-3. Mineralização**

As mineralizações na Serra do Expedito, via de regra, estão encaixadas em uma espessa seqüência de rochas piroclásticas e sedimentos vulcanogênicos, constituindo-se em acumulações maciças e semi-maciças de sulfetos de Zn e Pb e disseminações subordinadas de sulfeto de Cu e Au nativo.

A integração dos dados mineralógicos obtidos em testemunhos de sondagem com as observações de afloramentos das mineralizações, incluindo as zonas de alteração e de ocorrência de brecha, sugere que o depósito é formado de diversas lentes, veios e pipes,

constituídos por pirita, pirrotita, esfalerita, galena, calcopirita e arsenopirita com substituição de parte dos sulfetos por magnetita.

O minério apresenta uma paragênese rica em Zn e Pb, com teores subordinados de Cu e Au, este último, localmente enriquecido por efeito de remobilização direta de níveis sulfetados. Em geral são observadas elevados índices de correlação positiva entre Pb e Ag, Cu e Au e Zn e Pb.

Os corpos de sulfetos maciços e semi-maciços encontram-se hospedados na seqüência de vulcânicas piroclásticas, mas se apresentam discordantes, sem controle estratigráfico definido em termos de afinidade a níveis vulcanoclásticos específicos.

As rochas encaixantes incluem, predominantemente, tufos de lapilli e de cristal com intercalações de chert e sedimentos vulcanoclásticos, os quais são interpretados como resultantes de material piroclástico depositado em ambiente sub-aquático e originários de atividades de centros vulcânicos distais.

O modo de ocorrência da mineralização sulfetada mais comum é como minério maciço, constituindo junto com minerais de alteração, a matriz de brechas. Os sulfetos ocorrem ainda como vênulas e veios com texturas crustiformes preenchidos por sulfetos. Estas feições demonstram que a deposição dos sulfetos se deu em sub-superfície, em ambientes epizonais provavelmente conectados à superfície. Não é possível descartar, por este motivo, que com o detalhamento posterior dos trabalhos e o acesso direto ao minério durante as futuras atividades de lavra, sejam identificados corpos concordantes de minério como comumente ocorrem nos depósitos VMS.

#### **5-4. Alteração Hidrotermal**

A assembléia de minerais de alteração contém sericita, cloritas magnesianas, calcita, actinolita, magnetita e quartzo.

Uma característica principal das mineralizações da Serra do Expedito é a ampla alteração hidrotermal relacionada à deposição do minério. Extensas áreas de alteração são reconhecidas na lapa da maioria dos depósitos de sulfeto maciço. As análises de testemunhos de sondagem demonstraram a ocorrência de uma zonação simétrica na capa e lapa da alteração hidrotermal, caracterizada por intensa cloritização, com uma zona interior

dominada por brechas quartzo-carbonáticas e cálcio silicáticas gradando para uma zona a actinolita-magnetita, e para quartzo-clorita nas zonas externas.

Essa distribuição espacial de alteração foi também observada por Vivallo (1985) no depósito Paleoproterozóico de Garpenberg na Suécia. Aí as paragêneses de minério e da zona de alteração são semelhantes às descritas na Serra do Expedito, com exceção da ocorrência de flogopita, que foi interpretada como resultante de reação água do mar - rocha sob condições hidrotermais a temperaturas superiores a 300° C. Tanto em Garpenberg como em Aripuanã não foi observada a ocorrência de gipsita, comum nos depósitos VMS Fanerozóicos (ex. Kuroko). A ocorrência comum de carbonato associado à alteração sugere pressão parcial de CO<sub>2</sub> elevada no fluido hidrotermal.

É proposto para a Serra do Expedito a intervenção de múltiplos processos nos vários sítios de deposição dos sulfetos e minerais de alteração. Admite-se a ocorrência de modificações nas paragêneses minerais originais por efeito de processos de substituição metassomática posteriores, porém relacionados às fases tardias do evento vulcano-plutônico responsável pela mineralização.

Deve ser salientado que os dados geotermométricos, obtidos a partir da composição de arsenopirita, agrupam-se em torno de temperaturas no intervalo 100-200°C e no intervalo 300-550°C. O primeiro intervalo provavelmente representa re-equilíbrio de fases a baixas temperaturas, porém o segundo, coincidente os resultados termométricos obtidos em clorita na faixa 300-325°C, deve corresponder ao evento de deposição do minério sulfetado. Considera-se que as temperaturas mais elevadas, superiores a 350°C, devem estar indicando as condições nas quais ocorreu o desenvolvimento da alteração cálcio-silicática do depósito.

Considera-se que os fluidos responsáveis pela mineralização tipo skarn são, provavelmente, de origem magmática. A interação desses com fluidos mais oxidantes e salinos (água do mar) deve ter favorecido os processos de metasomatismo que afetaram o depósito incluindo a formação de magnetita em substituição aos sulfetos.

Dados isotópicos <sup>87</sup>Sr/<sup>86</sup>Sr obtidos em calcita indicam uma contribuição importante das rochas encaixantes na formação dos fluidos hidrotermais. Esses dados também sugerem ser improvável a hipótese de que a calcita seja resultante da remobilização de níveis sedimentares carbonáticos.

Levando-se em conta que na área estudada as rochas apresentam baixo grau metamórfico e que a presença de uma unidade carbonática não foi observada, sugere-se que a assembléia incomum de alteração hidrotermal, típica de skarn, tenha se produzido por aquecimento localizado decorrente da atividade plutônica.

### 5-5. Gênese e Classificação

O depósito é considerado como vulcanogênico, encaixado em rochas com permeabilidade e porosidade que favoreceram ampla circulação de fluidos, com consequente lixiviação de metais e posterior deposição em zonas de falhas, ativadas pelo próprio vulcanismo.

Interpreta-se que estas falhas sin vulcânicas funcionaram como dutos para a passagem e deposição de fluidos ricos em Ca, Na, Mg, Fe, metais base e nobres, em condições epizonais.

Assim, a formação do depósito se deu inicialmente através de fluidos hidrotermais enriquecidos em metais, oriundos de percolação das encaixantes pela água do mar aquecida, nas proximidades de fontes plutônicas epizonais de calor. A evolução do vulcanismo e plutonismo contemporâneo conduziram a fenômenos de colapso e subsidência e a formação de sistemas de falhamentos fissurais que canalizaram o fluxo das soluções mineralizantes, além de propiciarem pela abertura de espaço, ambientes para a deposição de sulfetos em sub-superfície.

As porções do depósito localizadas mais próximas de fontes de calor sofreram a ação de fluidos magmáticos de origem plutônica, originando, por substituição metassomática, a assembléia de minerais cálcio-silicáticos e magnetita.

O depósito do Expedito deve ter se formado durante o processo vulcano-plutônico por preenchimento de vazios gerados por falhas e fraturas e pela substituição das encaixantes constituídas de rochas vulcânicas, sedimentos vulcanoclásticos e sedimentos químicos (cherts), sendo assim considerados como singenéticos. Em decorrência do caráter discordante dos corpos de minério, atualmente observados, o depósito da Serra do Expedito devem ser mais apropriadamente classificado como fazendo parte do modelo VHMS - Volcanic Hosted Massive Sulfide.

Por outro lado, de acordo com a classificação proposta por Solomon (1976), baseada nas relações percentuais de teores Cu / ( Cu + Zn ) e Zn / (Zn + Pb), o depósito da Serra do Expedito pode ser caracterizado como do tipo Zn-Pb-Cu, ou mais apropriadamente como depósito de Zn-Pb (Cu, Ag, Au), considerando-se os baixos teores de Cu.

### 5-6. Critérios Prospectivos

Na região, as dificuldades para a descoberta de mineralizações em subsuperfície são aumentadas pelas restrições na utilização de métodos geoquímicos, em decorrência da falta de mapeamento em escala adequada e ocorrência de espesso manto de intemperismo, com intensa lixiviação de metais, decorrente da alta pluviosidade típica da Região Amazônica.

A utilização de magnetometria é favorecida pela grande quantidade de magnetita presente na mineralização e na zona de alteração cálcio-silicática dando um grande contraste com as vulcânicas félscicas que hospedam a mineralização.

As informações geológicas disponíveis, permitem considerar como indicadores de ambientes favoráveis para definição de novas concentrações sulfetadas, a ocorrência de grandes acumulações de rochas piroclásticas depositadas em ambientes sub-aquáticos.

Deve ser considerada ainda a importante associação dos depósitos descobertos com corpos plutônicos, que propiciaram altos gradientes de temperatura para a mobilização de fluidos, que através da lixiviação de encaixantes porosas foram enriquecidos em metais.

Do ponto de vista estrutural, pode se afirmar que os corpos mineralizados e respectivas zonas de alteração hidrotermal são controlados por sistemas fissurais de falhas sin vulcânicas, que, além de canalizar os fluidos, possibilitaram, com os fenômenos de subsidência e colapso, o posicionamento de rochas vulcânicas e plutônicas em níveis crustais equivalentes.

A interpretação de que ambientes distensionais permitiram através de falhamentos sin vulcânicos a colocação de corpos vulcânicos de forma passiva em níveis epizonais indica que devem ser consideradas como ambientes potenciais, as áreas em que acumulações de seqüências piroclásticas em íntima associação com corpos plutônicos, possibilitaram a aproximação de fontes de calor com rochas porosas e permeáveis, em ambiente subaquático, favorecendo a ampla circulação de fluidos hidrotermais com consequente lixiviação e reconcentração de metais das litologias vulcânicas.

## **5-7. RECOMENDAÇÕES**

Finalizando, são sugeridos alguns aspectos relevantes para pesquisas suplementares e detalhamento, que poderão em curto prazo ser de grande auxílio para um melhor entendimento dos depósitos como o da Serra do Expedito:

- 1- Trabalhos de mapeamento para definição criteriosa das diversas fácies vulcânicas observadas na região, com atenção na definição das unidades piroclásticas e sua associação com corpos plutônicos.
- 2- Execução de análises químicas com inclusão de um maior número de elementos traços e terras raras para melhor definição dos parâmetros geoquímicos das rochas regionais, encaixantes da mineralização e zonas de alteração.
- 3- Datações Ar-Ar em biotitas e outros minerais com potássio da zona de alteração dos diversos depósitos da região para confirmar as idades da mineralização e alteração e verificar a existência de fenômenos pós-mineralização
- 4- Estudo petrográfico de um número maior de amostras da zona de alteração para melhor definir os diferentes estágios progressivos ou regressivos do metassomatismo associado à assembleia de minerais cálcio-silicáticos.
- 5- Aumentar o número de análises Pb-Pb em sulfetos e material oxidado para melhor definir uma tendência para o distrito metalogênico (Pb/Pb array).
- 6- Efetuar estudos de inclusões fluidas para determinação de parâmetros das soluções hidrotermais.
- 7- Estudos de isótopos estáveis (C,O em calcita, O na magnetita, S nos sulfetos etc.)
- 8- Efetuar análises comparativas e integradas entre os diversos corpos de minério incluindo o Valley, Maçaranduba, Babaçu e as mineralizações contíguas nas áreas da Anglo American a Este e Oeste que não puderam ser amostradas.
- 9- A partir da comparação do depósito com outros relatados na literatura com alteração hidrotermal semelhante, deve ser verificada a hipótese de que a substituição metassomática empobreceu ou destruiu grande quantidade de minério em sua área de influência, como no caso do depósito Ansil. Existe a possibilidade, e deve ser investigada, que esta remobilização tenha ocasionado enriquecimento em Cu e Au em determinados setores das mineralizações. Esta hipótese é favorecida pela presença de magnetita maciça e porfiroblástica com estruturas de substituição em sulfetos e também em actinolita.

## **5-8. BIBLIOGRAFIA**

- Arnold, G.O , Sillitoe, R.H. 1989. Mount Morgan gold-copper deposit. Queensland, Australia. Evidence for a intrusion - related replacement origin. *Economic Geology.* (84) p.1805-1816.
- Barrie, T.C., Ludden, J.N., Green, Tony,H. 1993. Geochemistry of volcanic associated with Cu-Zn and Ni-Cu deposits in the Abitibi Province. *Economic Geology.* (88). 1341-1358.
- Basei, M.A.S. 1975. Idade do vulcanismo ácido-intermediário da Região Amazônica. Dissertação de mestrado. Universidade de São Paulo. Instituto de Geociências, 133p.
- Beams, S., Laing, W., O'Neill, D. 1989. The exploration history and geology of the polymetallic Reward Deposit, Mt. Windsor volcanic belt, north Queensland: North Queensland Gold '89 Conference. Townsville, Queensland. April 1989. Proceedings. P.95-102.
- Bodon, S.B.,Valenta, R.K. 1995.Primary and tectonic features of the Currawong Zn-Cu-Pb (-Au) massive sulfide deposit. Benambra Victoria:Implications for ore genesis.*Economic geology,* (90) p. 1694-1721.
- Costa, J.B.S., Hasui, Y., 1997. Evolução geológica da Amazônia. In: Costa, M.L. and Angélica, R.S., (Eds.), Sociedade Brasileira de Geologia, Contribuições à Geologia da Amazônia, p. 15-90.
- Doyle, G.H., Huston, D.L. 1999. The subsea-floor replacement origin of the ordovician Highway-Reward volcanic-associated massive sulfide deposit, Mount Windsor Subprovince, Australia. *Economic Geology.* (94). Pp.825-844.
- Finlow-Bates, T., Large, D.E. 11978. Water depth as major control on the formation of submsrine exhalative ore deposits. *Geol. Jahrb.* V.D30, p.27-39.
- Franklin, J.M., Lydon, J.W. and Sangster, D.F. 1981. Volcanic-associated massive sulfide deposits: *Economic Geology*, 75 th Anniversary Volume, p. 485-627.
- Franklin, J.M. 1990. Precambrian sulphide deposits, Geological Association of Canada, Special Paper 25: 255-295.

- Galley, A.G., D.H.Warkinson, Jonasson, I.R., Riverin, G., 1995. The subsea-floor formation of volcanic-hosted massive sulfide. Evidence from the Ansil deposit. Rouyn-Noranda, Canada. *Economic geology*, (90), p.2006-2017.
- Galley, A.G., Jonasson, I.R., D.H. Warkinson. 2000. Magnetite-rich calc-silicate alteration in relation to synvolcanic intrusion at the Ansil volcanogenic massive sulfide deposit, Rouyn-Noranda, Quebec, Canada. *Mineralium Deposit.* (35). 619-637.
- Goodfellow, W., Blaise, B. 1988. Sulfide formation and hydrothermal alteration of hemipelagic sediment in Middle Valley, N. Juan de Fuca Ridge. *Economic Geology*. (88). 675-696.
- Haas, J.L.Jr. 1971. The effect of salinity on the thermal gradient of a hydrothermal system at hydrostatic pressures. *Economic Geology*, (66), p.940-946
- Henley, R. W., Thornley, P. 1979. Some geothermal aspects of polymetallic massive sulfide formation. *Economic Geology* (74), p.1600-1612.
- Large, R. 1992. Australian Volcanic-Hosted Massive Sulfide Deposits: Features, Styles, and Genetic Models. *Economic Geology*. 97. p.471-510
- Lentz, D.R. 1998. Petrogenetic evolution of felsic volcanic sequences associated with Phanerozoic volcanic-hosted massive sulphide systems: the role of extensional geodynamics. *Ore geology reviews*. (12). 289-327
- Lesher, C.M., Goodwin, <sup>a</sup>M., Campbell,, I.H., Gorton, M.P. Trace-element geochemistry of ore-associated and barren, felsic metavolcanic rocks in the Superior Province Canada. *Can. J. Earth Sci.*(23), p.222-237.
- Lydon, J. W. 1984. Volcanogenic massive sulphide deposits Part I: A descriptive model: *Geosci. Canada*, 15. p.195-202.
- Pinho, M.S.A.B, Pinho, F. E. C., Quadros, A. P., Chemale Jr., F., 2001. Discussao do Termo Uatumã-Iriri, Região Norte do Estado de Mato Grosso – Brasil. Resumos Expandidos –VII Simpósio de Geologia da Amazônia, Sociedade Brasileira de Geologia, Belem, 15-18.
- Santos, J.O.S., 2000. Os terrenos paleoproterozóicos da Província Tapajós e as mineralizações de ouro associadas. Ph. D. thesis, Univ. Federal do Rio Grande do Sul, Porto Alegre-RS, 209 pp.

- Silva, H.A., Leal, J.W.L., Montalvão, R.M.G., Bezerra, P.E.L., Pimenta,O.N.S., Tassinari, C.C.G., Fernandes, C.A.C., 1980. Geologia. In: Projecto RADAM-BRASIL, Folha SC-21 Juruena., DNPM/MME, Rio de Janeiro, 21-116.
- Solomon, M. 1976. 'Volcanic' massive sulphide deposits and their host rocks - a review and explanation. In. Wolf, K.A. (Ed.). Handbook of Strata-bound and Stratiform Ore deposits: II. Regional studies and specific deposits. Elsevier, Amsterdam. p.21-50 .
- Tassinari, C. C. G. , Macambira, M.J.B. 1999. Geological provinces of the Amazonian Craton. *Episodes*. 22 n/3, pp.177773-182
- Tassinari, C.C.G., 1996. O Mapa Geocronológico do Cráton Amazônico no Brasil: Revisão dos dados isotópicos. Tese de livre Docência, Instituto de Geociências, Universidade de São Paulo, 139 p.
- Tassinari,C.C.G., Cordani, U.G., Nutman, P., Van Schmus, W.R., Bettencourt, J.S., Taylor, P.N., 1996. Geochronological systematics on basement rocks from the Rio Negro-Juruena Province (Amazonian Craton) and tectonic implications. *Intl. Geol. Review* 38, 161-175.
- Vivallo, W.1985. The geology and genesis of na Early proterozoic massive sulfide deposit at Garpensberg, Central Sweden. *Economic Geology*, (80), 17-32.
- Zierenberg, R.A., Shanks, W.C.III. 1983. Mineralogy and geochemical epigenetic features in metalliferous sediment. *Atlantis II Deep, Red Sea*. *Economic Geology*,(78), 57-72.

# **ANEXOS**

Tabela I – Relação de amostras e metodologias isotópicas utilizadas.

Nº Lab	Nº Campo*	Descrição	Material	R X	Rb/ Sr	Sr/ Sr	K/ Ar	Ar/ Ar	Sm/ Nd	Pb/ Pb	U/ Pb
	16/219	Minério Maciço	Galena							X	
	19/257	Minério Maciço	Galena							X	
	25/207	Minério Maciço	Galena							X	
34168	24/445.7	Minério Maciço	Galena							X	
34169	8/322.9	Veio de galena	Galena							X	
34170	19/231	Minério Maciço	Galena							X	
34171	19/220.5	Minério Disseminado	Galena							X	
34172	16/219	Carbonato	Calcita	X		X					
34173	19/220.5	Carbonato	Calcita	X		X					
34174	49/367	Carbonato	Calcita	X		X					
34175	8/144	Carbonato	Calcita	X		X					
34176	25/165	Minério Disseminado	Pirita	X		X				X	
34177	19/220.5	Minério Disseminado	Pirita	X		X				X	
34178	49/470.5	Minério Disseminado	Pirita	X		X				X	
34179	49/470.6	Zona de Alteração	Anfíbolio								
34180	20/355	Esfalerita	Esfalerita		X						
34183	Granito Paraibão	Granito	Pó-RT						X	X	X
34183	Granito Paraibão	Granito	Feldspato							X	
34184	Dacito Maçaranduba	Dacito							X		X
34455	19/267	Minério Disseminado	Galena							X	

\* O número de campo quando utilizando a barra significa nº do furo / profundidade.

Tabela II- Resultados de análises químicas de rochas (elementos maiores)

N lab.	Amostra	SiO <sub>2</sub>	Al <sub>2</sub> O <sub>3</sub>	Fe <sub>2</sub> O <sub>3</sub>	MnO	MgO	CaO	Na <sub>2</sub> O	K <sub>2</sub> O	TiO <sub>2</sub>	P <sub>2</sub> O <sub>5</sub>	P.F.	Total
		(%)	(%)	(%)	(%)	(%)	(%)	(%)	(%)	(%)	(%)	(%)	(%)
710	49/485	41.54	9.59	10.12	0.231	27.99	0.76	0.10	0.17	0.392	0.171	9.33	100.38
711	26	84.27	9.87	1.62	0.006	0.23	0.03	0.02	0.96	0.098	0.024	3.40	100.52
712	21	69.29	14.47	4.30	0.082	0.89	2.51	3.35	4.15	0.635	0.148	0.53	100.35
713	dacito	79.13	11.97	0.44	0.005	0.27	0.06	4.07	3.23	0.094	0.013	0.68	99.96
714	125	71.48	15.22	2.65	0.026	1.05	0.07	1.92	4.81	0.344	0.046	2.50	100.11
715	118	71.76	14.46	2.47	0.043	0.92	0.55	3.27	5.45	0.372	0.072	1.00	100.38
716calc.	49/723 sed	63.80	17.08	3.81	0.021	2.11	0.12	0.22	6.22	0.445	0.091	4.13	98.05
717calc.	24/349	71.13	14.18	1.77	0.030	3.20	0.02	0.13	4.42	0.138	0.016	3.35	98.38
718calc.	24/361	51.44	4.85	10.24	0.497	22.59	4.34	0.42	3.35	0.076	0.032	2.80	100.64
719	24/363	76.85	8.91	7.12	0.112	2.81	0.06	0.17	1.95	0.075	0.018	2.69	100.78
720	24/375	77.13	11.17	4.08	0.011	0.79	0.06	0.10	3.90	0.109	0.018	3.22	100.60
721	Gr.Paraião	74.89	12.88	2.31	0.024	0.33	1.33	3.60	3.47	0.235	0.049	0.53	99.66
722	18	48.41	15.30	11.65	0.206	8.56	11.23	2.15	0.48	0.962	0.097	0.81	99.87
723	22	48.97	14.40	12.95	0.244	7.61	9.97	2.41	1.12	1.059	0.087	1.54	100.36
724	22B	49.12	14.43	12.86	0.243	7.61	9.98	2.51	1.13	1.060	0.087	1.53	100.54
725	115	72.26	13.43	4.00	0.033	0.55	1.12	3.15	4.02	0.565	0.116	0.90	100.13
726	36+36B	50.55	15.74	9.06	0.140	7.52	12.02	2.47	0.37	0.899	0.092	1.26	100.12
727	57	76.14	12.46	2.97	0.048	1.28	0.03	0.08	5.01	0.143	0.015	2.48	100.66
728	62B	48.24	15.84	12.21	0.206	6.96	9.85	2.09	1.75	0.992	0.079	2.69	100.89
728D	62B	49.17	16.00	12.13	0.208	7.25	9.98	2.24	1.79	1.022	0.075	2.63	102.59
729	95	47.99	15.96	9.86	0.385	9.22	11.56	1.30	1.55	0.473	0.053	2.40	100.75
730	49/296	81.83	8.82	1.95	0.002	0.06	0.08	4.73	0.25	0.103	0.022	1.20	99.04
732calc.	98	70.82	13.95	2.81	0.064	0.62	1.13	4.33	4.28	0.583	0.062	0.75	99.40
733	110A	67.03	15.60	4.40	0.103	1.40	3.53	3.90	2.90	0.514	0.183	0.75	100.30
734calc.	34	47.50	15.05	11.61	0.217	9.61	11.52	1.72	0.54	0.625	0.055	1.59	100.05
735calc.	95B	47.83	15.95	9.61	0.373	9.19	11.42	1.39	1.55	0.471	0.047	2.77	100.59
736	36T	51.18	15.87	9.13	0.14	7.54	12.16	2.47	0.38	0.918	0.092	1.14	101.02
737calc.	110B	66.37	15.48	4.49	0.103	1.39	3.54	3.80	2.84	0.520	0.176	0.73	99.44
738	22T	48.98	14.34	12.90	0.240	7.57	10.00	2.40	1.11	1.067	0.085	1.83	100.50
738D	22T	48.90	14.32	12.91	0.238	7.57	9.98	2.43	1.11	1.072	0.086	1.83	100.43
739	18B	48.45	15.28	11.72	0.203	8.59	11.29	2.14	0.48	1.002	0.094	0.93	100.18
740	99	81.06	9.49	1.65	0.022	0.24	0.35	1.23	5.84	0.212	0.027	0.67	100.79
741calc.	35	74.79	12.73	2.41	0.020	0.35	0.53	3.69	4.88	0.300	0.036	0.62	100.36
742	101	71.92	13.86	3.45	0.029	0.06	0.54	3.04	6.69	0.393	0.063	0.72	100.77
743calc.	77	77.31	11.82	1.35	0.008	0.14	0.40	2.59	5.18	0.185	0.021	0.68	99.69
744	62B	73.68	13.71	1.77	0.044	0.27	0.94	2.99	5.53	0.176	0.051	0.71	99.86
744D	62B	74.14	13.77	1.70	0.044	0.27	0.95	3.13	5.53	0.177	0.051	0.71	100.46
745calc.	117	68.70	13.13	4.57	0.028	1.68	0.27	2.05	7.71	0.617	0.109	0.49	99.35
WSE ( V. rec.+1σ )		50.70±0. 58	13.78± 0.28	13.15±0. 37	0.17±0. .01	5.55±0. .21	8.95±0. .25	2.47±0. .14	1.00±0. .06	2.40±0.0 8	0.30±0.0 4		
WSE(V. obtido)		51.16	13.82	13.09	0.172	5.58	9.00	2.52	1.00	2.403	0.312		
BAC(V. rec.)		52.25	13.43	12.12	0.160	4.25	7.87	2.63	2.39	3.500	0.490		
BAC(V. obtido)		51.68	13.71	12.13	0.161	4.29	7.81	2.72	2.35	3.524	0.517		

Tabela III- Resultados de análise químicas de rochas (elementos menores.)

N Lab.	Amostra	Ba ppm	Cr ppm	Cu ppm	Nb ppm	Ni ppm	Pb ppm	Rb ppm	Sr ppm	Th ppm	V ppm	Y ppm	Zn ppm	Zr ppm
710	49/485	<5	<2	75	12	6	358	15	6	<2	34	10	813	173
711	26	141	<2	12	10	<2	4	32	4	14	3	25	13	110
712	21	984	6	14	15	4	14	139	188	13	42	45	53	327
713	dacito	574	4	32	15	<2	4	49	19	18	<3	29	0	136
714	125	666	20	2	16	5	2	183	39	21	22	26	21	200
714D	125	671	31	2	16	5	2	184	40	21	22	27	21	201
715	118	1076	2	3	15	3	6	130	83	16	23	21	23	228
716	49/723 sed	1048	8	660	20	24	824	198	8	<2	35	69	241	370
717	24/349	450	<2	4	13	<2	16	134	7	17	3	52	57	192
718	24/361	83	<2	113	6	5	725	247	4	<2	8	14	757	103
719	24/363	347	5	113	11	<2	2	57	9	13	3	29	123	103
720	24/375	343	<2	62	12	<2	9	120	7	15	3	41	17	145
721	Gr.Paraiçâo	1193	<2	3	11	<2	4	82	108	13	10	42	17	169
722	18	35	323	150	1	145	<2	16	122	<2	285	23	68	40
723	22	407	229	71	1	80	8	88	231	<2	339	27	114	50
724	22B	385	222	71	1	79	8	88	234	<2	338	28	114	49
725	115	1181	10	2	18	5	5	76	97	20	24	51	28	410
726	36+36B	67	283	49	2	98	<2	20	304	2	255	25	53	56
727	57	1249	<2	2	15	0	4	185	9	18	5	31	21	174
728	62B	295	163	95	1	80	<2	115	238	<2	309	28	82	48
728D	62B	292	159	93	1	79	<2	115	239	<2	309	28	81	48
729	95	517	421	93	1	167	<2	119	170	<2	219	17	103	24
730	49/296	94	9	55	8	<2	20	5	17	7	<3	24	11	146
732	98	1501	4	5	18	4	2	167	123	13	9	59	33	438
733	110A	1106	5	17	9	3	9	86	394	9	58	25	56	187
733D	110A	1110	6	17	9	4	9	87	394	8	58	25	56	186
734	34	341	78	93	1	126	<2	32	197	<2	208	20	74	33
735	95B	467	419	81	2	164	<2	120	171	<2	216	17	92	24
736	36T	70	278	49	2	96	<2	21	305	<2	257	25	54	56
737	110B	1090	3	17	9	2	8	86	395	8	60	26	56	189
738	22T	377	219	71	1	79	8	86	235	<2	332	28	112	49
739	18B	28	323	133	2	137	<2	15	121	<2	285	23	63	40
740	99	1235	10	23	12	5	3	156	44	13	7	17	24	262
741	35	707	4	5	17	2	1	108	53	19	3	100	15	367
742	101	1023	4	5	20	8	3	206	54	19	9	35	14	441
743	77	717	7	3	13	<2	7	172	62	17	6	20	9	159
744	62B	742	10	3	11	2	38	260	141	69	13	18	18	194
744D	62B	755	15	3	10	3	38	260	141	68	10	18	18	194
745	117	1966	16	4	14	8	4	245	45	16	38	32	21	304
BHVO(V. rec. $\pm$ 1 $\sigma$ )		130 $\pm$ 13	280 $\pm$ 19	127 $\pm$ 7	18 $\pm$ 2	119 $\pm$ 7		9.8 $\pm$ 1.0	389 $\pm$ 2.3	1.2 $\pm$ 0.3	317 $\pm$ 1.3	26 $\pm$ 2	103 $\pm$ 6	172 $\pm$ 1
BHVO(V. obitido)		132.4	283.8	128.9	18.4	122.6	3.7	9.1	389	1.2	316.5	25.8	104.8	171.5
WSE (V <sub>rec</sub> $\pm$ 1 $\sigma$ )		338 $\pm$ 27.52	99 $\pm$ 9.984	65 $\pm$ 10.84	18 $\pm$ 2.51	55 $\pm$ 7.5.26	13.8 $\pm$ 2.26	25 $\pm$ 4.87	410 $\pm$ 2.562	3 $\pm$ 0.761.83	340 $\pm$ 31.84	30.4 $\pm$ 3.64	117 $\pm$ 10.92	195 $\pm$ 17.07.07
WSE		350.0	98.4	62.8	17.5	57.2	12.8	26.1	410.8	3.1	342.5	31.4	117.0	200.3
Limites de Detecção (3 $\sigma$ )		5	2	1	1	2	2	1	2	2	3	1	1	1

Tabela IV – Resultados de análises químicas de esfaleritas (Microssonda)

Amostra	Análise	%Fe	%S	%Zn	%Cu	Total	Mole % FeS
F16-139	Pto. 4	6.33	32.18	59.21	0.02	97.73	11.12
F16-139	Pto. 5	6.19	33.59	59.84	0.04	99.67	10.81
F16-139	Pto. 6	7.07	33.31	58.01	0.02	98.41	12.49
F16-139	Pto. 7	6.87	32.86	59.61	0.01	99.34	11.89
F16-139	Pto. 8	6.60	33.03	59.74	0.12	99.84	11.45
F16-139	Pto. 9	6.81	32.54	59.23	0.01	98.58	11.86
F16-139	Pto. 9	6.57	32.59	59.13	0.02	98.67	11.51
F16-139	Pto. 10	6.00	32.85	59.86	0.02	98.73	10.50
F16-139	Pto. 12	5.97	32.92	59.71	0.20	98.81	10.48
F16-139	Pto. 13	7.03	33.22	59.40	0.01	99.66	12.17
F16-139	Pto. 14	6.27	33.09	60.46	0.01	99.83	10.82
F16-139	Pto. 17	5.82	32.99	60.82	-	99.63	10.08
F16-139	Pto. 19	6.86	32.96	59.77	-	99.59	11.85
F16-139	Pto. 20	6.53	32.67	58.73	0.01	97.95	11.52
F16-139	Pto. 21	6.15	33.10	59.59	-	98.84	10.79
F16-139	Pto. 22	6.73	33.08	57.30	2.36	99.47	12.09
F16-139	Pto. 23	6.25	33.10	60.76	0.01	100.14	10.75
F16-139	Pto. 25	6.89	33.05	58.99	0.02	98.96	12.03
F8-138.9	Pto. 26	5.91	32.42	60.90	0.17	99.40	10.21
F8-138.9	Pto. 27	6.90	31.97	59.25	0.71	98.84	12.00
F8-138.9	Pto. 28	5.95	31.75	60.61	0.04	98.36	10.31
F8-138.9	Pto. 29	6.84	32.24	59.39	0.01	98.48	11.88
F8-138.9	Pto. 30	7.01	33.24	60.36	0.01	100.61	11.97
F8-138.9	Pto. 31	17.53	33.90	48.15	0.04	99.61	29.88
F8-138.9	Pto. 32	7.70	32.95	58.19	1.16	99.99	13.41
F8-138.9	Pto. 33	7.42	33.08	58.68	0.25	99.43	12.90
F8-138.9	Pto. 34	7.68	32.89	59.07	0.04	99.68	13.22
F8-138.9	Pto. 36	7.58	32.33	58.36	1.22	99.49	13.20
F8-138.9	Pto. 38	5.80	33.01	60.45	0.02	99.29	10.10
F8-138.9	Pto. 39	5.17	32.41	61.39	0.07	99.04	8.97
F8-138.9	Pto. 40	26.79	45.12	28.59	0.00	100.50	
F8-138.9	Pto. 42	8.20	32.90	58.21	0.01	99.32	14.16
F8-138.9	Pto. 43	5.83	34.21	60.66	-	100.70	10.12
F8-138.9	Pto. 44	7.39	31.95	59.48	0.09	98.90	12.70
F8-138.9	Pto. 45	7.68	32.53	58.35	0.99	99.54	13.35
F8-138.9	Pto. 46	6.88	32.39	59.47	0.98	99.72	11.92

Tabela V – Resultados de análises químicas de arsenopiritas (Microssonda)

Análise	S%	As%	Fe%	Total	Mole %As
Pto.2	19.45	47.15	34.59	101.18	33.93
Pto.3	19.64	47.10	34.50	101.24	33.82
Pto.12	20.09	46.92	35.77	102.78	33.08
Pto.11	20.16	46.81	35.34	102.31	33.12
Pto.6	20.03	46.58	35.00	101.60	33.19
Pto.1	19.99	46.56	34.76	101.30	33.28
Pto.10	19.94	46.50	35.20	101.64	33.14
Pto.13	20.12	46.47	35.10	101.69	33.06
Pto.9	19.98	46.44	34.96	101.38	33.16
Pto.5	19.67	46.36	34.63	100.65	33.41
Pto.4	20.34	45.76	34.86	100.96	32.67
Pto.7	20.11	45.72	34.98	100.80	32.74
Pto.8	20.18	45.45	35.25	100.88	32.49
Pto.21	21.12	44.42	35.03	100.57	31.56
Pto.28	21.02	44.21	34.81	100.05	31.57
Pto.29	21.33	43.32	35.02	99.67	30.91
Pto.25	20.84	43.14	34.36	98.34	31.28
Pto.22	21.74	43.08	35.26	100.08	30.51
Pto.24	21.62	42.97	35.54	100.13	30.44
Pto.15	21.00	42.64	34.35	97.99	30.95
Pto.14	21.73	42.58	34.91	99.23	30.37
Pto.32	21.10	42.50	34.47	98.07	30.78
Pto.34	20.95	42.48	34.03	97.46	30.99
Pto.27	23.22	41.78	35.98	100.99	28.95
Pto.26	22.78	41.14	35.43	99.34	28.99
Pto.31	23.64	38.70	35.14	97.48	27.43
Pto.33	24.08	37.56	36.23	97.88	26.37

Tabela VI – Resultados de análises químicas de anfibólios (Microssonda)

Análise	%SiO <sub>2</sub>	%TiO <sub>2</sub>	%Al <sub>2</sub> O <sub>3</sub>	%FeO	%MnO	%MgO	%CaO	%Na <sub>2</sub> O	%K <sub>2</sub> O	%F	%Cl	Total
Pto.21	37.51	0.62	12.73	15.91	0.52	16.12	0.00	0.10	9.63	0.00	0.00	93.14
Pto.27	38.02	0.70	12.26	14.92	0.57	17.17	0.02	0.07	9.20	0.00	0.00	92.94
Pto.22	38.62	0.77	13.00	15.38	0.50	16.80	0.00	0.06	9.86	0.00	0.00	95.00
Pto.30	39.24	0.79	12.40	14.42	0.42	17.60	0.00	0.06	9.57	0.00	0.00	94.49
Pto.24	39.24	0.69	12.32	15.19	0.50	17.65	0.00	0.08	9.54	0.00	0.00	95.20
Pto.28	39.31	0.68	12.49	14.59	0.43	17.96	0.00	0.07	9.50	0.00	0.00	95.04
Pto.25	39.37	0.84	12.34	14.83	0.48	17.51	0.00	0.07	9.69	0.00	0.00	95.12
Pto.26	39.45	0.66	12.54	14.55	0.46	17.60	0.00	0.09	9.32	0.00	0.00	94.66
Pto.15	40.69	0.55	12.96	9.95	0.48	20.06	0.08	0.00	7.57	1.46	0.01	93.82
Pto.16	41.98	0.01	7.72	12.01	0.74	22.82	5.48	0.08	0.48	0.68	0.01	91.98
Pto.11	48.34	0.04	1.08	7.28	1.29	22.35	11.20	0.19	0.03	0.53	0.00	92.32
Pto.2	49.16	0.07	2.57	9.44	1.47	19.86	10.84	0.53	0.05	0.42	0.00	94.41
Pto.9	49.64	0.00	0.40	6.16	1.75	22.09	10.94	0.13	0.03	0.42	0.02	91.56
Pto.4	50.21	0.03	2.27	7.70	2.45	21.17	9.58	0.44	0.07	0.56	0.02	94.49
Pto.14	50.33	0.08	1.86	7.37	1.29	20.36	11.52	0.33	0.16	0.36	0.01	93.68
Pto.3	50.60	0.11	3.18	10.39	1.52	18.95	10.94	0.52	0.04	0.52	0.01	96.77
Pto.20	51.25	0.03	0.98	12.56	2.27	17.48	9.29	0.21	0.02	0.00	0.00	94.10
Pto.1	51.73	0.09	3.86	11.60	1.69	17.59	10.23	0.57	0.04	0.25	0.01	97.65
Pto.13	53.06	0.08	2.45	7.84	2.19	19.30	10.61	0.43	0.05	0.27	0.01	96.27
Pto.6	53.19	0.01	0.98	6.55	0.95	20.46	11.85	0.12	0.14	0.48	0.02	94.75
Pto.10	53.30	0.01	0.52	5.50	1.26	22.30	12.31	0.09	0.02	0.44	0.01	95.77
Pto.19	54.27	0.05	1.11	11.73	1.74	17.58	10.71	0.24	0.02	0.00	0.00	97.44
Pto.7	54.33	0.05	0.82	6.58	1.11	20.35	12.01	0.13	0.03	0.67	0.00	96.09
Pto.23	54.40	0.09	1.33	10.86	1.29	17.94	11.20	0.30	0.03	0.00	0.00	97.43
Pto.12	54.42	0.07	1.20	6.03	0.88	21.97	10.12	0.06	0.09	0.36	0.00	95.20
Pto.5	54.96	0.00	0.42	4.04	1.04	22.69	12.41	0.05	0.04	0.34	0.01	95.99
Pto.29	55.45	0.00	0.71	9.92	1.16	18.47	12.17	0.14	0.02	0.00	0.00	98.04
Pto.8	55.46	0.05	0.93	6.48	2.47	20.86	10.47	0.21	0.04	0.39	0.01	97.36
Pto.18	55.53	0.02	0.75	6.35	0.74	20.36	12.60	0.11	0.05	0.43	0.01	96.94
Pto.17	55.62	0.00	0.75	6.43	0.97	20.70	12.22	0.11	0.02	0.48	0.00	97.30

Tabela VII– Resultados de análises químicas de cloritas (Microssonda)

Amostra	Análise	%SiO <sub>2</sub>	%TiO <sub>2</sub>	%Al <sub>2</sub> O <sub>3</sub>	%FeO	%MnO	%MgO	%CaO	%Na <sub>2</sub> O	%K <sub>2</sub> O	Total
L24393	p1	25.998	0.051	21.139	26.481	0.932	16.076	0.018	0.043	0.018	90.993
L24393	p2	26.011	0.039	20.849	27.292	0.922	15.556	0.029	0.031	0.017	90.875
L24393	p3	25.997	0.019	20.599	26.864	0.891	15.127	0.011	0.019	0	89.581
L24393	p4	26.089	0.028	20.638	26.957	0.940	15.190	0.008	0.026	0	89.962
L24393	p5	25.739	0.100	20.846	26.674	0.819	15.706	0.002	0.039	0	90.132
L24393	p6	25.465	0.027	20.798	26.809	0.930	15.384	0.019	0.048	0	89.602
L24393	p7	25.650	0.079	20.364	26.555	0.782	15.602	0.002	0.005	0.013	89.163
L24393	p8	25.978	0.065	21.018	27.684	0.867	14.750	0.007	0.096	0.028	90.620
L24393	p9	25.893	0.081	20.528	26.622	0.809	15.653	0.003	0.022	0.007	89.785
L24393	p10	25.158	0.064	19.770	26.949	0.948	15.633	0	0.037	0	88.695
L24393	p11	25.404	0.089	20.722	28.508	0.908	14.439	0.029	0.048	0.005	90.229
L24393	p12	25.936	0.028	20.427	26.817	0.775	14.458	0.061	0.146	0.071	88.872
L24393	p13	25.915	0.066	20.647	27.016	0.860	15.297	0.003	0.02	0.025	89.936
L24393	p14	26.041	0.075	20.209	26.909	0.843	15.497	0.043	0.059	0.049	89.813
L24393	p15	25.692	0.053	20.141	27.422	0.938	14.781	0.049	0.085	0.035	89.400
L98130	p1	25.965	0.057	20.994	26.664	0.796	15.687	0.022	0.026	0	90.393
L98130	p2	25.538	0.048	20.447	27.064	0.746	15.217	0.029	0.049	0.021	89.304
L98130	p3	25.323	0.026	20.751	27.975	0.849	14.640	0.037	0.03	0.016	89.766
L98130	p4	26.820	0.036	19.938	25.913	0.749	16.311	0	0.01	0.006	89.976
L98130	p5	26.164	0.019	20.338	26.156	0.792	15.721	0.006	0.007	0.01	89.442
L98130	p6	26.229	0.000	20.160	28.990	0.796	14.574	0.049	0.053	0.04	91.079
L98130	p7	27.140	0.049	18.664	26.079	0.716	16.525	0.005	0.034	0.019	89.556
L98130	p8	25.438	0.078	20.634	27.831	0.819	13.997	0.013	0.031	0.001	88.855
L98130	p9	26.748	0.063	18.857	26.696	0.720	15.998	0.004	0.044	0.02	89.333
L98130	p10	26.061	0.067	19.937	27.822	0.818	15.233	0.038	0.034	0	90.210

Tabela VIII- Descrição resumida do furo 21

From	To	Descrição
0	58.8	Saprolito
58.8	64.5	Argilito
64.5	64.9	Argilito
64.9	66.7	Argilito
69.7	73.3	Grauvaca
73.3	80.1	Argilito
80.1	80.5	Zona de Falha
80.5	92.0	Sedimento Indiferenciado
92.0	92.6	Zona de Falha
92.6	98.8	Argilito
98.8	99.5	Zona de Falha
99.5	116.7	Sedimento Indiferenciado
116.7	132.7	Tufo de Cinzas Félsicas
132.7	137.4	Sedimento Indiferenciado
137.4	138.1	Chert
138.1	143.4	Sedimento Indiferenciado
143.4	161.7	Tufo félsico
161.7	162.5	Zona de Cisalhamento
162.5	164.3	Sedimento Indiferenciado
164.3	165.9	Brecha a Quartzo e Clorita
165.9	169.1	Sedimento Indiferenciado
169.1	174.0	Tufo félsico
174.0	174.8	Chert
174.8	176.1	Tufo félsico
176.1	181.1	Argilito
181.1	181.9	Chert
181.9	184.4	Tufo de Cinzas Félsicas
184.4	184.6	Chert
184.6	187.4	Zona de Cisalhamento
187.4	188.0	Chert
188.0	195.2	Tufo félsico
195.2	196.4	Chert
196.4	200.1	Tufo félsico
200.1	202.5	Tufo félsico com cherts intercalados
202.5	204.1	Chert
204.1	220.9	Tufo félsico
220.9	224.1	Argilito
224.1	233.2	Tufo de Cinzas Félsicas
233.2	252.2	Tufo félsico
252.9	267.5	Tufo félsico
267.5	270.8	Tufo félsico intercalados com sedimentos indif.
270.8	278.0	Tufo félsico
278.0	278.5	Tufo félsico de Lapilli
278.8	287.4	Tufo félsico intercalados com sedimentos indif.
284.4	294.0	Argilito
294.0	296.2	Tufo félsico
296.2	299.4	Argilito
299.4	300.2	Tufo félsico com sulfetos Semi-Macícios
300.2	304.1	Tufo félsico
304.1	307.4	Zona de alteração cálcio-silicática e cloritização

Tabela VIII – Continuação

From	To	Description
307.4	307.7	Sulfetos maciços
307.7	309.3	Tufo félscico cloritizado
309.4	316.4	Zona de Falha
316.4	316.55	Zona de Cloritização
316.55	318.45	Sulfetos Semi-maciços
318.45	318.6	Sulfetos maciços
318.6	319.6	Zona de Alteração Clorítica à magnetita
319.6	319.9	Sulfetos maciços
319.9	322.6	Zona de Cloritização
322.6	325.8	Zona de Alteração Cálcio-Silicática
325.8	326.2	Zona de Alteração Clorítica à magnetita
326.2	326.8	Sulfetos Semi-maciços
326.8	327.6	Cloritização em Zona de Shear
327.6	328.1	Sulfetos Semi-maciços
328.1	331.2	Cloritização em tufos de Cinzas Félscicas
331.2	331.5	Sulfetos Semi-maciços
331.5	333.1	Zona de Cloritização
333.1	334.05	Sulfetos Semi-maciços
334.05	336.1	Zona de Alteração Clorítica à magnetita
336.1	337.5	Zona de Alteração Clorítica à magnetita
337.5	340.0	Zona de Cloritização
340.0	341.2	Sulfetos Semi-maciços
341.2	342.0	Cloritização em Zona de Falha
342.0	342.7	Sulfetos maciços
342.7	350.8	Zona de Alteração Clorítica à magnetita
350.8	352.3	Sulfetos maciços
352.3	354.6	Zona de Alteração Clorítica à magnetita
354.6	355.3	Zona de alteração calcio-silicatica em zona de Bx
355.3	365.6	Zona de Alteração Clorítica à magnetita
365.6	367.1	Zona de carbonatação,silicif., clorit. e brechação
367.1	367.7	Zona de Alteração Clorítica à magnetita
367.7	377.6	Zona de carbonatação,silicif., clorit. e brechação
377.6	379.1	Zona de Alteração Clorítica à magnetita
379.1	379.7	Zona de carbonatação,silicif., clorit. e brechação
379.7	381.4	Zona de Alteração Clorítica à magnetita
381.4	382.3	Sulfetos Semi-maciços
382.3	383.6	Zona de Alteração Clorítica à magnetita
383.6	384.1	Zona de carbonatação,silicif., clorit. e brechação
384.1	390.0	Zona de Alteração Clorítica à magnetita
390.0	390.4	Zona de carbonatação,silicif., clorit. e brechação
390.4	390.8	Zona de Alteração Clorítica à magnetita
390.8	391.6	Zona de carbonatação,silicif., clorit. e brechação
391.6	392.45	Sulfetos Semi-maciços
392.45	394.55	Sulfetos maciços
394.55	396.2	Zona de Alteração Clorítica à magnetita
396.2	397.6	Sulfetos maciços
397.6	405.3	Zona de Alteração Clorítica à magnetita
403.5	405.8	Zona de carbonatação,silicif., clorit. e brechação
405.8	406.5	Zona de Alteração Clorítica à magnetita

Tabela VIII – Continuação

406.5	408.3	Zona de carbonatação,silicif., clorit. e brechação
408.3	411.65	Zona de Alteração Clorítica à magnetita
411.65	412.9	Sulfetos Semi-maciços
412.9	420.6	Sulfetos maciços
420.6	421.6	Sulfetos Semi-maciços
421.6	423.2	Zona de Alteração Clorítica à magnetita
423.2	428.1	Zona de Alteração Clorítica à magnetita
428.1	434.5	Zona de Alteração Cálcio-Silicática
434.5	436.05	Sulfetos Semi-maciços
436.05	437.1	Zona de Cloritização
437.1	438.5	Zona de cloritização e silicificação
438.5	451.4	Agilito
451.4	453.7	Sulfetos Semi-maciços
453.7	455.9	Zona de Cloritização
455.9	457.1	Sulfetos maciços
457.1	458.9	Zona de Cloritização
458.9	460.6	Sulfetos Semi-maciços
460.6	462.6	Zona de Alteração Cálcio-Silicática
462.6	464.2	Zona de Alteração Cálcio-Silicática
464.2	466.6	Zona de carbonatação,silicif., clorit. e brechação
466.6	469.71	Sedimento Laminado
469.71	472.3	Zona de carbonatação,silicif., clorit. e brechação
472.3	475.3	Zona de Cloritização
475.3	478.0	Zona de Cloritização e biotitização
478.0	487.4	Zona de cloritização e silicificação
487.4	502.9	Sedimento Laminado
502.9	509.7	Chert
509.7	542.5	Sedimento Laminado

Tabela IX – Resultados de análises químicas de testemunhos de sondagem do furo 21.

AR97-21 Amostra	De	Até	Comp	Pb	Zn	Cu	Ag	Au
	m	m	m	%	%	%	glt	ppb
61813	145.8	146.4	0.6	0.33	0.8	0.05	12	201
61814	147.2	147.5	0.3	0.15	0.07	0.07	21	439
61815	164.3	165.9	1.6	0.02	0.66	0.02	3	27
61816	185.5	187	1.5	0.07	1	0	3	16
62151	288	288.5	0.5	0.22	0.5	0.01	4	34
62152	288.5	289.9	1.4	2.79	3.59	0.03	36	24
62153	289.9	291	1.1	0.21	0.84	0.05	4	7
62154	291	291.6	0.6	0.58	0.97	0.07	9	14
62155	291.6	292.6	1	0.16	0.04	0	5	46
62156	298.4	299.4	1	0.09	0.97	0.01	5	27
62157	299.4	300.2	0.8	4.2	9.8	0.04	34	35
62158	304.1	304.8	0.7	0.12	0.26	0.02	2	44
62159	304.8	305.1	0.3	0.95	12.69	0.35	14	98
62160	305.1	305.4	0.3	1	0.19	0.1	12	140
62161	305.4	306.3	0.9	0.02	0.01	0	1	16
61817	307.4	307.7	0.3	0.08	0.25	0.81	19	11
61818	307.7	309.3	1.6	0.03	0.06	0.02	3	95
61819	309.3	310.4	1.1	0.24	4.09	0.18	17	63
61820	310.4	312.4	2	0.13	1.29	0.04	10	35
61821	312.4	314.4	2	0.02	0.15	0.02	3	15
61822	314.4	316.4	2	0.2	1.5	0.01	9	22
61823	316.4	316.6	0.2	1.2	16.29	0.02	28	70
61824	316.6	317.5	0.9	0.1	1.39	0.02	7	16
61825	317.5	317.7	0.2	0.13	13.89	0.1	11	109
61826	317.7	318.5	0.8	0.14	1.2	0.01	7	22
61827	318.5	318.6	0.2	1.1	2.09	0.22	27	33
61828	318.6	319.1	0.5	0.49	0.56	0.02	14	22
61829	319.1	319.6	0.5	1.1	5	0.08	32	11
61830	319.6	319.9	0.3	1.29	4.44	0.02	26	135
61831	319.9	321.2	1.3	0.86	4.5	0.02	13	44
61832	321.2	322.6	1.4	1.7	6.9	0.02	21	49
61833	322.6	324.2	1.6	0.81	2.29	0.02	10	24
61834	324.2	325.8	1.6	0.49	2.59	0.05	10	22
61835	325.8	326.2	0.4	0.17	1.6	0.05	5	14
61836	326.2	326.8	0.6	1.2	5.3	0.14	16	16
61837	326.8	327.6	0.8	0.04	0.14	0.02	5	8
61838	327.6	328.1	0.5	0.11	0.09	0.05	13	5
61839	328.1	329.4	1.3	0.01	0.05	0.02	2	11
61840	329.4	330.4	1	0.07	0.17	0	3	10
61841	330.4	331.2	0.8	0.04	0.11	0.01	1	14
61842	331.2	331.5	0.3	0.75	0.08	0.35	21	122
61843	331.5	333.1	1.6	0.01	0.04	0.38	9	193
61844	333.1	334.1	0.9	0.01	0.04	0.17	5	65
61845	334.1	335.1	1.1	0	0.05	0.12	3	22
61846	335.1	336.1	1	0.01	0.1	0.29	3	190

Tabela IX- Continuação

Amostra	De m	Até m	Comp M	Pb %	Zn %	Cu %	Ag g/t	Au ppb
61847	336.1	337.5	1.4	0.01	0.08	0.09	5	64
61848	337.5	338.5	1	0.02	0.09	0.13	4	25
61849	338.5	340	1.5	0.02	0.05	0.35	8	142
61850	340	341.2	1.2	0.12	0.71	0.78	19	793
61851	341.2	342	0.8	0.02	0.4	0.08	5	15
61852	342	342.7	0.7	0.92	9.39	0.14	19	125
61853	342.7	343.7	1	0.01	0.78	0.03	2	5
61854	343.7	344.7	1	0.46	0.76	0.03	8	16
61855	344.7	345.7	1	1.1	2.09	0.02	16	35
61856	345.7	346.7	1	2	4.69	0.04	31	57
61857	346.7	347.7	1	0.13	2.29	0.04	5	16
61858	347.7	348.7	1	0.14	0.83	0.03	3	44
61864	348.7	349.7	1	0.16	2.29	0.03	4	16
61859	349.7	350.8	1.1	0.84	4.3	0.04	11	35
61860	350.8	352.3	1.5	4.09	11.8	0.03	52	281
61861	352.3	353.4	1.1	0.94	3.59	0.03	12	63
61862	353.4	354.6	1.2	1	4.3	0.03	17	90
61863	354.6	355.3	0.7	0.29	2.29	0	4	8
61865	355.3	357.2	1.9	1.1	6	0.04	12	30
61866	357.2	359.2	2	0.67	2.9	0.03	14	27
61867	359.2	361.2	2	1.1	2.7	0.03	25	35
61868	361.2	363.2	2	1.1	3.29	0.01	10	25
61869	363.2	365.6	2.4	0.89	2.2	0.01	9	14
61870	365.6	367.1	1.5	0.17	0.22	0	5	16
61871	367.1	367.7	0.6	0.02	0.44	0	1	8
61872	367.7	368.7	1	0.06	0.08	0	1	16
61873	376.6	377.6	1	0.01	0.06	0	1	3
61874	377.6	379.1	1.5	0.01	1.5	0.02	2	14
61875	379.1	379.7	0.6	0.51	0.9	0	9	5
61876	379.7	381.4	1.7	0.91	3.4	0.01	12	25
61877	381.4	382.3	0.9	0.65	2	0.01	10	57
61878	382.3	383.6	1.3	0.9	4	0	14	38
61879	383.6	384.1	0.5	0.57	0.17	0	7	14
61880	384.1	385.6	1.5	1.2	3.9	0.01	16	35
61881	385.6	387.6	2	0.34	2.29	0	7	11
61882	387.6	388.5	0.9	0.17	3.9	0	4	11
61883	388.5	390	1.5	0.35	3.59	0	5	19
61884	390	390.4	0.4	0.46	1.1	0	5	11
61885	390.4	390.8	0.4	0.01	0.62	0	2	5
61886	390.8	391.6	0.8	0.08	0.23	0	2	7
61888	391.6	392.5	0.8	0.13	2.5	0.01	5	155
61889	392.5	393.6	1.2	1.89	8.8	0.02	23	310
61890	393.6	394.6	0.9	2.64	4.55	0.03	13	395
61891	394.6	396.2	1.6	0.06	1.89	0.01	4	23
61892	396.2	397.6	1.4	0.32	6.69	0.04	8	162
61893	397.6	399.6	2	0.02	0.71	0.06	3	79

Tabela IX- Continuação

AR97-21	Amostra	De	Até	Comp	Pb	Zn	Cu	Ag	Au
		m	m	m	%	%	%	g/t	ppb
	61894	399.6	401.6	2	0.07	0.63	0.07	7	122
	61895	401.6	403.6	2	0.05	1.1	0.01	2	79
	61896	403.6	405.3	1.7	0.51	4.59	0.02	5	19
	61897	405.3	405.8	0.5	0.1	0.59	0	2	11
	61898	405.8	406.5	0.7	0.57	4.69	0	6	33
	61899	406.5	408.3	1.8	0.4	0.95	0	7	11
	61900	408.3	409.4	1.1	1.2	3.79	0	14	55
	62101	409.4	410.5	1.1	1	2.5	0	9	52
	62102	410.5	411.7	1.1	0.73	4.3	0.02	9	52
	62103	411.7	412.9	1.3	1.6	9	0.03	19	321
	62104	412.9	414.1	1.2	1.89	7.69	0.03	25	825
	62105	414.1	415	0.9	0.97	2.4	0.02	24	409
	62106	415	415.7	0.7	1.29	3.59	0.02	15	190
	62107	415.7	416.3	0.6	1.79	10.89	0.03	18	390
	62108	416.3	417.4	1.1	1.1	3.09	0.02	15	283
	62109	417.4	418.4	1	1.7	4.69	0.02	20	164
	62110	418.4	419.4	1	1.2	2.7	0.03	15	196
	62111	419.4	420.6	1.2	1.5	5.8	0.03	14	256
	62112	420.6	421.6	1	2.2	7.5	0.02	22	152
	62113	421.6	423.2	1.6	0.23	0.91	0.01	3	14
	62114	423.2	425.2	2	0.91	2.79	0.02	9	54
	62115	425.2	426.8	1.6	0.9	2.29	0.03	8	65
	62116	426.8	428.1	1.3	0.24	1.89	0.02	4	41
	62117	428.1	430.1	2	0.09	1	0	3	11
	62118	430.1	432.1	2	1.7	1.5	0	26	46
	62119	432.1	434.5	2.4	1.29	1.29	0.02	21	25
	62120	434.5	435.2	0.6	0.35	3.9	0.19	9	65
	62121	435.2	436.1	0.9	0.14	2.7	0.14	8	144
	62123	436.1	437.1	1.1	0.02	0.14	0.35	8	165
	62124	437.1	438.5	1.4	0.07	0.2	2.7	49	1288
	62125	438.5	440.3	1.8	0.01	0.03	0.06	3	19
	62126	440.3	441.6	1.3	0.01	0.09	0.04	2	11
	62127	441.6	442.7	1.1	1.29	0.03	0.38	27	235
	62128	442.7	443.8	1.1	0.04	0.05	0.11	4	22
	62129	443.8	444.8	1	0.12	0.12	0.11	8	19
	62130	444.8	445.7	0.9	0.03	0.19	0.19	6	38
	62131	445.7	446.7	1	0.02	0.15	0.17	4	46
	62132	446.7	448.4	1.7	0.05	0.14	0.11	3	11
	62133	448.4	449.4	1	1.1	0.1	0.06	33	16
	62134	449.4	450.2	0.8	0.62	0.09	0.15	28	65
	62135	450.2	451.4	1.2	0.1	1	0.06	6	11
	62136	451.4	452.4	1	0.02	1.89	0.17	5	38
	62137	452.4	453.7	1.3	0.05	1.6	0.39	10	82
	62138	453.7	454.7	1	0.51	2.09	0.1	8	26
	62139	454.7	455.9	1.2	0.01	4.09	0.07	7	35

Tabela IX- Continuação

AR97-21

Amostra	De m	Até m	Comp m	Pb %	Zn %	Cu %	Ag g/t	Au ppb
62140	455.9	457.1	1.2	2.7	9.3	0.06	30	74
62141	457.1	458.9	1.8	1.2	6.09	0.04	17	57
62142	458.9	459.5	0.6	0.42	8.39	0.03	8	65
62143	459.5	460.6	1.1	1.79	2.5	0.05	22	74
62144	460.6	461.4	0.8	0.09	1.89	0.05	4	18
62145	461.4	462.2	0.8	5.69	7.8	0.05	75	79
62146	462.2	464.2	2	0.33	0.82	0.02	15	24
62147	464.2	465	0.8	0.35	0.58	0.01	12	44
62148	> 465	466.6	1.6	0.35	0.76	0	9	22
62149	466.6	468.1	1.5	0.08	0.09	0	2	3
62150	468.1	469.7	1.6	0.17	0.47	0	4	11
61919	470.9	471.8	0.9	0.02	0.04	0.02	2	0
61920	471.8	472.3	0.5	0.22	0.2	0	8	0
61921	472.3	473	0.7	0.01	0.06	0	2	0
61922	478.2	478.7	0.5	1.2	4.3	0	42	0.05

Tabela VIII- Análise químicas de amostras do furo 21

Sample	From	To	SiO <sub>2</sub>	TiO <sub>2</sub>	Al <sub>2</sub> O <sub>3</sub>	Fe <sub>2</sub> O <sub>3T</sub>	MnO	MgO	CaO	Na <sub>2</sub> O	K <sub>2</sub> O	P <sub>2</sub> O <sub>5</sub>	LOI	Total	Ba	Rb	Sr	Ti	Nb	Zr	Y
61619	7750	7870	75.1	0.25	12.2	2.64	0.08	3.4	0.09	0.03	4.34	0.05	2.05	98.18	1140	134	4	1427	16	214	42
61620	8750	8870	77.4	0.17	12	2.11	0.05	2.49	0.05	0.01	4.05	0.02	2.1	98.35	997	131	2	970.36	14	157	34
61621	10910	11030	72.9	0.23	13	2.85	0.06	3.74	0.1	0.04	3.92	0.04	2.9	96.88	655	123	2	1312.84	13	186	41
61622	13150	13260	75.7	0.27	12.4	2.8	0.01	1.39	0.08	0.05	4.46	0.05	2.8	97.21	681	151	5	1541.16	17	215	44
61623	15210	15320	80.1	0.16	10.1	1.57	0.01	0.93	0.11	1.31	3.06	0.02	1.55	97.37	1370	86	4	913.28	12	199	42
61624	18260	18400	75.4	0.2	12.6	1.96	0.1	2.18	0.71	0.62	4.3	0.02	2	98.09	1180	143	24	1141.6	16	252	47
61625	20880	21000	75.1	0.23	12.4	2.96	0.02	1.96	0.08	0.01	4.09	0.04	2.85	96.89	655	133	4	1312.84	13	176	42
61626	22250	22400	69	0.19	12.2	4.6	0.21	5.22	0.62	0.21	4.62	0.02	2.8	96.89	627	182	30	1084.52	15	258	49
61627	24990	25140	73.5	0.2	12.6	2.1	0.13	2.19	1.06	0.35	4.84	0.02	1.65	96.99	1360	150	25	1141.6	17	251	48
61628	26500	26670	72.1	0.23	14.1	2.26	0.08	3.46	0.09	0.03	4.59	0.03	2.6	96.97	953	143	4	1312.84	18	307	51
61629	28480	28570	67.2	0.38	14.3	3.93	0.08	4.7	0.15	0.01	4.41	0.08	4	95.24	852	137	2	2169.04	17	280	50
61630	30230	30320	75.5	0.37	13.3	1.77	0.01	1.32	0.12	0.06	5.02	0.06	2.55	97.53	661	160	2	2111.96	18	165	31